Sigrid Strand

An Investigation of HOR Activity in Alkaline Solution on Nickel Electrode

Master's thesis in MTKJ
Supervisor: Svein Sunde
Trondheim, December 2018

Master's thesis

NTNU
Norwegian University of Science and Technology
Faculty of Natural Sciences
Department of Materials Science and Engineering

NTNU
Norwegian University of
Science and Technology

Sigrid Strand

An Investigation of HOR Activity in Alkaline Solution on Nickel Electrode

Master's thesis in MTKJ
Supervisor: Svein Sunde
Trondheim, December 2018

Norwegian University of Science and Technology
Faculty of Natural Sciences
Department of Materials Science and Engineering

NTNU
Norwegian University of
Science and Technology

Preface

This master's thesis is the final work of the Master's program "Industrial Chemistry and Biotechnology" at the Norwegian University of Science and Technology (NTNU), resulting in a Master of Science degree in Chemical Engineering, specialized in Materials Science. This thesis was part of a collaboration project with SINTEF and two universities from Israel and Taiwan. It was written during the Autumn of 2018 at the department of Materials Science and Engineering. The goal was to investigate the kinetics of the hydrogen oxidation reaction on polycrystalline platinum and bulk-nickel electrodes in an alkaline fuel cell. The experimental work has been conducted by the author, but some data was collected from a specialization project which this master thesis is a continuation of. The specialization project "Electrochemical Analysis of Nickel for the Alkaline Fuel Cell" was conducted by the author during the spring semester of 2018, where HOR properties were investigated during electrochemical formation of α-$Ni(OH)_2$ and β-$Ni(OH)_2$.

Declaration of Compliance

I hereby declare that this is an independent work according to the exam regulations of the Norwegian University of Science and Technology.

Trondheim, 2018-12-10

Sigrid Strand

Sigrid Strand

Acknowledgement

I would like to thank my supervisor, Professor Svein Sunde[1], for his patience and thorough guidance, and for the opportunity to be part of this exciting project. I would also like to thank my co-supervisor, Postdoctoral Fellow Maidhily Manikandan[1], for all help experimentally and theoretically, and for sharing her knowledge with a smile on her face.

Finally, I would like to thank my friends and fellow students for 5 amazing years in Trondheim.

[1] The Department of Materials Science and Engineering, NTNU, Trondheim

Abstract

Finding new and sustainable energy sources is of great importance as the population, technological advancement, and consumption is ever increasing. Fuel cell (FC) technology has been thoroughly investigated the past decades, and is considered to be one of the most promising renewable and sustainable energy sources of the future.

The objective of this study was to investigate the properties and kinetics of hydrogen oxidation reaction (HOR) in the alkaline fuel cell, using polycrystalline platinum and bulk nickel electrodes. Cyclic Voltammetry (CV) and Electrochemical Impedance Spectroscopy (EIS) was conducted to investigate properties such as pH dependence, hydrogen evolution and charge transfer resistance (R_{ct}). EIS measurements showed a decrease in R_{ct} with increasing polarization below 0 V and an increase in R_{ct} with increasing polarization above 0 V. The effect of rotation was investigated, but gave contradicting results. The overall R_{ct} was much lower on Pt compared to Ni, which was as expected due to catalytic properties. Further evaluation and investigation of the data must be conducted. Suggestions are put in further works.

When conducting CV's on Pt electrode, proof of hydrogen evolution was found at 0 V, as the the peak at this potential was suppressed with rotation. During studies conducted on the Ni electrode, it was found that HOR activity was best promoted in H_2(g) saturated 0.1M KOH at low scan rates. It was also found that hydrogen evolution increases as the stating potential of the CV scan is set to more negative potentials. Rotation of the electrode showed significant effect in 0.1M KOH, but did not have any effect in 1M KOH. The theory behind hydrogen binding energy (HBE) was used used to explain the rotation effect and the pH dependence, however this theory is yet to be proven and further work must be conducted.

The kinetics of HOR was investigated by a simulation of CV curves in MATLAB based on a kinetic HOR model, both made by Professor Svein Sunde. Valuable information like rate constants, reaction rates, and coverage can be extracted from the simulation, giving a much better understanding of the HOR kinetics. However, it proved to be difficult achieving a perfect fit to the experimental data. Further improvement of the simulation is necessary before collecting the much desired data. A suggestion on how to solve this is provided in further works.

Sammendrag

Å finne nye og bærekraftige energikilder er av stor betydning ettersom befolkning, teknologisk utvikling og forbruk øker. Brenselcelle (FC)-teknologi har blitt grundig undersøkt de siste tiårene, og regnes som en av fremtidens mest lovende fornybare og bærekraftige energikilder.

Målet med dette studiet var å undersøke egenskaper og kinetikk hos hydrogenoksidasjonsreaksjonen (HOR) i den alkaliske brenselcellen ved bruk av polykrystallinske platinum- og bulknikkel elektroder. Syklisk voltammetri (CV) og elektrokjemisk impedansspektroskopi (EIS) ble utført for å undersøke egenskaper som pH-avhengighet, hydrogenevolusjon og ladningsoverføringsresistens (R_{ct}).

EIS-målinger viste en nedgang i R_{ct} med økende polarisasjon under 0 V, og en økning i R_{ct} med økende polarisasjon over 0 V. Effekten av rotasjon ble undersøkt, men ga motstridende resultater. Den totale R_{ct} var mye lavere for Pt sammenlignet med Ni, som var som forventet fra katalytiske egenskaper. Videre evaluering og undersøkelse av dataene må gjennomføres. Forslag legges i videre arbeid. Ved utførelse av CV på Pt-elektroden ble det funnet bevis på hydrogenutvikling ved 0 V, da toppen ved dette potensialet ble undertrykt ved rotasjon av elektroden. Gjennom studier utført på Ni-elektroden ble det funnet ut at HOR-aktivitet var best fremmet i H_2(g) mettet 0.1M KOH ved lave skannehastigheter. Det ble også funnet at hydrogenevolusjonen øker ettersom startpotensialet til CV-skanningen ble satt til mer negative potensialer. Rotasjon av elektroden viste signifikant effekt i 0.1M KOH, men hadde ingen effekt i 1M KOH. Teorien bak hydrogenbindende energi (HBE) ble brukt til å forklare rotasjonseffekten og pH-avhengigheten, men denne teorien er ennå ikke bevist, og ytterligere arbeid må utføres.

Kinetikken til HOR ble undersøkt ved en simulering av CV-kurver i MATLAB basert på en kinetisk HOR-modell, begge laget av professor Svein Sunde. Verdifull informasjon som hastighetskonstanter, reaksjonshastigheter og dekningsgrad kan hentes fra simuleringen, noe som gir en mye bedre forståelse av HOR kinetikken. Imidlertid viste det seg å være vanskelig å oppnå en perfekt passform til de eksperimentelle dataene. Videre forbedring av simuleringen er nødvendig før ønskede dataene kan bli samlet. Et forslag til hvordan man løser dette er gitt i videre arbeid.

Contents

Abbreviations and nomenclature

List of Abbreviations

AAEMFC	Alkaline anion exchange membrane fuel cell
AEM	Anion exchange membrane
AFC	Alkaline fuel cell
CA	Chronoamperometry
CE	Counter electrode
CV	Cyclic voltammetry
EIS	Electrochemical impedance spectroscopy
FC	Fuel cell
HBE	Hydrogen binding energy
HER	Hydrogen evolution reaction
HOR	Hydrogen oxidation reaction
LSV	Linear sweep voltammetry
NTNU	Norwegian University of Science and Technology
OER	Oxygen evolution reaction
ORR	Oxygen reduction reaction

$PEMFC$	Proton exchange membrane fuel cell
$PGM-free$	Platinum group metal free
$RDEs$	Rotatin disk electrode
rds	Rate determining step
RE	Refrence electrode
RHE	Reversible hydrogen electrode
rpm	Rotations per minute
WE	Working electrode

List of Nomenclature

β	Tafel slope
δ	New objective
η	Dynamic viscosity
$\frac{\partial c_i(x,t)}{\partial x}$	Concentration gradient
ν	Voltage sweep rate
ν_L	Levich number
ω	Angular velocity
ω	Radial frequency [rad/sec]
ϕ	Phase shift angle
ρ	Density
A	Electrode surface area
c_R^*	Bulk concentration of species R
D_i	Diffusion coefficient for species i

E	Cell potential
E_0	Initial potential
E_l	Lower potential
E_{rev}	Reversible potential
E_u	Upper potential
F	Faraday's constant
f	Frequency [Hz]
i	Current density
I_0	Current amplitude
i_0	Exchange current density
i_f	Measured current density in chosen point
i_{kin}	Kinetic current density
i_{lim}	Limited current density
i_{rem}	Removal controlled current density
I_t	Current at time T
J	Diffusion Flux
j	Current
n	Number electrons transferred
O	Oxidized species
P	Probability factor
R	Gas constant
R	Reduced species
R	Resistance

R_{ct}	Charge transfer resistance
T	Temperature
t	Time
Z	Impedance
Z'	Real part of Z
Z''	Imaginary part of Z

Chapter 1

Introduction

1.1 Motivation

The technological advancement and rapid increase in the population of today have led to an over-consumption of energy that pollutes the environment to the point of no return. The use of fossil fuels such as oil, coal, and gas must be replaced by new ways of generating and saving electricity in a sustainable matter. Fuel cell technology has been around since the early 20th century, and much of research has been conducted in this field the past decade. In 2015, the first commercialized fuel cell vehicles were launched [1] as a result of extensive research. However, there are many obstacles concerning this technology as well. For example, in proton exchange membrane fuel cells (PEMFCs), noble metals such as platinum (Pt) and palladium (Pd) are used as electrode materials as they have the best catalytic properties. Unfortunately, these are very expensive materials as their reservoir are limited. By changing the membrane to an anion exchange membrane (AEM), using hydroxide ions (OH^-) as carriers, a whole new arena of platinum group free (PGM-free) catalysts opens, thus leading to a substantial decrease of the overall production costs of a fuel cell [1]. Hydrogen gas (H_2(g)) is used as fuel in the alkaline anion exchange membrane fuel cell (AAEMFC), and is perfectly suited as an energy carrier. H_2(g) does not pollute, and the only by-product in AAEMFCs with H_2(g) as a fuel is water. The kinetics of HOR in alkaline condition is two orders of magnitude slower than that in acidic [2], which is

why a thorough investigation of HOR is of great interest and importance to further improve and develop the fuel cell technology[3].

1.2 Previous Work

To further enhance the AAEMFC technology of today, a thorough investigation of the hydrogen oxidation and evolution reactions is needed, as their mechanisms and properties are poorly understood [4]. Nickel is a commonly used PGM-free metal due to its good catalytic properties. M.Alsabet (2011) [5] used the electrochemical measurement techniques such as cyclic voltammetry (CV), electrochemical impedance spectroscopy (EIS), and chronoamperometry (CA) to investigate the electrochemical growth of surface oxide on nickel, and how the resulting current was affected by the phenomenon of place exchange. It was found that Langmuir-type adsorption, electron tunnelling, the point defect model, and the nucleation-and-growth model does not apply to the growth of α-Ni$(OH)_2$. Oshchepkov (2018) [6] investigates how the kinetics of HOR/HER are affected by temperature and surface oxidation by conducting CV and microkinetic modeling. This study suggests that HOR/HER on metallic nickel follows a Heyrovsky-Volmer mechanism, due to the characteristically low reaction rate and strong adsorption of hydrogen intermediates. By monitoring the adsorption and desorption of hydrogen at the electrode surface, the kinetics can be investigated. In the work of Conway (1987) [7], impedance measurements were conducted on HER kinetics at activated and un-activated Pt cathodes. By using sets of rate constants in the HER, a quantitatively simulation of the kinetic behavior was performed. A similar approach was used by Professor Svein Sunde in his first edition of a kinetic HOR model, which is used in this thesis to investigate the rate constant of HOR on nickel.

This master thesis is the continuation on the studies conducted on the nickel surface. The surface oxidation of Ni, its activity and stability for HOR in alkaline environment was studied by two major electrochemical techniques such as CV and LSV. Both α-Ni$(OH)_2$ and β-Ni$(OH)_2$ were formed electrochemically by conducting CV in different potential ranges. It was observed that parameters like scan rates and rotation influences the HOR. The HOR testes were also conducted on both Ar and H_2 atmosphere [8]. The main goal was to achieve a mechanistic under-

standing of the HOR on the surface of bulk Ni electrode. A detailed interpretation of all these findings are explained in a best possible way in this thesis.

1.3 Scope of Work

This master thesis focuses on HOR on the nickel in alkaline solution. The CVs were conducted in 1M KOH, which was compared to the CVs conducted in 0.1M KOH in the project thesis [8]. To have an extensive comparison. some more CV measurements were carried out in 0.1 M KOH in this thesis. By comparing CV scans in different concentrations, pH dependence was investigated. EIS was conducted to further investigate the stability and activity of HOR on a nickel surface. A kinetic model of the HOR, developed by Professor Svein Sunde, was used to simulate the CV. The algorithm "Simulated Annealing" was used in MATLAB to fit the simulation to the experimental curves. Important rate constants was then collected from the simulated curve. The code in Matlab was also written by Professor Svein Sunde.

1.3.1 Outline

Chapter 1 is an introduction of this thesis, briefly describing the motivation and aim for this work. A short overview of earlier work is also presented here. Chapter 2 is a theoretical introduction, discussing Alkaline fuel cells (AFCs), hydrogen and its application, the electrochemical methods such as CV, LSV, and EIS, Pt, Ni and their properties, and a small section about MATLAB as a tool, and how the algorithm "Simulated Annealing" works is also given in a small section. Chapter 3 is a description of experiments and how they were conducted. Chapter 4 presents the results obtained during this study, which is further discussed in chapter 5. Chapter 6 presents a conclusion, and chapter 7 is further work.

Chapter 2

Basic Theory

This section is based on the theory section in [8].

2.1 Alkaline fuel cells

The world population is rapidly increasing and by 2050 the population is estimated to be 9.8 billion[9]. The energy demand will increase proportionally with the rising population and technological advancement, and there are not enough resources on earth to meet future demands in a sustainable matter. The only way to solve this issue is to find new, clean, and renewable energy sources which can replace the non-renewable and polluting energy sources of today[10]. Hydrogen is an excellent energy source as it both carries and stores energy [11]. It can be obtained from for example water electrolysis, driven by clean energy sources such as solar, wind and hydro power etc. The only bi-product of this reaction is water, making it a 100% clean and sustainable energy source, as long as the applied energy source is clean [11, 12]. By combining hydrogen and its properties with fuel cell technology, sustainable electricity is generated. Fuel cell technology has been thoroughly investigated in past decades and is considered to be one of the most promising energy technologies of the future. The proton exchange membrane fuel cell has earlier been the main focus when it comes to fuel cell technology, but the past decades, alkaline fuel cell technology has been revisited and as it allows the utilization of PGM-free catalysts

such as Ni [3, 13, 14]. PGM-free metals have proven to have great catalytic properties in alkaline environment concerning the oxygen reduction reaction (ORR) and oxygen evolution reaction (OER), however, the kinetics of HOR and HER are a lot slower in this environment, resulting in a larger load on the catalyst [15].

The main principle of a fuel cell (FC) is to convert chemical energy from chemical reactions directly into electrical energy without any intermediate steps [2]. This one-step process is a much more efficient mechanism compared to combustion based technology. Energy is lost between each step in the combustion based power source. It also consumes natural resources such as oil, gas, and coal as fuel, and pollutes the environment, enhancing the already too high global warming. One of the greatest perks of FC technology is its sustainability. FCs provides a clean and sustainable mechanism where renewable energy sources can be utilized [16].

The idea of fuel cell technology has existed since the 1800s, however the technology was not applicable until the 1950s. AFCs was the first fuel cell technology to generate electricity from hydrogen reactions, and it was used in the first Apollo spacecraft that went to the moon [16]. A lot of research and development was conducted through the 1960s and 1970s, but commercially there were many issues such as safety, costs, and reliability. Soon, the development of the PEMFC became a more important research field and the interest of AFC declined [16, 17]. However, the past decades new insight in the alkaline fuel cell technology has received a lot of attention. Anion exchange membrane fuel cells (AEMFCs) provides an opportunity to use non-noble metal catalysts, which drastically reduces the costs per kilowatt of power[17]. The concept of AEMFCs is quite similar to PEMFCs, the difference lies in the alkaline solid membrane transferring hydroxide (OH^-) ions instead protons (H^+) in the acidic solid membrane. Also, the OH^- in the AEMFCs is transported from the cathode to the anode. This is opposite compared to PEMFC, where the hydrogen atom is transported from the anode to the cathode. Improvement of the AEM and its availability has made the AEMFCs reach much higher and better values for the conductivity, yielding great improvement of the overall cell performance [18].

The outline of a FC is a quite simple concept, much similar to batteries considering the anode, cathode, and reactions taking place at the electrode surface. The fuel cell consists of an anode where fuel is oxidized, a cathode where fuel is reduced and an electrolyte between these elec-

trodes. There is a constant fuel and oxidant supply in the fuel cell which drives the reactions and generates electric energy [16]. Oxidation and reduction reactions takes plaxe at the anode and cathode in the fuel cell [2, 17]. These can be viewed in equations 2.1.1-2.1.2.

$$2H_2 + 4OH^- \longrightarrow 4H_2O + 4e^- \qquad (Anodic) \tag{2.1.1}$$

$$O_2 + 4e^- + 2H_2O \longrightarrow 4OH^- \qquad (Cathodic) \tag{2.1.2}$$

and an overall cell reaction becomes

$$2H_2 + O_2 \longrightarrow 2H_2O + \text{electric energy} + \text{heat} \tag{2.1.3}$$

The reaction at the cathode is the well-known ORR. OH^- ions are transferred from the cathode to the anode where it reacts with the fuel (hydrogen was used as fuel in 2.1.1) and produces water as a by-product [18]. Twice the amount of water is produced per electron in AFCs compared to PEMFCs, and the water produced can actually be used as drinking water, which was how they provided water during the Apollo space craft mission to the moon [16]. The water and the heat have to be removed if the cell is to function properly. The electrolyte can be recycled and used to cool down the system, while the water can be utilized in other matters or be evaporated[2]. A schematic representation of the alkaline fuel cell can be viewed in figure 2.1.1.

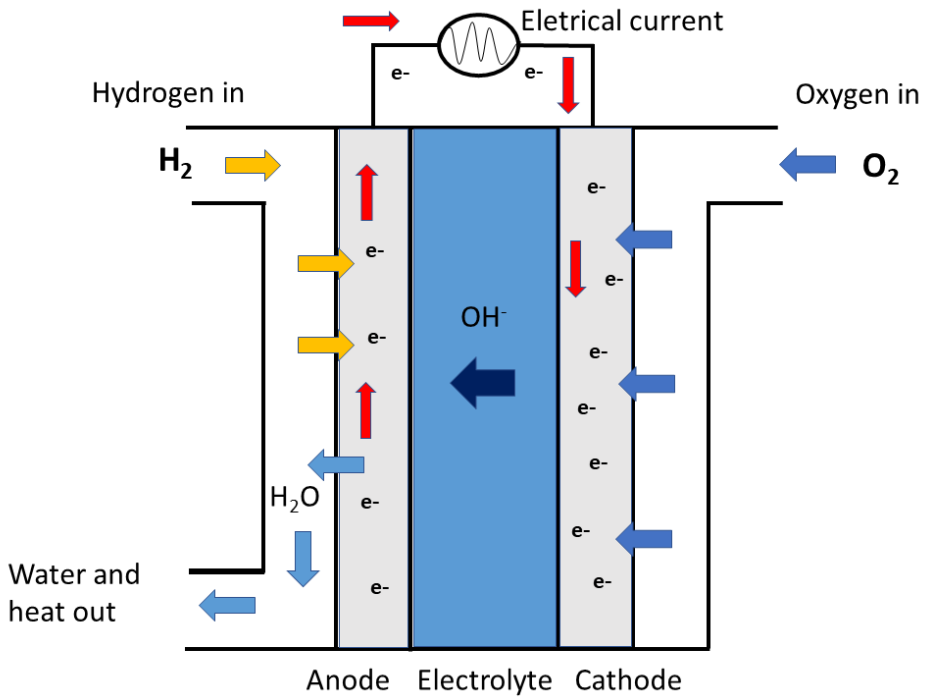

Figure 2.1.1: Schematics of an alkaline fuel cell, from [16]. The reactions at the anode and the cathode can be viewed in equations 2.1.1 and 2.1.2, respectively. Electron transfer occurs from the anode to the cathode while positive current flow the opposite direction.

The electrolyte in an AFC is of course an alkaline solution. There are several options, but one of the best choices is potassium hydroxide (KOH) as it is very cheap, highly soluble and has good corrosion properties [16]. However, liquid electrolyte can be replaced by solid membranes, on which extensive studies are being conducted [4].

There are several advantages using AFCs compared to other fuel cells. An AFC has a lower activation overvoltage at the cathode compared to fuel cells with an acidic electrolyte, yielding a lower voltage loss in the cell. The cathode kinetics are faster in alkaline media, leading to a more rapid ORR. The enhanced ORR is one of the most important properties of the AFC, allowing the utilization of PGM-free catalysts [17, 16]. AFC is a low-cost fuel cell compared to other fuel cell technologies. The KOH electrolyte is very cheap and could be used in almost all kinds of AFC. There is also a broader fuel selection for AFC compared to other fuel cells [18]. As mentioned earlier, the electrodes can be made from non-noble metals, providing a cheaper and more sustainable option. AFC does not have bipolar plates like PEMFC, and this lowers the production costs substantially. However, bipolar plates are also important for maintaining a high power

density, which is a huge drawback in AFC [16].

There are some drawbacks concerning AFC, but the main issue has to do with the alkaline electrolyte. As air contaminated with CO_2(g) goes into the cell and reacts with the electrolyte, carbonates ($CO_3{}^{-2}$) will form and precipitate [16, 17].

$$2\,OH^- + CO_2 \longrightarrow CO_3{}^{2-} + H_2O \tag{2.1.4}$$

The formation of carbonates has several unfortunate outcomes

- Reduction of the reaction rate at the anode, as a result of a reduction in the OH^- concentration
- An increase of the viscosity, which again lowers the diffusion rates and thus the limiting currents. This yields a higher mass transport loss.
- $(CO_3)^{-2}$ is less soluble and will precipitate after a while, which could block pathways and pores at the electrode surface, causing damage to the electrodes.
- The cathode experiencing a higher activity loss because the oxygen solubility decreases.
- A lower conductivity in the electrolyte, hence an increase in ohmic losses.
- Possible degradation of electrode performance.

Removal of CO_2 from the air is a necessity if the AFC is to operate over a longer period of time, however implementing such a device would increase both size, mass, complexity, and costs of the fuel cell [16].

To evaluate the electrochemical performance of fuel cells, the relationship between the cell potential (E) and current density (i) should be investigated. If mass transport limitations are assumed negligible, the relationship can be written as

$$E = E_0 - \beta log i - Ri \tag{2.1.5}$$

with

$$E_0 = E_r + \beta log i_0 \tag{2.1.6}$$

where E_0 is the initial potential, E_r is the reversible thermodynamic potential, β is the Tafel slope, i_0 is the exchange current density for the cathodic reaction, i is the current density, and R is the cell resistance [17]. By differentiating Eq. 2.1.5 the relationship between electrode kinetics and electric resistance can be written as

$$\frac{\partial E}{\partial i} = -\frac{\beta}{i} - R \tag{2.1.7}$$

Equation 2.1.7 gives the relationship between current density and resistance. A high current density combined with low cell resistance and low values for Tafel slopes gives the most optimal performance for the fuel cell system [17]. The cell resistance is mainly dependent on the ionic and protonic resistivity of the electrolyte. There are several electrochemical methods to characterize properties of the fuel cell systems and the reactions that develop within the cell.

The greatest obstacle of AFCs today is the slow reaction kinetics of the HER and HOR. A more thorough investigation of these mechanisms and their current densities is critical to achieve higher performance, as low kinetics consequently reduces the cell efficiency, leading to a higher load of the catalysts [19].

2.2 Hydrogen and its applications

Hydrogen has been investigated for years as a clean and renewable energy source an is viewed a worthy candidate that can be used as an alternative to fossil fuel due to high gravimetric energy density and sustainability [20]. It is the smallest element in existence, consisting of one proton and one electron. However, it is not found naturally as a gas and is bound to other elements such as oxygen, nitrogen and carbon (i.e water and hydrocarbons). H_2(g) can be produced by splitting water, using external power sources such as hydro power, solar power, biomass, coal,

nuclear power etc [11, 12, 21].

Hydrogen has several applications, among them being an energy carrier. It becomes an energy carrier when an external power source is applied and will carry this electricity as chemical energy for future use. One of the greatest perks being an energy carrier is the vast application range: from small scale batteries to large-scale plants. Its application as an energy carrier can be divided into four subcategories

- *Mobile*: Objects in motion, such as cars, boats and aeroplanes.
- *Stationary*: Stationary objects, such as power plants and fuel cells.
- *Backup*: A portable energy source
- *Specialty*: Advanced technologies and applications

Another critical feature of hydrogen is its storage ability. It can store electricity produced by sustainable sources and utilize it a desired time. This property will be very important in the years to come, as the demand of sustainable energy rapidly increases [12].

The utilization of hydrogen faces many difficulties despite of its small size and many applications. It is a secondary energy source as it does not exist in a free state and has to be separated from other compounds in order to use it. Hydrogen is very flammable, and difficult to store due to its small size. It is a very light element with low solubility. In comparison to other compounds, hydrogen contains less usable energy volumetrically. It can also cause great damage in the industry in the form of hydrogen embrittlement [22].

In order to transport, store and deliver energy, there are two fundamental mechanisms: Hydrogen oxidation reaction and hydrogen evolution reaction, which takes place on the anodes and cathodes used in fuel cells and electrolyzers [4]. These reactions have been thoroughly investigated for decades, and it is found that the current density of HOR in an alkaline environment is 2-3 times lower compared to the HOR in acidic environment[23, 24]. Sluggish kinetics in the HOR mechanism yields performance losses and a higher consumption of precious metals in AEMFCs as a higher overpotential is required[25]. HER is the best known mechanism compared to the HOR as the performance of HOR is poor in the alkaline environment and less studies have

been conducted on HOR. The kinetics of the reactions are dependent on several factors such as electrolyte composition, the chemical and physical nature of the electrode, pH, pressure, temperature and applied potential[26].

The overall HOR mechanism in alkaline media can be written as

$$H_2 + 2\,OH^- \rightleftharpoons 2H_2O + 2\,e^- \tag{2.2.1}$$

which is divided into the Tafel, Heyrovsky and Volmer step, respectively:

$$H_2 \rightleftharpoons 2H_{ads} + 2e^- \tag{2.2.2}$$

$$H_2 + OH^- \rightleftharpoons H_{ads} + e^- + H_2O \tag{2.2.3}$$

$$H_{ads} + OH^- \rightleftharpoons H_2O + e^- \tag{2.2.4}$$

Where the Tafel reaction is a chemical desorption, the Heyrovsky reaction is an electrochemical desorption, and the Volmer reaction is an electrochemical hydrogen adsorption. The overall reaction is either a combination of Heyrovsky-Volmer mechanisms or Tafel-Volmer mechanisms with the Volmer mechanism as rate determening step (rds), or Heyrovsky-Volmer where the Heyrovsky mechansism is rds [1, 15, 27, 28, 29].

The hydroxide can be adsorbed at the electrode surface and be further reduced to OH_{2ads} [1].

$$H_2(aq) + OH{-}(aq) \rightleftharpoons OH_{ads} + e^- \tag{2.2.5}$$

$$OH_{ads} + OH{-}(aq) \rightleftharpoons OH_{2ads} + e^- \tag{2.2.6}$$

By using equations 2.2.2-2.2.6, a model for the kinetics of the HOR on a metal surface, Ni for instance, can be developed.

Extensive studies has been conducted to find the perfect catalyst for the HER reaction. This is not an easy task, as HOR requires a considerable overpotential to achieve an acceptable effi-

ciency. Noble metals such as Pt, Ru, and Rh have the best properties, but they cannot be used in industrial processes due to their high costs and limited reservoir [21, 29]. The kinetics of HOR in alkaline media is considered to be a major restriction, concidering further advancement of the water-splitting technology for hydrogen production of high purity [4, 19, 23, 30]. Even though a lot of research has been conducted on the HOR/HER mechanism, important parameters like the reaction order with respect to hydrogen concentration, and rate constants for the reactions in equations 2.2.2-2.2.6 remains unknown [4]. A lot of research is currently being conducted in this field.

2.3 Electrochemical measurements

2.3.1 Linear Sweep Voltammetry (LSV)

LSV is a tool used in electrochemistry to analyze the current that moves between electrodes in an electrochemical cell at increasing or decreasing potential [31, 32]. The resulting graph is a current-voltage plot that can be used to characterize the properties of the chosen materials in the cell. The increase or decrease in potential can be written as

$$E(t) = E_0 \pm \nu t \tag{2.3.1}$$

where E(t) is the potential at a given time, t, ν is the voltage sweep rate, and E_0 is the starting potential which is set to a such low potentials that no reactions will occur.

LSV measurements are dependent on many factors. The reaction rate of the electron transfer reaction(s), the reactivity of the species and the scan rate are some of the most important ones [33]. If the scan rate is increased, the current will also increase. This can be justified by considering how long it takes to record the scan, as well as the size of the diffusion layer. The size of the diffusion layer will vary with the voltage and scan rate, as a high scan rate gives a shorter recording time and vice versa. The diffusion layer will grow much closer to the electrode in a high scan rate compared to a slow scan rate, hence the flux to the electrode will be larger at fast

scan rates. The flux and the current are proportional, which justifies why the current increases with increasing scan rate [33].

The flux can be described by Fick's first law

$$J_i(x,t) = -D_i \frac{\partial c_i(x,t)}{\partial x} \tag{2.3.2}$$

where J_i is the flux of species i, D_i is the diffusion coefficient and $\frac{\partial C_i(x,t)}{\partial x}$ is the concentration gradient. Species i will later be described as O or R, referring to oxidized or reduced species, respectively. The diffusion is described by Fick's second law, which predicts how concentration changes over time as a result of diffusion [31].

$$\frac{\partial c_O}{\partial t} = D_O\left(\frac{\partial^2 c_O}{\partial x^2}\right) \tag{2.3.3}$$

$$\frac{\partial c_R}{\partial t} = D_R\left(\frac{\partial^2 c_R}{\partial x^2}\right) \tag{2.3.4}$$

with the boundary conditions

$$i = -nFD_R\left(\frac{\partial c_O}{\partial x}\right)_0 = nFD_R\left(\frac{\partial c_R}{\partial x}\right)_0 \tag{2.3.5}$$

where i is the current density, n is the number of transferred electrons, F is Faraday's constant and R is the gas constant. To be able to solve these equations, some additional boundary conditions has to be taken into consideration [31, 32, 34].

1. The initial conditions states that

$$c_R(x,0) = c_R^* \qquad \text{For all values of x} \tag{2.3.6}$$

$$c_O(x,0) = 0 \qquad \text{For all values of x} \tag{2.3.7}$$

   where c_O is the concentration of species O, c_R is the concentration of species R c_R^* is the bulk concentration of species R. Initially, the solution is uniform and there are no oxidized species present.

2. Whether the concentration gradients reaches the cell walls or not during electrolysis can be used as a boundary condition. The cell used in LSV is normally very large compared to the diffusion layer thickness, leading to the assumption that diffusion is semi-infinite at large distances.

$$\lim_{x\to\infty} C_R(x,t) = C_R^* \qquad \text{For all values of t} \tag{2.3.8}$$

$$\lim_{x\to\infty} C_O(x,t) = 0 \qquad \text{For all values of t} \tag{2.3.9}$$

3. Electrode surface concentrations depends on the electrode potential.

$$\frac{C_O(0,t)}{C_R(0,t)} = f(E) \tag{2.3.10}$$

   For fast kinetics, the Nernst equation holds, and is applicable to the boundary conditions.

$$E = E_t + \nu t = E^0 + \frac{RT}{nF}\ln\left(\frac{c_O^s}{c_R^s}\right) \tag{2.3.11}$$

$$\frac{c_O^s}{c_R^s} = exp\left[\frac{nF}{RT}(E_i - \nu t - E_{rev})\right] \tag{2.3.12}$$

where T is temperature, ν is the voltage sweep rate, t is the time and E_{rev} is the reversible potential.

2.3.2 Cyclic Voltammetry (CV)

If the current from the LSV is reversed back to E_0 after reaching an upper potential, it is called cyclic voltammetry. All the equations and boundary conditions stated for LSV in the previous section holds for CV. The currents in the cell are positive going or negative going, corresponding to anodic or cathodic currents, respectively. It is used for investigating reactions and their mechanisms occuring close to the electrode surface [31, 35]. A potential is swept between a lower potential limit (E_l) to an upper potential limit (E_u), and it can be swept back and forth for as many cycles as desired. The generated current will stabilize after a certain amount of cycles, which is can be observed when the two last cycles displays the same current [35].

A one-electron oxidation and reduction reaction takes place during the conducted voltammetry

$$R(soln) \rightleftharpoons e^- + O(soln) \tag{2.3.13}$$

where R represents a reduced species and O represents an oxidized species [31]. During oxidation, the reaction will move from left to right. Conversely, the reaction moves from right to left during reduction. The potential in the one-electron transfer CV is described by

$$E(t) = E_{rev} \mp |-\nu t \pm (E_{rev} - E_0)| \tag{2.3.14}$$

where E_{rev} is the potential at which the scan is reversed and the || is the absolute value of its con-

tent. The equation represents the potential program in oxidative and reductive CV, respectively[31].

The forward peak in oxidative CV occurs as a result of increasing current. The increase in current travels hand in hand with increasing potential, as this leads to a higher rate of the oxidation: R → O. As time passes, the availability of R will become low and the current starts decreasing again. O will be in excess, and as the potential is reversed, O will slowly start to reduce: R ← O. A negative backward peak will occur as the reduction rate increases and the availability of O decreases [31, 34].

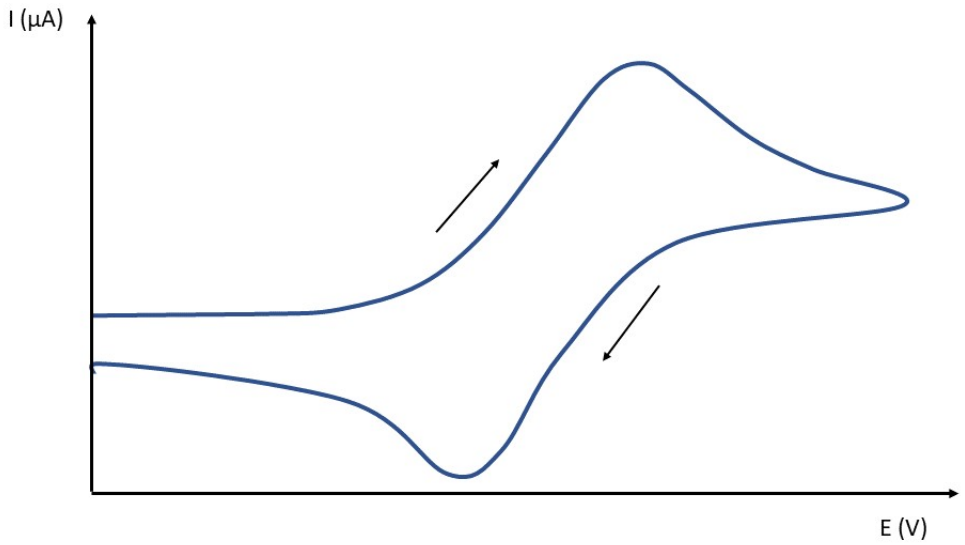

Figure 2.3.1: A schematic representation of CV. Re-sketched from [31]

2.3.3 Electrochemical Impedance Spectroscopy (EIS)

EIS is an electrochemical tool used to investigate electrical properties of conducting electrodes by measuring the resistance of the electric current flow between two electrodes in an electrochemical cell after applying a potential to it [36, 37]. The current flow is the result of a red.ox reaction occurring close to the surface of the electrode, leading to a charge transfer. The kinetics of this charge transfer is dependent on the mass transfer, which is a measure of consumption and production of reactants in the reaction[38].

The measured impedance spectra can be divided into two sub-sections: The high-frequency range (>100 Hz) and the low-frequency range (<0.01 Hz). Generally, charge transport in the cat-

alytic layer is dominating in the high-frequency region while mass transport in the gas diffusion layer, the membrane, and the catalyst layer are dominating in the low-frequency region. The mass transport is in general dependent on the overpotential and its steady-state value present in the electrochemical cell as EIS is conducted. Low overpotentials yields low mass transport resistance, making charge transfer in the catalyst layer the most important contributor to the impedance measurements. As the overpotential rises, contributors like water, gas, and proton transport will affect the impedance. However, at high overpotentials the most dominant contributor to the impedance is the gas diffusion taking place in the catalyst layer. Using air as an oxidant will elevate this contribution further [39].

The processes at the electrode surface start oscillating after applying an ac potential. The response signal of this oscillation can be analyzed as a sum of sinusoidal functions [36]. A pseudo-linear response is achieved by using small excitation signals. A phase shift in the current occurs in response to a sinusoidal potential in pseudo-linear systems, which can be viewed in figure 2.3.2.

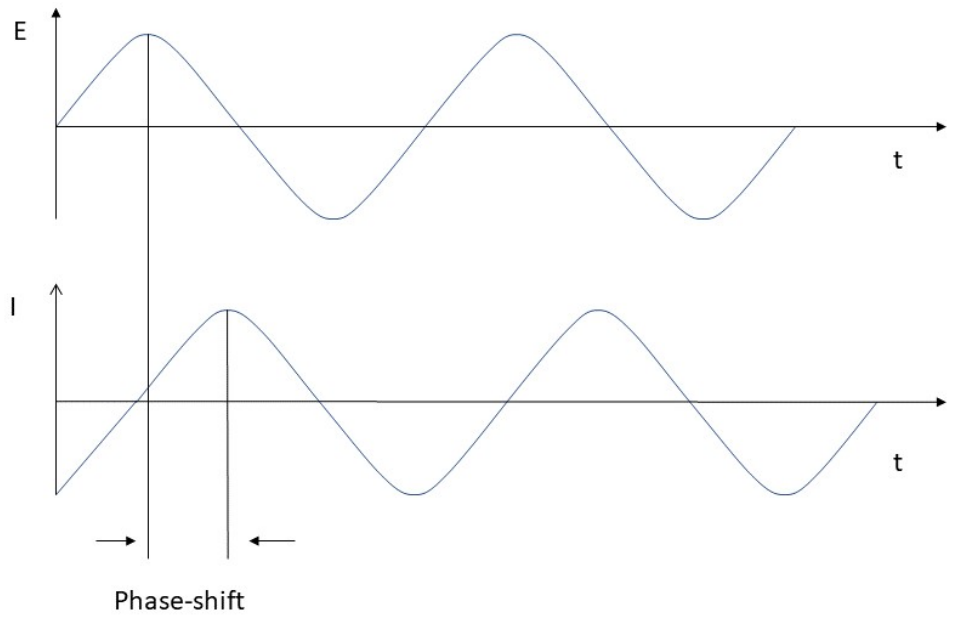

Figure 2.3.2: Sinusiodal current respons in a linear system. Potential vs time and current vs time. A phase shift in the current is observed. From [36]

The excitation signal is described by

$$E(\omega, t) = E_0 sin(\omega t) \tag{2.3.15}$$

where $E_{\omega,t}$ is the potential for the excitation signal at a given frequency and time, E_0 is the potential amplitude of the signal, and ω is the radial frequency [rad/sec] [36, 37]. The expression for radial frequency is

$$\omega = 2\pi f \tag{2.3.16}$$

where f is frequency [Hz]. Further, the response signal in a linear (or pseudo linear) system is described by

$$I(\omega, t) = I_0 sin(\omega t + \phi) \tag{2.3.17}$$

where $I_{\omega,t}$ is the response current with respect to phase shift and time, I_0 is the amplitude of the signal, and ϕ represents a phase shift. This implies that the response current has a different amplitude than I_0 [36, 37].

Impedance is defined as the relationship between voltage and current, and by combining the expressions Eq. 2.3.15 and Eq. 2.3.17, impedance can be expressed by ohm's law as

$$Z(\omega, t) = \frac{E(\omega, t)}{I(\omega, t)} = \frac{E_0 sin(\omega t)}{I_0 sin(\omega t + \phi)} = Z_0 \frac{sin(\omega t)}{sin(\omega t + \phi)} \tag{2.3.18}$$

[36]

where $Z_{\omega,t}$ is the impedance with respect to frequency and time and Z_0 is the frequency amplitude. Because of the phase angle that is incorporated in the impedance measurements, complex algebra is often used to get a proper representation of the impedance [31]. The voltage and cur-

rent can be expressed as

$$E(\omega, t) = E_0 e^{i\omega t} \tag{2.3.19}$$

$$I(\omega, t) = I_0 e^{i(\omega t - \phi)} \tag{2.3.20}$$

where i is an imaginary number. Now, equation 2.3.18 is rewritten to

$$Z(\omega, t) = \frac{E(\omega, t)}{I(omega, t)} = \frac{E_0}{I_0} e^{i\phi} = |Z(\omega)| e^{i\phi} \tag{2.3.21}$$

where $|Z_\omega|$ is the impedance modulus. The imaginary part of equation 2.3.21 can be modified using Euler's formula, which states that

$$e^{ix} = cos(x) + isin(x) \tag{2.3.22}$$

yielding

$$Z(\omega, t) = |Z(\omega)|(cos(\phi) + isin(\phi)) == Z'(\omega) + iZ''(\omega) \tag{2.3.23}$$

where Z'(ω) corresponds to the real part $|Z(\omega)|cos(\phi)$ and Z"(ω) corresponds to the imaginary part $|Z(\omega)|sin(\phi)$ [40].

Impedance data is mainly represented in a Bode plot or a Nyquist plot. The Nyquist plot presents the imaginary plane, where Z" is displayed as a function of Z'. However, it has a major drawback compared to the Bode plot, as it is not possible to tell the frequency of each point in the Nyquist plot. In a Bode plot, the frequency is plotted against both phase and magnitude, making it an explicit value[36, 40].

Conducting EIS measurements and achieving good results is not always easy, and can also be very time consuming. There are several factors that may affect and cause problems for the measurements. For instance, the system must be in a steady state at all times during the experiments. Solution resistance, current distribution, electrical double layers, polarization, charge transfer resistance, and diffusion are some phenomena that may occur in the electrochemical

cell and affect the measurements, and therefore must be considered when analyzing the resulting spectra[36].

Nowadays, a three-electrode potentiostat is the most common instrument used in EIS measurements. This type of potentiostat will make compensations for solution resistance that occurs between the reference and counter electrode, lowering its influence on the impedance. However, solution resistance must always be considered during analysis as could be a significant factor. Calculating an exact solution resistance has proven to be difficult, as the current distribution across a chosen electrolyte area in the electrochemical cell is rarely uniform. There will always exist an electrical double layer at the interface between an electrode and electrolyte. This phenomenon occurs as ions in the electrolyte adsorb at the electrode surface due to separation of the charged electrode and ions. It is normal to assume that the contribution from the double layer capacitance is between 20 and 60 μF for every 1 cm^2 electrode surface area[36]. The double layer capacitance is affected by temperature, electrode potential, type of ions, ionic concentration, oxide layers, impurities etc. Polarization occurs whenever the electrode potential is forced away from its original value at open circuit, leading to current flowing through electrochemical reactions that takes place on the electrode surface. The current is regulated by the kinetics of the reaction, as well as diffusion of reactants[36].

In practice, steady-state conditions can be difficult to achieve. The cell can change through adsorption of solution impurities, growth of an oxide layer, build up of reaction products in solution, coating degradation, or temperature changes, etc.

2.4 Material selection

Finding catalysts with properties that provides efficient kinetics for HOR/HER in AFC is not an easy task. The catalyst must have a good catalytic activity, provide a low overpotential for the HOR, have high stability and a low cost [41]. The main difficulties regarding the catalysts used in FCs today are the full utilization of active surface and efficient charge transfer [20]. Some research has been conducted on hydrogen binding energy, where it was found that catalysts with moderate HBE between adsorbed species and the electrode surface promotes HOR, and

that HBE decreases with decreasing pH [19]. However, not enough research has been conducted to prove this theory.

2.4.1 Platinum

Platinum is a precious transition metal with excellent catalytic and electrocatalytic properties, by forming alloys with other metals with desired properties. Magnetic properties also could be achieved by alloying the Pt [42]. It is a popular catalyst in fuel cells due to its electrocatalytic activity and high stability for the oxidation of H_2(g) and small organic molecules. Due to its high exchange current density and small Tafel slope, it is also one of the most popular catalysts for HER [43].

However, Pt is a very expensive material due to its limited reserve on earth. Due to the slow kinetics in alkaline media which leads to high consumption, Pt is being replaced by PGM-free catalysts [1].

2.4.2 Nickel

Ni is a d-block metal that exists with valences +2 and +3. It has many excellent properties in the field of magnetism, catalysis and hydrogen storage applications [17, 44]. It is chemically stable with a generally high activity, making Ni and Ni-based compounds among the best catalysts in water electrolysis for fuel cells and electrolyzers, using alkaline electrolytes. However, their high overpotentials and large Tafel slopes limits their performance [29, 45]. Compared to Pt-group metals, Ni as a catalyst is still preferred due to its low costs and large reservoir [6]. Unfortunately, Ni is easily oxidized when exposed to air already at ambient conditions which could result in formation of a thick oxide film consisting of NiO and $Ni(OH)_2$ [46, 47].

Transition metal oxides and hydroxides on nanoscale have a wide range of applications as passive electronic components, ceramic materials and catalysts [48]. Nanoparticles have new properties that are entirely different from their bulk counterparts. $Ni(OH)_2$ is widely used as an active material in portable electronics, positive electrodes, power tools etc. $Ni(OH)_2$ has an extensive

set of applications and is considered to be one of the most essential materials in its category. $Ni(OH)_2$ is formed when bulk nickel is exposed to a basic aqueous solution such as KOH. The hydroxide exists in two polymorphs, α-$Ni(OH)_2$ and β-$Ni(OH)_2$. β-$Ni(OH)_2$ is an oxidized state of α-$Ni(OH)_2$. This oxidation is an irreversible reaction. α-$Ni(OH)_2$ exists in the potential range 0 V $\leq$ E $\leq$ 0.5 V with respect to the reversible hydrogen electrode (RHE), while β-$Ni(OH)_2$ is formed as the potential moves beyond 0.5 V [49].

As stated earlier, $Ni(OH)_2$ has an extensive set of applications. However, it is dependent on morphology, structural characteristics and size. The two polymorphs of $Ni(OH)_2$ have different properties, and it is found that the electrochemical properties of α-$Ni(OH)_2$ is significantly better compared to β-$Ni(OH)_2$. γ-NiOOH is the product of α-$Ni(OH)_2$ oxidation, and is produced at a lower potential compared to the corresponding oxidation to β-$Ni(OH)_2$. Another advantage of the α-$Ni(OH)_2$ is the discharge capacity, which is higher compared to β-$Ni(OH)_2$. When α-$Ni(OH)_2$ is stabilized the charge capacity is much higher compared to β-$Ni(OH)_2$, and it can be reversibly converted into γ-NiOOH without any complications. However, α-$Ni(OH)_2$ is not stable when exposed in highly basic media and will be oxidized into β-$Ni(OH)_2$ [50].

2.5 Matlab

Matlab is a great tool when it comes to solving equations, plotting, simulate models, testing, and solving optimization problems etc. By using the global optimization tool box and the algorithm "Simulated Annealing", bound-constrained and unconstrained optimization problems can be solved. The simulated annealing algorithm is a model for heating of a material, followed by slowly lowering the temperature to remove and decrease defects within the structure, minimizing the total energy of the system. The simulated annealing algorithm uses iterations to solve the problem. For each iteration, a new point is generated randomly. The distance between the newly generated point and the old one is based on a probability distribution which is proportional to the temperature of the material. The main goal of the algorithm is to approach an ideal set of parameters, giving the best fit possible for the initial set of parameters. The best fit is achieved as the generated points decreases in value. This is referred to as "lowering the

objective". Some of the randomly generated points will end up in local minimas. Normally, algorithms gets stuck when they end up in the local minima. This is what distinguishes simulated annealing from other algorithms. Simulated annealing accepts points that raises the objective as well, allowing the simulation to proceed and explore other options after being trapped in a local minima. The probability of acceptance is defines as

$$P = \frac{1}{1 + exp\left(\frac{\Delta}{max(T)}\right)} \tag{2.5.1}$$

where T is the current temperature and Δ is the new objective - the old objective.

The temperature is systematically decreased while the algorithm is running. This reduces the extent of the algorithms search to converge to a minimum. The chances of finding an optimal solution gets higher when decreasing the temperature more slowly. However, this will also be more time consuming . In other words: temperature affects both the distance from an old point to a new one and the probability of accepting a new point which elevates the objective[51, 52, 53].

Chapter 3

Experimental

Experimental measurements were carried out in a three electrode cell using an Iviumn stat as the potentiostat that is a multichannel electrochemical analyser. A teflon cell was used as the electrochemical cell, and a rotating disk electrode (RDE) from Pine Research Instrumentation. Three different electrochemical methods were applied to characterize bulk nickel properties: LSV, CV, and EIS. The measurements were conducted in both 0.1 M KOH and 1 M KOH electrolyte. The electrochemical cell had the same setup for all the experiments except for when the working electrode (WE) was changed from polycrystalline platinum to bulk-nickel. Hg/HgO was used as reference electrode (RE) and Pt foil as counter electrode (CE). All experiments were performed at room temperature ($22^{\circ}C \pm 1.5^{\circ}C$) and all measurements were conducted with respect to RHE. The Hg/HgO electrode was calibrated prior to every experiment. The calibration was conducted by sparging the electrolyte for 30 min with H_2. Then, the cell was assembled with Pt-wire as working electrode, Pt foil as counter electrode and the Hg/HgO electrode as reference electrode. A forward LSV scan was conducted, and the potential at which the curve crossed 0 A was set to be the reference potential.

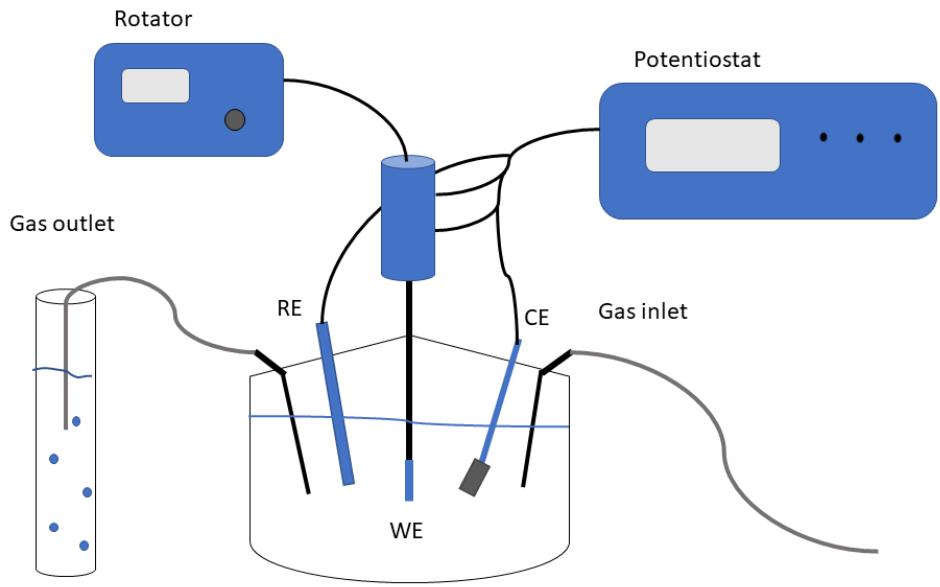

Figure 3.0.1: A schematic representation of the three electrode system used for the electrochemical studies.

The electrodes were polished with an alumina suspension to make sure that there was no contamination on the electrode surface. The Pt electrode was polished with an alumina (Al_2O_3) suspension with particle size 0.05 μm, while the Ni electrode was first polished with a suspension of particle size 0.3 μm, followed by particle size 0.05 μm. The polishing motion was in figure eights to achieve a more uniformly polished surface. The electrode was rinsed with de-ionized water before the electrochemical cell was assembled and connected to the IVIUM potentiostat. The electrode surface of Ni(poly) was protected with a droplet of de-ionized water and a cap to make sure that it was not exposed to air, preventing formation of oxide layers at the electrode surface.

3.1 Preparation of 1M KOH

1M KOH was prepared by using KOH pellets of 85% purity. The molar mass of KOH is 56.11 g/mol. To make 500 mL 1 M KOH, 33.01 g KOH pellets were added to a clean polypropylene beaker with de-ionized water. The pellets were dissolved, and the de-ionized water was gradu-

ally added until the solution reached 500 mL.

$$\frac{56.11 g mol^{-1}}{2 \cdot 0.85} = 33.01 g mol^{-1} \tag{3.1.1}$$

3.2 Electrochemical impedance spectroscopy of Pt and Ni electrode

After calibrating the electrode, the impedance measurements were conducted. The electrolyte had to be re-sparged for 40 min with Ar-gas when impedance measurements were conducted in Ar atmosphere. The electrode was immersed in the cell. The starting frequency was set to 1 MHz and the ending frequency was set to 0.1 Hz. Impedance was measured at the potentials -40 mV, -20 mV, 0 mV, 10 mV, 20 mV, 30 mV, 40 mV, 50 mV, 60 mV, 70 mV, 80 mV, 90 mV and 100 mV with rotation rate 1600 rpm and without rotation. The potential was then held at a constant while the impedance was measured at different rotation rates. The measurements were conducted at 0 mV, 5 mV, 10 mV and 15 mV, each with rotations 0 rpm, 400 rpm, 800 rpm, 1200 rpm, 1600 rpm, 2000 rpm, 2400 rpm. These measurements were conducted for both Pt and Ni electrode in both Ar and H_2 atmosphere, first in 0.1 M KOH, then repeated in 1.0 M KOH.

3.3 Cyclic Voltammetry

The reference electrode was caliberated by purging the electrolyte with H_2 for 30 min. After the caliberation, the electrolyte was re-sparged with Ar gas for 40 min before the background CV's were measured. Thereafter CV's with H_2 were conducted by purging the solution for 40 min with the H2 gas.

To have an extensive set of measurements in 0.1M KOH, some extra experiments had to be conducted. These are listed below. The same procedure as explained in the next sections were used here.

- CV on Pt in H_2(g) saturated atmosphere in the potential range from 0.0 V to 1.2 V with scan rate ν = 100 mVs^{-1}, 50mVs^{-1}, and 20mVs^{-1}, with and without rotation 1600 rpm
- CV on Ni in H_2(g) saturated atmosphere, from E_l = -0.2 V to E_u = 0.3 V, 0.4, 0.5 V. Scan rate ν = 100 mVs^{-1}, 20 mVs^{-1}, and 1 mVs^{-1}, with and without rotation 1600 rpm
- CV on Ni in Ar (g) saturated atmosphere, from E_l = -0.2 V to E_u = 0.3 V, 0.4 V, 0.5V. Scan rate ν = 100 mVs^{-1}, 20 mVs^{-1}, and 1mVs^{-1}, with rotation 1600 rpm.

Platinum electrode

CV's were conducted on a Pt electrode in the potential range of 0V to 1.2 V vs RHE with different scan rates. The effect of rotation has also been studied by doing the measurments with and without rotation . A constant rotation speed of 1600 rpm is kept for all the measurments.

Nickel electrode

CV's were conducted on a bulk-Ni electrode in the potential range of E_l = -0.2 V to E_u = 0.3 V, 0.4 V, and 0.5 V, with and without rotation. A constant rotation speed of 1600 rpm is kept for all the measurments. Like the measurements conducted for the Pt, the CV's were also meassured at various scan rates set to be ν = 100 mVs^{-1}, 20 mVs^{-1}, 5 mVs^{-1}, and 1 mVs^{-1},.

Effect of hydrogen

It is important to know the effect of H_2(g) gas inside the electrochemical cell as the potential below 0 V could evolve H_2(g) gas, which can influence the HOR reaction. The effect of H_2(g) evolution and the effect of rotation on the removal of evolved H_2 was investigated. 0.1 M KOH was used as electrolyte. The reference electrode was calibrated, and CV was conducted on a bulk-Ni electrode from different starting potentials. The potential intervals were from E_l = -0.2 V, -0.15 V, -0.10 V,-0.05 V and 0 V to E_u = 0.5 V. All these measurements were conducted at 5 mVs^{-1} with and without rotation (the rotation speed was kept constant as 1600 rpm). Another set of

experiments with 1 mVs^{-1} scan rate was also carried out without rotation. All the measurements were done in both Ar and H_2 atmosphere.

Polarization

A final set of CV scans were conducted after using a pre-treatment scheme. The electrolyte used for this experiment was 0.1 M KOH. The reference electrode was calibrated, then the working electrode was polarized at -0.5 V for 1200 seconds in H_2 atmosphere to reduce traces of oxides and hydroxides. Further polarization was conducted at 0.0 V for 1800 seconds, sparged with Ar(g), to remove H_2(g) that was generated during the previous step. The electrode was rotated with the rotation speed of 1600 rpm at all times. CV's were conducted in Ar atmosphere in the potential range from E_l =0.0 V to E_u = 0.5 V, with scan rate of ν = 5 mVs^{-1} and rotation speed of 1600 rpm.

3.4 Simulation

The initial script used for simulation was provided by Professor Svein Sunde based on his first draft of the kinetic HOR model, which can be viewed in Appendix C, and MATLAB R2018a was used for its implementation. More than half of the semester was spent working on this code in collaboration with Professor Svein Sunde, and different approaches were conducted to obtain the best simulated fit of the CV curves. Expressions for the coverages were found from the rate expressions in the HOR model, equations C.1.7-C.1.11, and implemented into the code without any luck. It was found that using dimensionless parameters would simplify the calculations in MATLAB. How to find these can be viewed in the HOR model in Appendix C. There were some issues regarding time and the reverse sweep in the earlier development of the code. This was solved by using a function that finds the forward and reverse maximum sweep. It was made an attempt to solve for the rate constants numerically and then implement these in the MATLAB code, however this became very demanding mathematically. Another approach was to find irreversible approximations of the current in forward and reverse direction using expressions for dimensionless rate constants and plot this current vs potential.The "lsqcurvefit" function was

used to solve the equations in the code. This function implements two algorithms and is used to solve non-linear least square problems.

The final edition of this script used the algorithm "Simulated annealing" in stead of lsqcurvefit. Simulated annealing generates a random point and uses iterations to generate new points that lowers the objective, thus fitting the simulated curve to the experimental one. How the algorithm works can be viewed in the theory section MATLAB. Help functions were generated to convert parameters to dimensionless parameters, finding the forward and reverse sweep maximum, and implementing equations for coverage. The coverage and the reaction rates were plotted seperately. The plot of the reaction rates is essential, as it displays whether the kinetics are fast or slow in equations C.1.2-C.1.6, thus implying how to adjust the rate constants in order to achieve a better fit of the simulation. The main script runs the simulated annealing and fits the simulation to the experimental curve. Initial conditions were collected from the supplementary data in [1].

Chapter 4

Results

4.1 Electrochemical Impedance Spectroscopy

4.1.1 Platinum electrode

EIS was conducted on a poly-crystalline platinum electrode at potentials -40 mV, -20 mV, 0 mV, 10 mV, 20 mV, 30 mV, 40 mV, 50 mV, 60 mV, 70 mV, 80 mV, 90 mV, and 100 mV with rotation 1600 rpm and without rotation in both 0.1M KOH and 1M KOH, which can be viewed in figures 4.1.1 and 4.1.2. All measurements were conducted in Ar and H_2 atmosphere. The frequency range was set from 1 MHz to 0.1 Hz with an potential amplitude of 0.01 V.

An immediate observation is that the solution resistance remains the same for all impedance measurements, unaffected by factors such as rotation and atmosphere. From the figure 4.1.1, it is clear that the rotation does not affect the R_{ct} in both 0.1 as well as 1M KOH under the Ar atmosphere. But when comparing to two different electrolyte concentration, 1M KOH showed higher R_{ct}. Increasing the potential below 0 V reduces the size of the impedance arc whereas polarizing the potential above 0 V increased the size of the arc and R_{ct} increased with an increase in potential. The R_{ct} became constant after a certain potential in the case of both 0.1M and 1M KOH.

Under H_2 environment, the Pt electrode in 1M KOH did not show much change in the R_{ct} with

and without rotation. The increase in R_{ct} with an increase in voltage is noticed, and that is almost similar in every case irrespective of the rotation. But under H_2 environment, the electrode in 0.1M KOH showed a slightly different tendency compared to the same measurement done in Ar atmosphere. Here the impedance spectrum without rotation showed slightly higher R_{ct} compared to the spectrum with rotation. When compared the spectrum for the electrode in two different electrolyte concentrations with and without rotation,the resistance is high for the KOH having higher concentration . When compare the spectrum under Ar atmosphere with H_2, the electrolyte saturated with H_2 showed the higher R_{ct}.

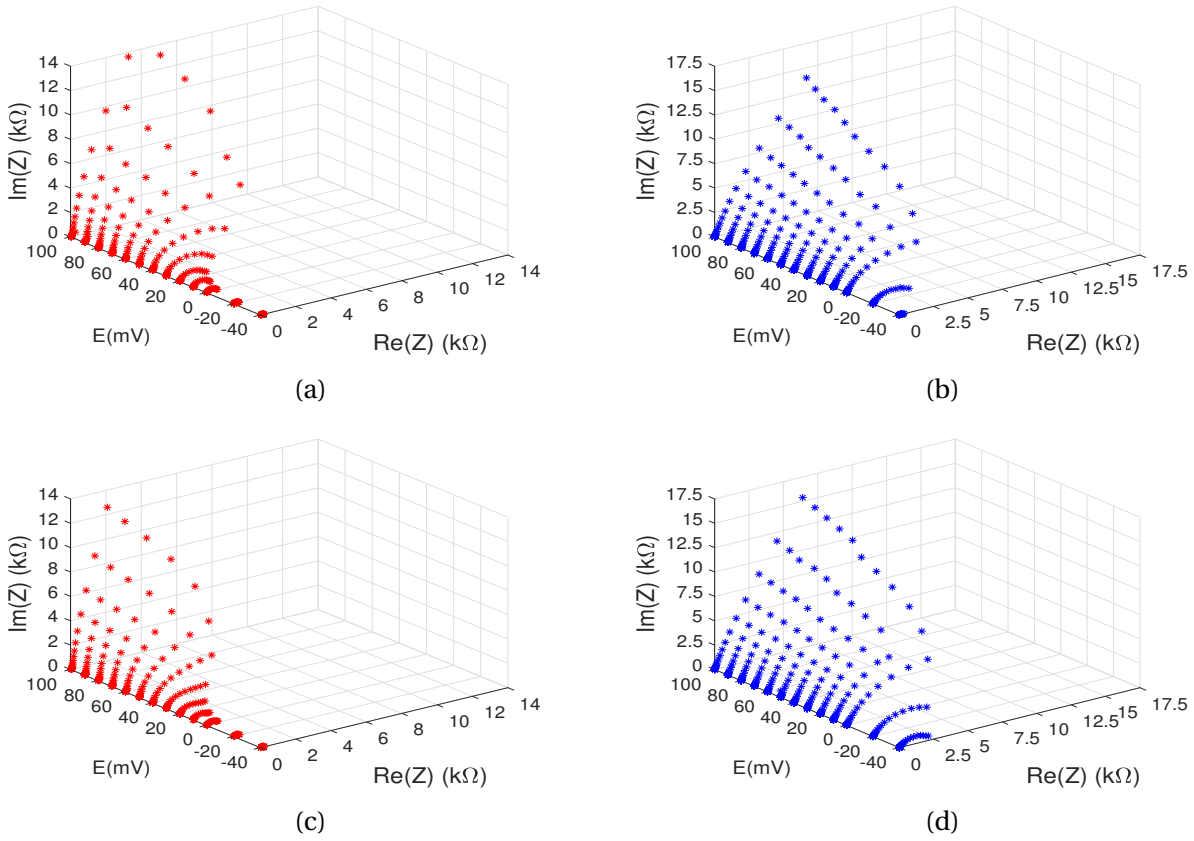

Figure 4.1.1: A comparison of EIS conducted on a Pt electrode immersed in Ar(g) saturated electrolyte at potentials -40 mV, -20 mV, 0 mV, 10 mV, 20 mV, 30 mV, 40 mV, 50 mV, 60 mV, 70 mV, 80 mV, 90 mV and 100 mV at in a) 0.1M KOH with ν = 1600 rpm b) 1M KOH with ν = 1600 rpm c) 0.1M KOH without rotation d) 1M KOH without rotation.

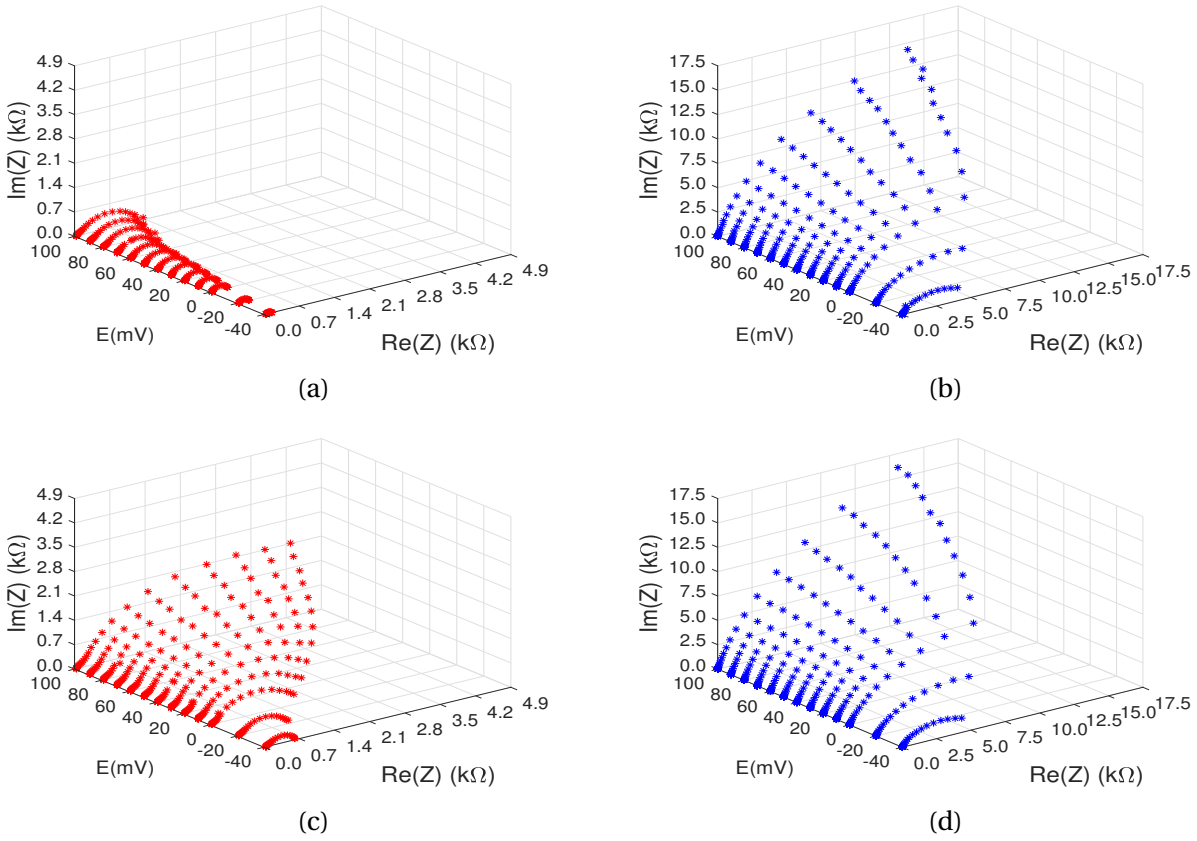

Figure 4.1.2: A comparison of EIS conducted on a Pt electrode immersed in H_2(g) saturated electrolyte at potentials -40 mV, -20 mV, 0 mV, 10 mV, 20 mV, 30 mV, 40 mV, 50 mV, 60 mV, 70 mV, 80 mV, 90 mV and 100 mV at in a) 0.1M KOH with ν = 1600 rpm b) 1M KOH with ν = 1600 rpm c) 0.1M KOH without rotation d) 1M KOH without rotation.

The increase of charge transfer resistance stagnates after reaching a set potential. These potentials are summarized in table 4.1.1 below, and are collected from the impedance measurements presented in figure 4.1.1 and 4.1.2. The charge transfer resistance stagnates at a higher potential in 0.1M KOH compared to 1M KOH.

Rotation	E(mV) 0.1M KOH	E(mV) 1M KOH	Atmosphere
1600 rpm	70 mV	20 mV	Ar
No rotation	60 mV	20 mV	Ar
1600 rpm	70 mV	10 mV	H_2
No rotation	30 mV	10 mV	H_2

Table 4.1.1: This table summarizes potentials at which the charge transfer resistance stagnates, in different environments and conditions. The potentials are collected from figure 4.1.1 and 4.1.2

The effect of rotation was further investigated by holding the potential at a constant while conducting impedance measurements at different rotation rates. The potential was set to 0.0 V, 5 mV, 10 mV, and 15 mV, and the impedance measurements were conducted in both Ar and H_2 atmosphere, immersed in 0.1M KOH and 1M KOH. Their resulting Nyquist plots can be viewed in figure 4.1.3 and 4.1.4, respectively.

The effect of rotation was also studied by polarizing the electrode in 4 different potentials above 0 V. The R_{ct} increased with increase in potential but the rotation did not have any effect on the R_{ct} . But under the reactant gas H_2, the Pt electrode showed higher resistance compared to the system saturated with Ar. The effect of rotation was more or less the same for the Pt in both 0.1 as well as 1M KOH. But when comparing the effect of concentrations, 1M KOH yields higher resistance compared to 0.1M KOH which is consistent with the previous observations.

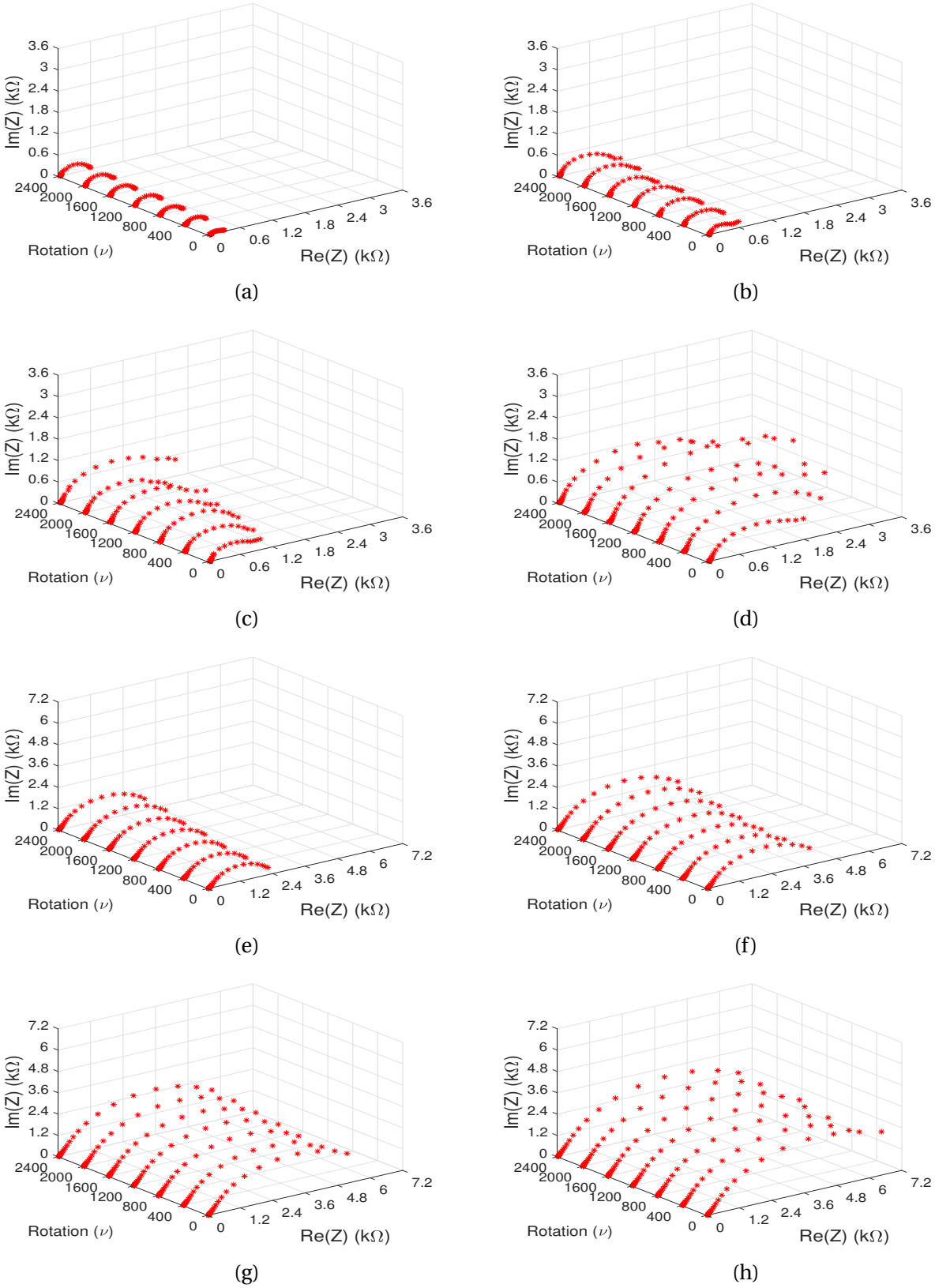

Figure 4.1.3: A comparison of EIS conducted on a Pt electrode immersed in Ar (g) saturated 0.1M KOH. Rotation speed was set to 400 rpm, 800 rpm, 1200 rpm, 1600 rpm, 2000 rpm and 2400 rpm at a constant potential a) 0 V b) 5 mV c) 10 mV d) 15 mV, and in H_2 atmosphere at constant potential e) 0 V f) 5 mV g) 10 mV h) 15 mV

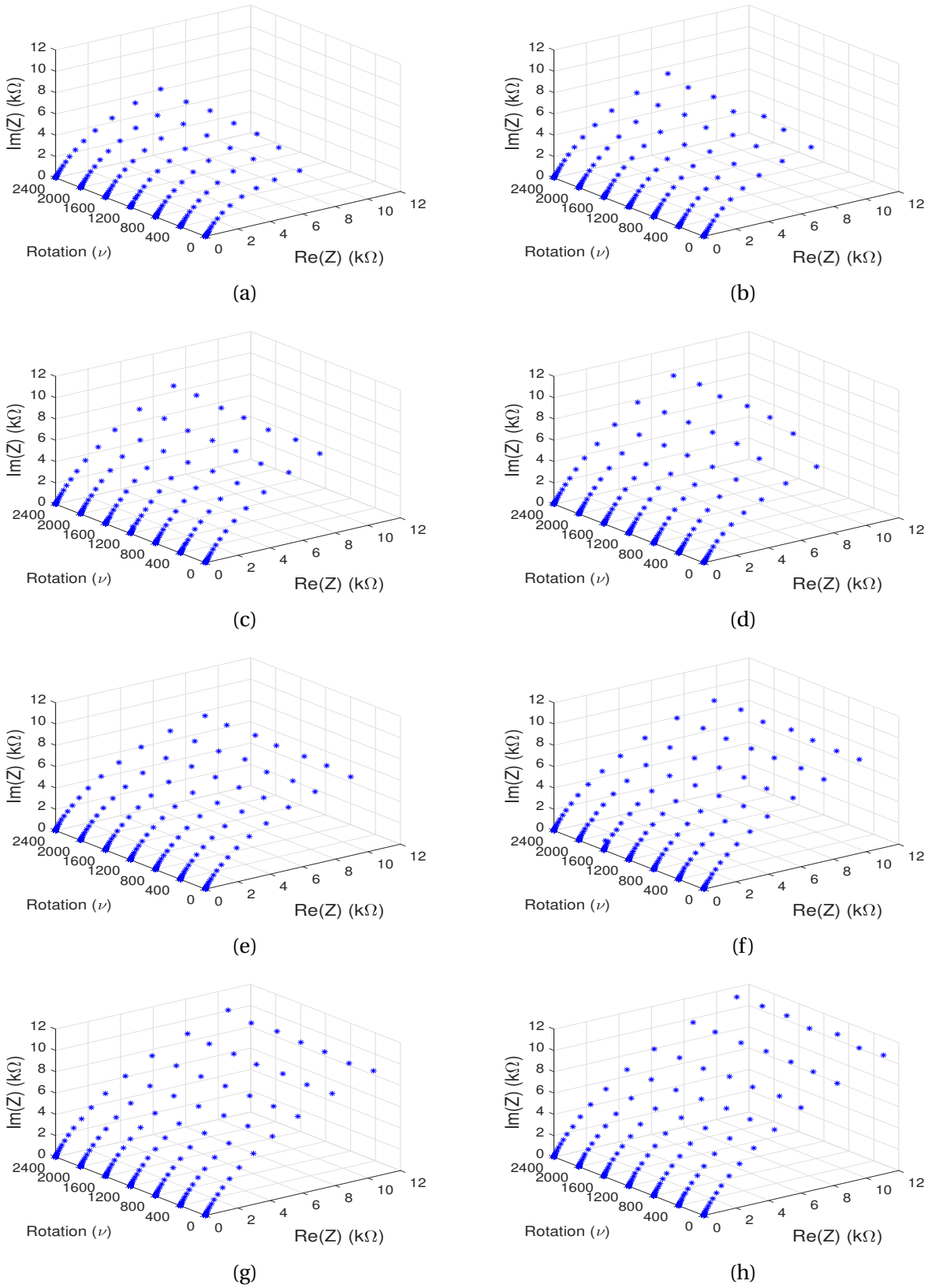

Figure 4.1.4: A comparison of EIS conducted on a Pt electrode immersed in Ar(g) saturated 1M KOH. Rotation speed was set to 400 rpm, 800 rpm, 1200 rpm, 1600 rpm, 2000 rpm and 2400 rpm in Ar atmosphere at a constant potential a) 0 V b) 5 mV c) 10 mV d) 15 mV, and in H_2 atmosphere at constant potential e) 0 V f) 5 mV g) 10 mV h) 15 mV

The more thorough investigation of rotational effect on impedance measurements conducted on poly-crystalline platinum electrode confirmed the trends observed earlier. The charge transfer resistance is higher when conducting EIS at higher potential, but remains unaffected by rotation. Hydrogen atmosphere and higher electrolyte concentration promotes charge transfer resistance.

4.1.2 Bulk-Nickel electrode

The same set of experiments described in the previous section was conducted on a bulk-nickel electrode. The solution resistance remains the same, unaffected by environment and rotation. The polarization phenomenon that was described for Pt has the same effect here; increasing the polarization below 0 V decreases the impedance arc while increasing the polarization above 0 V increases the arc.

Conversely to the R_{ct} found with Pt as catalyst, 0.1M KOH generates a higher R_{ct} compared to 1M KOH. The rotation seems to have some effect, especially at the lower potentials. These trends are consistent in both 0.1M and 1M KOH, in both Ar and hydrogen atmosphere. H_2(g) saturated electrolyte generates higher R_{ct} than Ar(g).

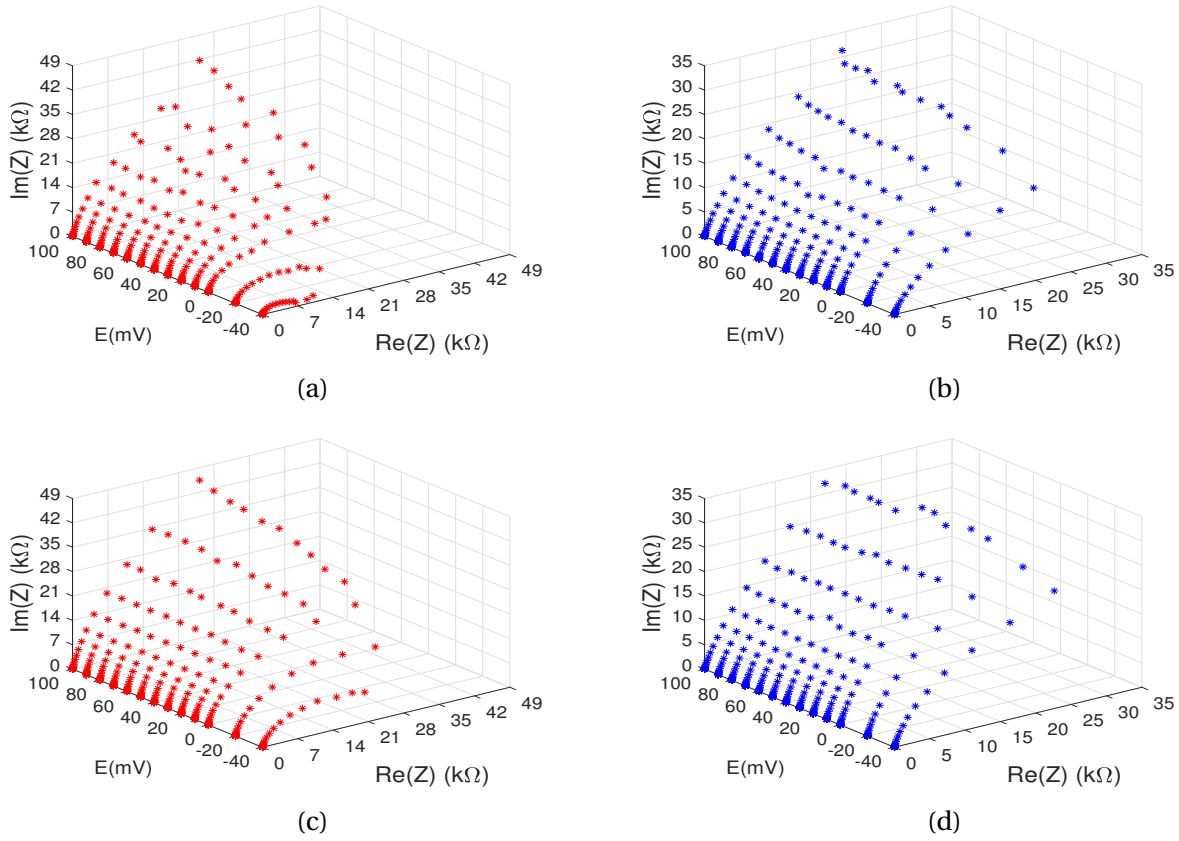

Figure 4.1.5: A comparison of EIS conducted on a Ni electrode immersed in Ar(g) saturated electrolyte at potentials -40 mV, -20 mV, 0 mV, 10 mV, 20 mV, 30 mV, 40 mV, 50 mV, 60 mV, 70 mV, 80 mV, 90 mV and 100 mV at in a) 0.1M KOH with rotation speed 1600 rpm b) 1M KOH with rotation speed 1600 rpm c) 0.1M KOH without rotation d) 1M KOH without rotation.

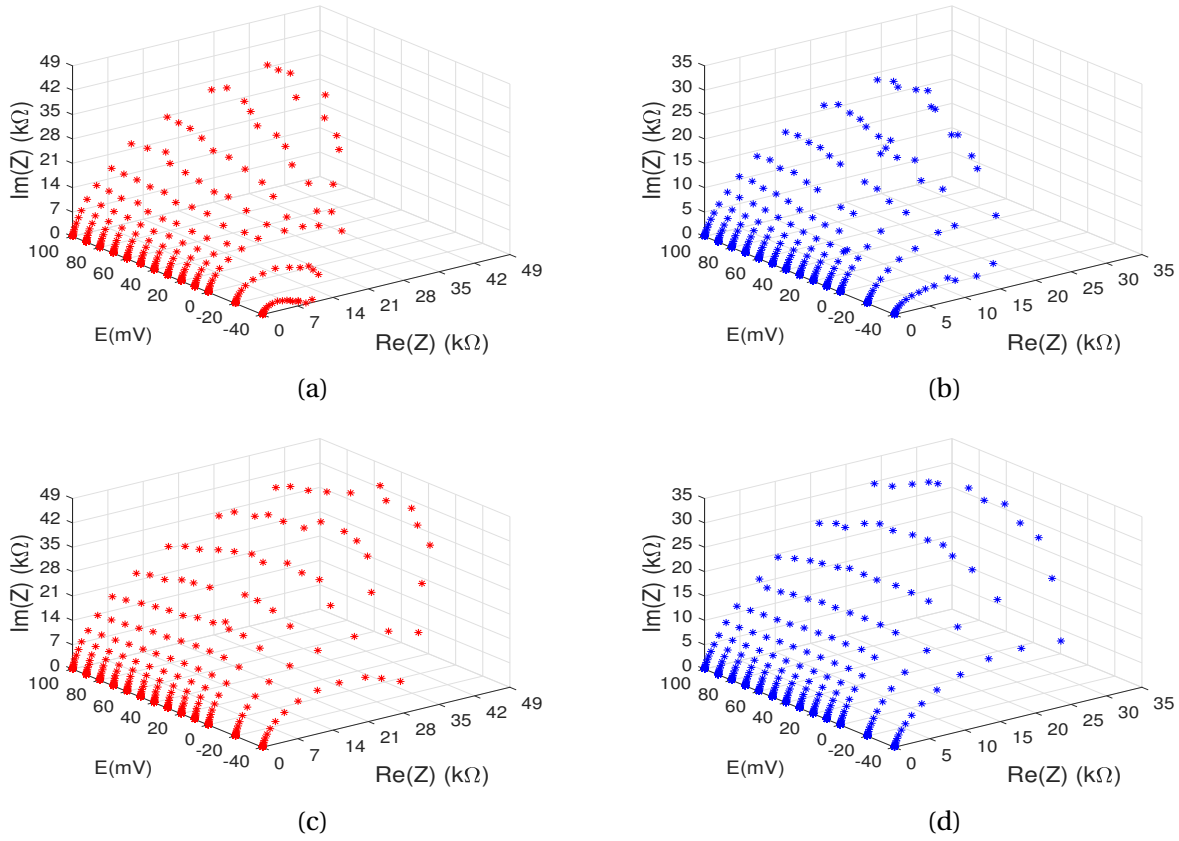

Figure 4.1.6: A comparison of EIS conducted on a Ni electrode immersed in H_2(g) saturated electrolyte at potentials -40 mV, -20 mV, 0 mV, 10 mV, 20 mV, 30 mV, 40 mV, 50 mV, 60 mV, 70 mV, 80 mV, 90 mV and 100 mV at in a) 0.1M KOH with rotation speed 1600 rpm b) 1M KOH with with rotation speed 1600 rpm c) 0.1M KOH without rotation d) 1M KOH without rotation.

A summary of approximately where the charge transfer resistance stagnates when conducting EIS on a bulk-Ni electrode can be viewed in table 4.1.2 below. The charge transfer resistance generally stagnates at higher potentials when EIS is conducted in 0.1M KOH. The R_{ct} stagnates at higher potentials when EIS is conducted in H_2(g) saturated electrolyte with rotation.

Rotation	E(mV) 0.1M KOH	E(mV) 1M KOH	Atmosphere
1600 rpm	20 mV	-20 mV	Ar
No rotation	0 mV	-20 mV	Ar
1600 rpm	30 mV	20 mV	H_2
No rotation	20 mV	0 mV	H_2

Table 4.1.2: This table summarizes potentials at which the charge transfer resistance stagnates, in different environments and conditions. The potentials are collected from figure 4.1.5 and 4.1.6

When comparing the values in table 4.1.1 and 4.1.2, it was observed that the charge transfer resistance stagnated at higher potential using a Pt catalyst. However, the charge transfer resistance is much higher when conducting EIS with Ni catalyst.

The effect of rotation was further investigated on the bulk-nickel electrode as well. Potentials 0.0 V, 5 mV, 10 mV, and 15 mV were held at a constant while the rotation was varied between 400-2400 rpm. The measurements were conducted in both Ar and H_2 atmosphere in 0.1M KOH and 1M KOH.

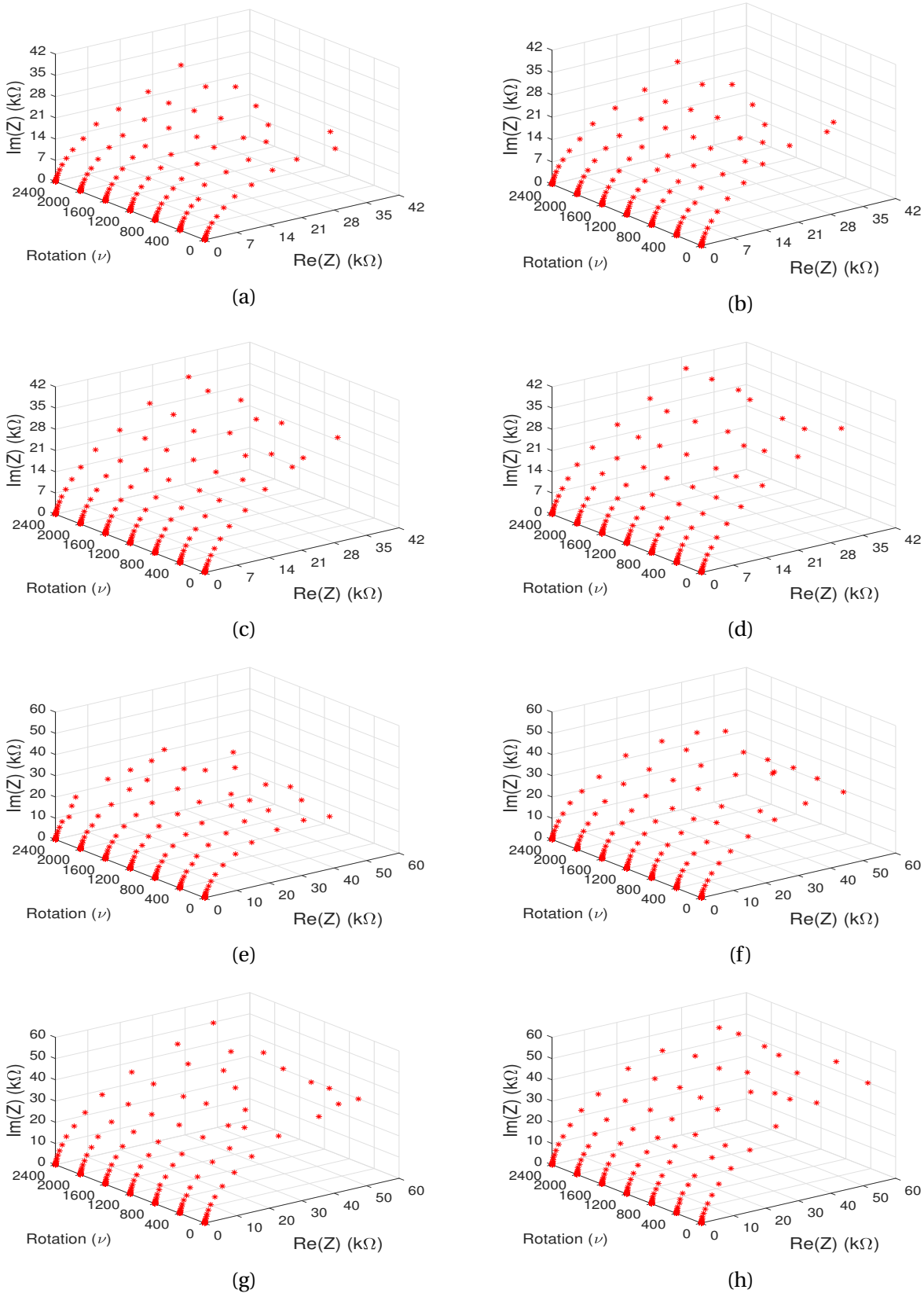

Figure 4.1.7: A comparison of EIS conducted on a Ni electrode immersed in Ar(g) saturated 0.1M KOH. Rotation speed was set to 400 rpm, 800 rpm, 1200 rpm, 1600 rpm, 2000 rpm, and 2400 rpm at constant potentials a) 0 V b) 5 mV c) 10 mV d) 15 mV, and in H_2 atmosphere at constant potential e) 0 V f) 5 mV g) 10 mV h) 15 mV

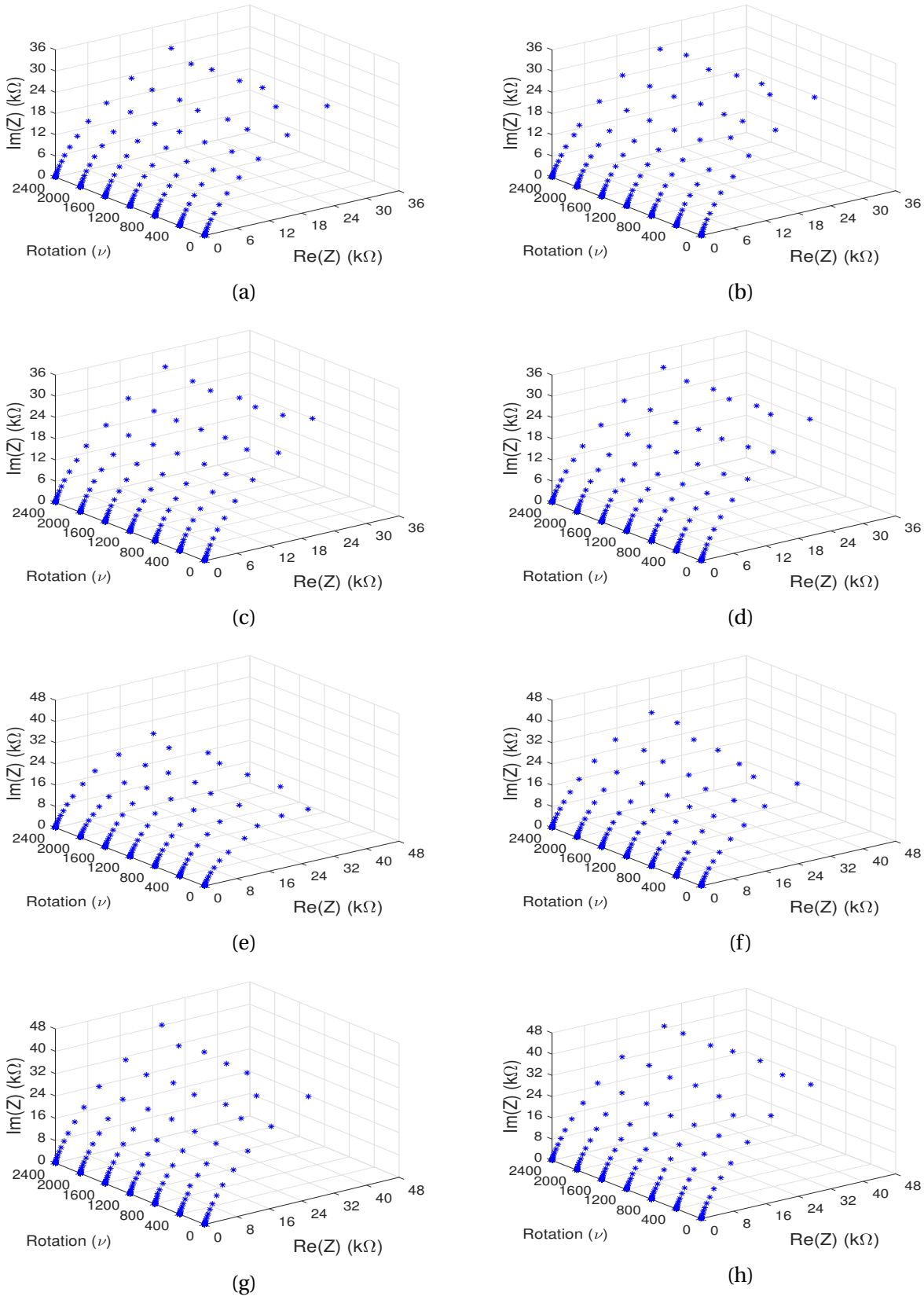

Figure 4.1.8: A comparison of EIS conducted on a Ni electrode immersed in Ar(g) saturated 1M KOH. Rotation speed was set to 400 rpm, 800 rpm, 1200 rpm, 1600 rpm, 2000 rpm, and 2400 rpm in Ar atmosphere at a constant potential a) 0 V b) 5 mV c) 10 mV d) 15 mV, and in H_2 atmosphere at constant potential e) 0 V f) 5 mV g) 10 mV h) 15 mV

The same trend concerning the effect of rotation rate at a constant potential is observed. The rotation has no effect in either Ar nor H_2 atmosphere. The charge transfer resistance remains the same for each rotation paralell.

4.2 Cyclic Voltammetry

4.2.1 Pt electrode

CV was conducted on a Pt electrode immersed in 0.1 M and 1M KOH. The CV scans were conducted in the potential range from 0.0 V to 1.2 V, first in Ar atmosphere, then repeated in H_2 atmosphere. Scan rate was set to ν = 100 mVs^{-1}, 50 mVs^{-1} and 20 mVs^{-1}, and the scans were conducted with and without rotation. Rotation speed 1600 rpm is kept constant for all the measurments with rotation. The results can be viewed in figure 4.2.1 and 4.2.2 below, for Ar and H_2 atmosphere, respectively.

The voltammograms and their behavior are as expected in figure 4.2.1. Hydrogen adsorption, followed by an electrolytic double layer, oxygen adsorption, and oxygen oxidation in forward sweep, as well as oxygen desorption, a new electrolytic double layer, hydrogen desorption, and hydrogen oxidation in backward sweep. These reactions have all been elaborated in section 4.2 in the previous study[8], from where figure 4.2.1c and 4.2.1d are collected from. However, when the platinum electrode is rotated, the first hydrogen oxidation peak in anodic direction is suppressed. When comparing the behavior in 1M KOH and 0.1M KOH in figure 4.2.1a and 4.2.1c, respectively, it is observed that the hydrogen adsorption is higher in 0.1 M KOH, thus generating a higher current in this specific area. However, when the potential moves past 0.4 V, a larger amount of oxygen adsorption occurs in 1M KOH.

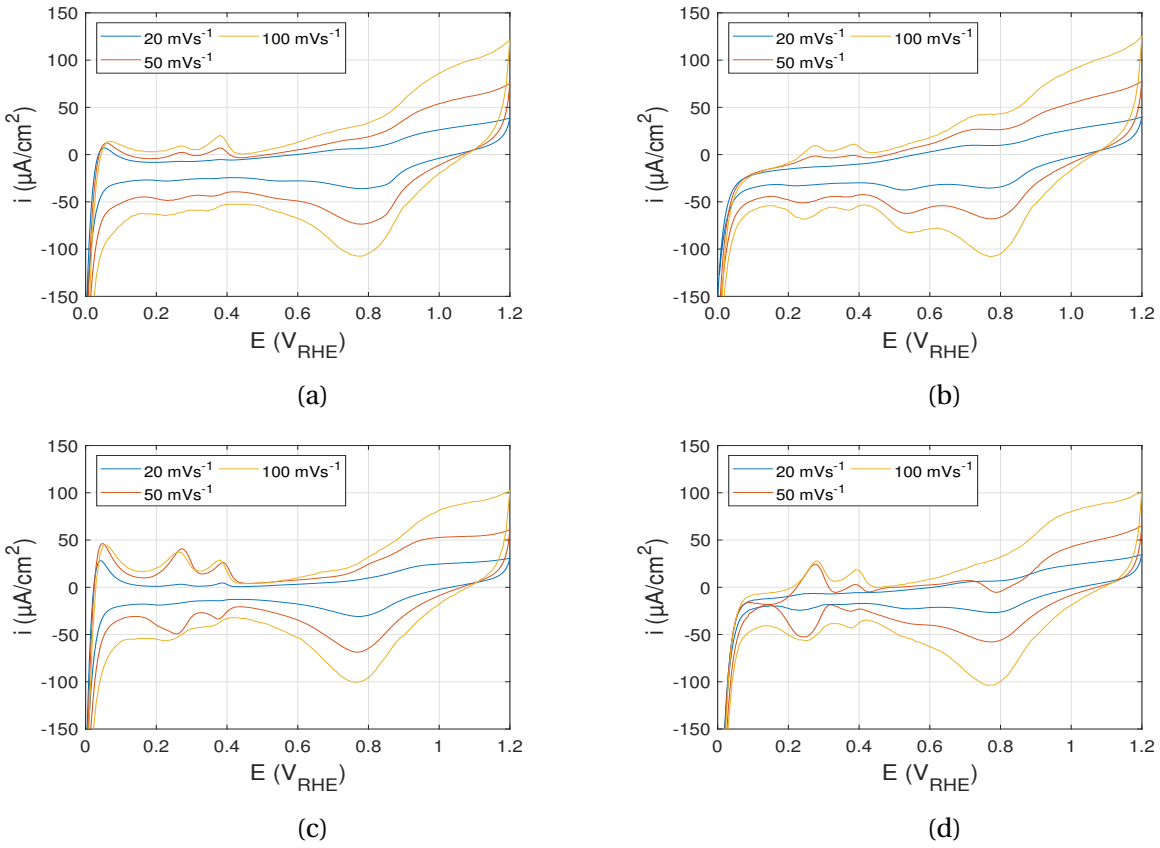

Figure 4.2.1: A comparison of CV scans conducted on a Pt electrode immersed in Ar (g) saturated electrolyte with scan rate ν = 100 mVs^{-1}, 50 mVs^{-1} and 20 mVs^{-1} a) In 1M KOH without rotation b) In 1M KOH, rotated at 1600 rpm c) In 0.1M KOH without rotation [8] d) in 0.1M KOH, rotated at 1600 rpm

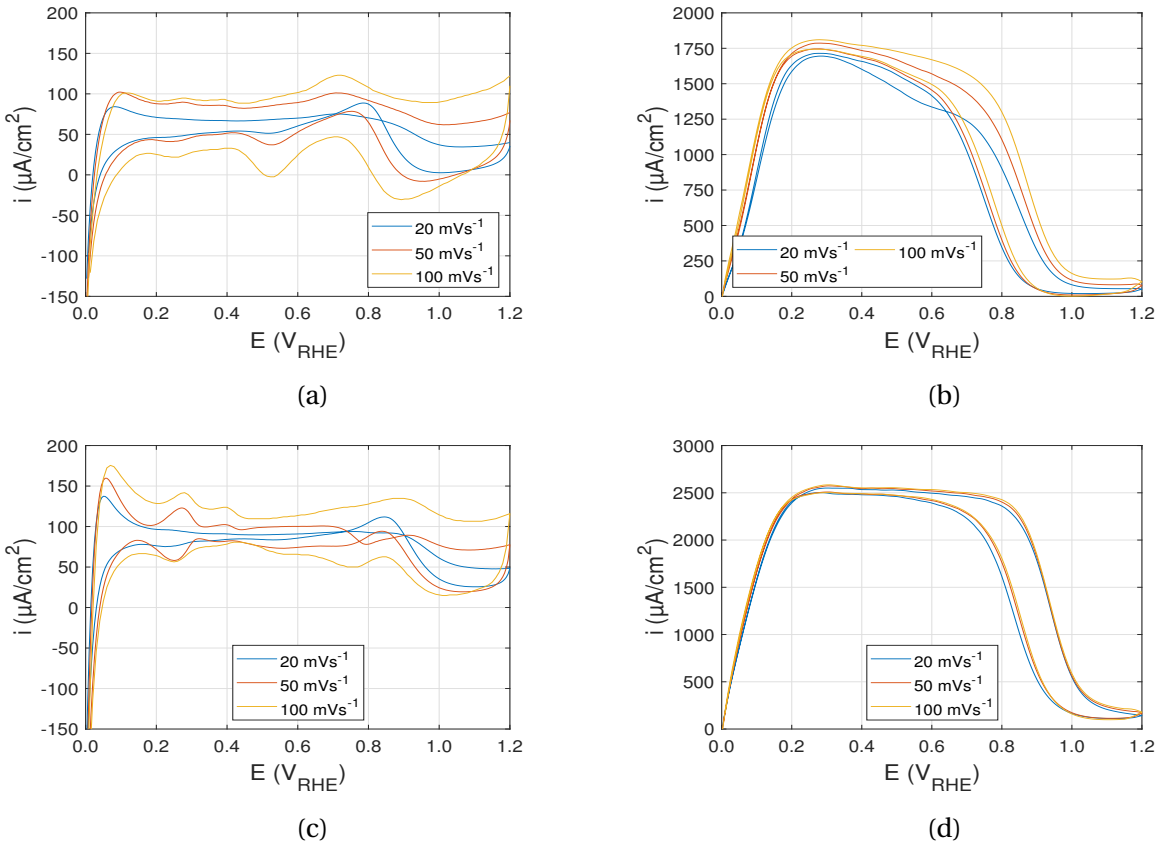

Figure 4.2.2: A comparison of CV scans conducted on a Pt electrode immersed in H_2(g) saturated electrolyte with scan rate 100 mVs^{-1}, 50 mVs^{-1} and 20 mVs^{-1} a) Without rotation, 1M KOH b) Rotation 1600 rpm, 1M KOH, c) Without rotation, 0.1M KOH d) Rotation 1600 rpm, 0.1M KOH

4.2.2 Nickel electrode

CV's were conducted on a Ni electrode immersed in 1M KOH and 0.1M KOH. The series of conducted experiments are summarized in table 4.2.1 and 4.2.2 for 1M KOH and 0.1M KOH, respectively.

Atmosphere	E_l [V]	E_u [V]	Scan rate [mVs^{-1}]	Rotation [rpm]
Ar and H_2	-0.2	0.3	100, 20, 5, 1	1600 rpm and No rotation
Ar and H_2	-0.2	0.4	100, 20, 5, 1	1600 rpm and No rotation
Ar and H_2	-0.2	0.5	100, 20, 5, 1	1600 rpm and No rotation

Table 4.2.1: A summary of all experiments conducted on Ni electrode immersed in 1M KOH

Atmosphere	E_l [V]	E_u [V]	Scan rate [mVs^{-1}]	Rotation [rpm]
Ar and H_2	-0.2	0.3	100, 20, 1	1600 rpm and No rotation
Ar and H_2	-0.2	0.4	100, 20, 1	1600 rpm and No rotation
Ar and H_2	-0.2	0.5	100, 20, 1	1600 rpm and No rotation

Table 4.2.2: A summary of all experiments conducted on Ni electrode immersed in 0.1M KOH

The E_u were chosen to observe the formation of α-$Ni(OH)_2$. At 100 mVs^{-1} a peak appeared at 0.3 V which is the formation of α-$Ni(OH)_2$, the peak started growing at 0.3 V at 100 mVs^{-1}, and after 0.4 V the current started reducing. The formed α-$Ni(OH)_2$ during the forward scan was completely reduced back during the backward scan, which agrees well with the literature saying that α-$Ni(OH)_2$ is completely reversible[5, 54]. The trend was similar when the CV's measured in 0.1M KOH, except the fact that the magnitude of α-$Ni(OH)_2$ current was higher in 0.1M KOH compared to 1M KOH. In 1M KOH the peaks were less prominent. The measurements also seem to be more accurate in 0.1M KOH, implying more disturbance in 1M KOH. It was also observed that the scan rate influences the peak position, where an increase in scan rate shifts the peak to a more positive potential. In the CV curves in both 1M and 0.1M KOH, the formation of α-$Ni(OH)_2$ started at 0.1 V, and the growth was completed at 0.3 V.

Figure 4.2.3 and 4.2.4 are a compilation of CV's conducted in 1M KOH and 0.1M KOH, respectively.

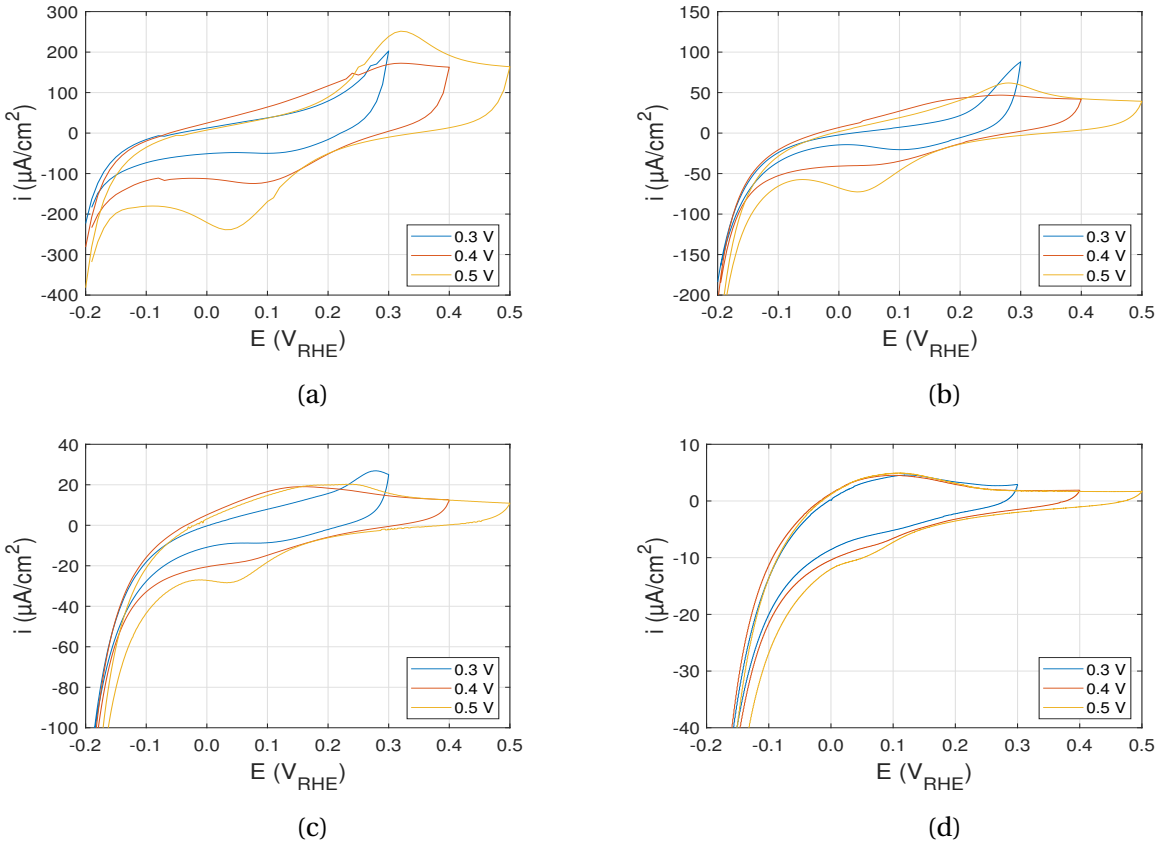

Figure 4.2.3: A comparison of CV conducted on a Ni electrode immersed in Ar saturated 1M KOH in the potential range from 0.0 V to 0.5 V. Different scan rates were used, no rotation. a) ν = 100 mVs^{-1} b) ν = 20 mVs^{-1} c) ν = 5 mVs^{-1} d) ν = 1 mVs^{-1}

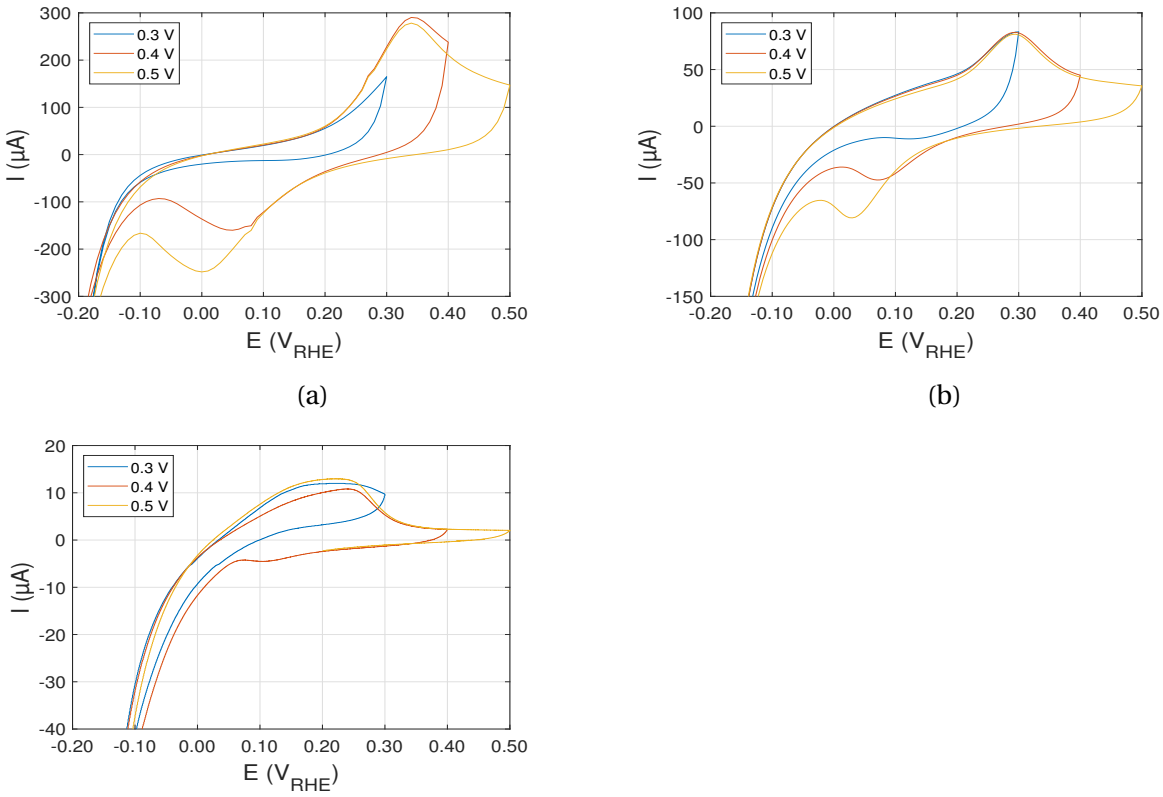

Figure 4.2.4: A comparison of CV conducted on a Ni electrode immersed in Ar saturated 0.1M KOH in the potential range from 0.0 V to 0.5 V. Different scan rates were used, no rotation. Collected from [8] a) $\nu = 100$ mVs^{-1} b) $\nu = 20$ mVs^{-1} c) $\nu = 1$ mVs^{-1}

The similar set of CV measurements were done with a rotation speed of 1600 rpm in both 0.1M KOH and 1M KOH, which can be viewed in figure 4.2.5 and 4.2.6. A very slight difference in current density is observed when comparing the CV scans of 1M KOH with and without rotation. It is slightly higher for low scan rates when the electrode is not rotated. However, the measurements conducted in 0.1M KOH are affected by the rotation. The α-Ni(OH)$_2$ peak current density is insignificant at various scan rates when the electrode was rotated in 0.1M KOH

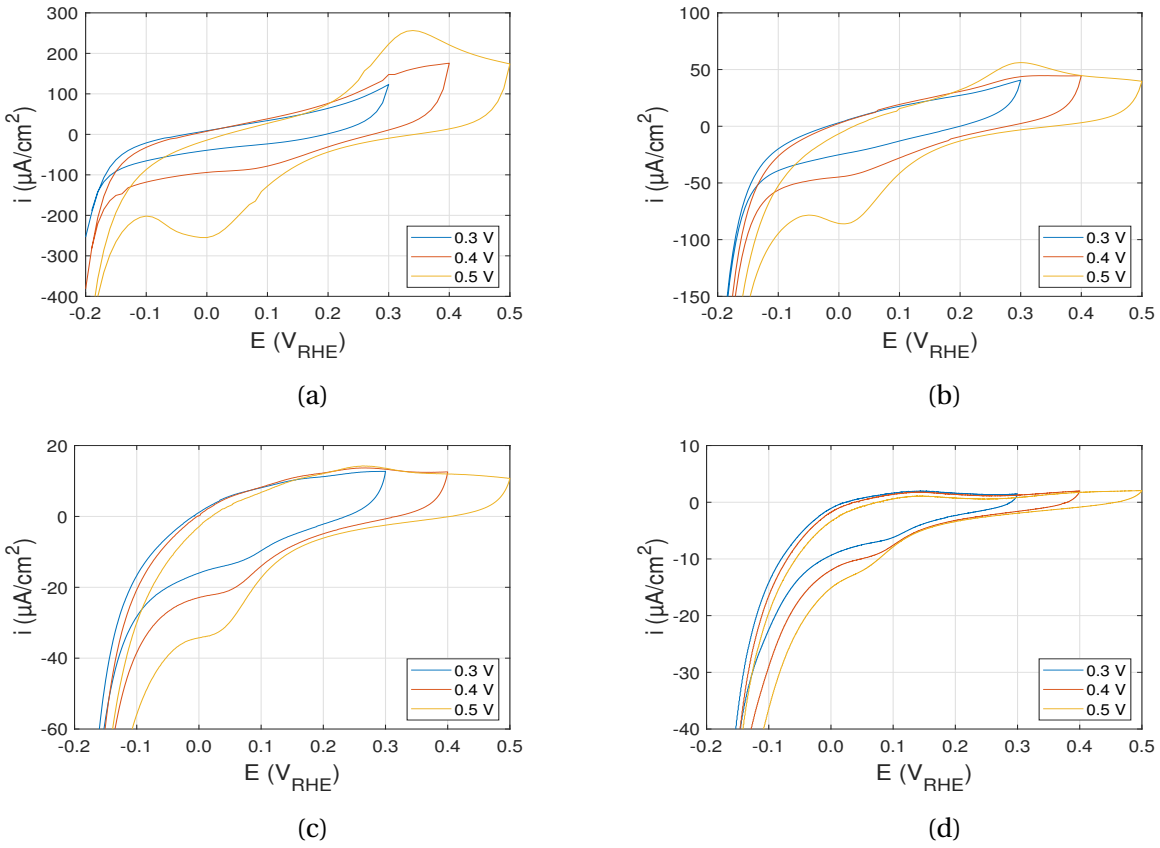

Figure 4.2.5: A comparison of CV conducted on a Ni electrode immersed in Ar saturated 1M KOH in the potential range from 0.0 V to 0.5 V. Different scan rates were used, and the electrode was rotated at 1600rpm. a) $\nu = 100$ mVs^{-1} b) $\nu = 20$ mVs^{-1} c) $\nu = 5$ mVs^{-1} d) $\nu = 1$ mVs^{-1}

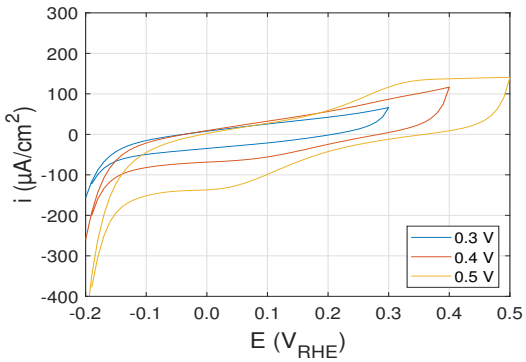

(a)

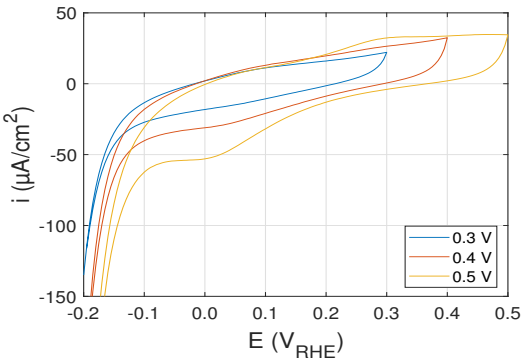

(b)

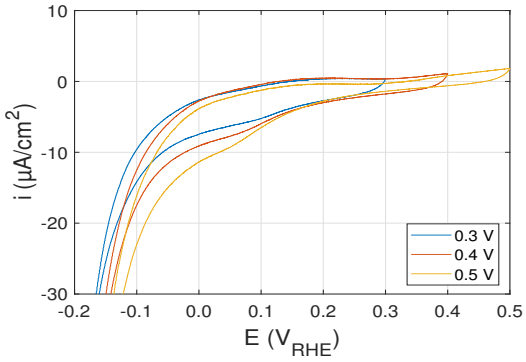

(c)

Figure 4.2.6: A comparison of CV conducted on a Ni electrode immersed in Ar saturated 1M KOH in the potential range from 0.0 V to 0.5 V. Different scan rates were used, and the electrode was rotated at 1600rpm. a) $\nu = 100$ mVs^{-1} b) $\nu = 20$ mVs^{-1} c) $\nu = 1$ mVs^{-1}

The system was saturated with H_2(g) and CV's were conducted with similar measurements, reported in figure 4.2.7 - 4.2.10. When comparing the CV's conducted in Ar with H_2 at 1M KOH, no significant improvement in current was observed without rotation. However, at lower scan rate (1 mvs^{-1}), a small increase in current due to the HOR is observed. But overall, the HOR activity in bulk Ni electrode is negligible. When the electrode is rotated at 1600, the effect was more or less the same. Not much difference in current was noticed in H_2 compared to Ar environment at higher scan rates such as 100 mvs^{-1}, 50 mvs^{-1} and 5 mvs^{-1}. But at the lowest scan rate (1 mvs^{-1}) the trend was the same as that of the curves without rotation. The HOR current is noticeable compared to the background scan with Ar, which confirms the effect of scan rate on the HOR activity.

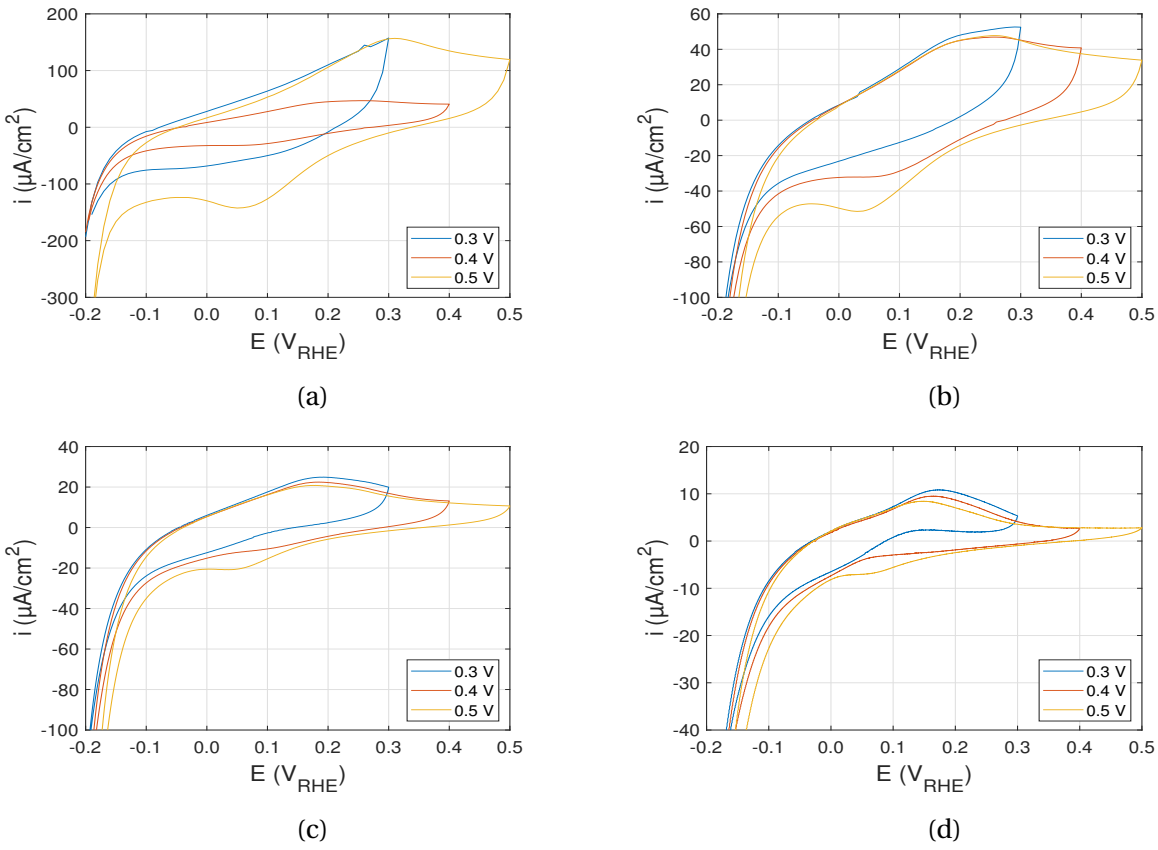

Figure 4.2.7: A comparison of CV conducted on a Ni electrode immersed in H_2 saturated 1M KOH in the potential range from 0.0 V to 0.5 V. Different scan rates were used, without rotation a) ν = 100 mVs^{-1} b) ν = 20 mVs^{-1} c) ν = 5 mVs^{-1} d) ν = 1 mVs^{-1}

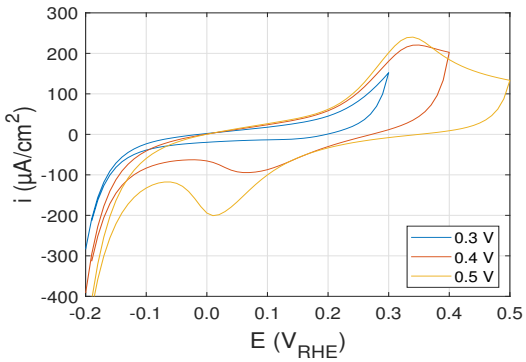

(a)

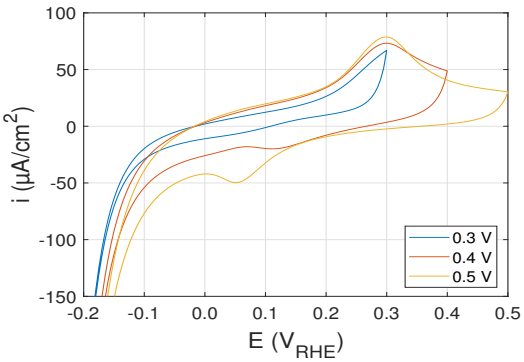

(b)

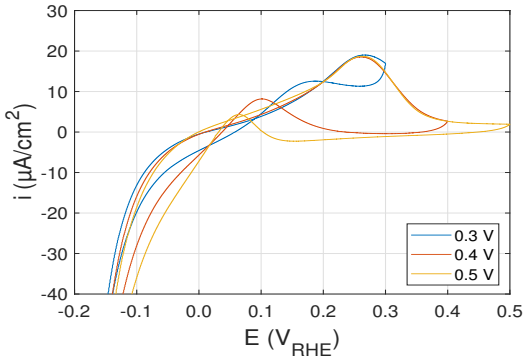

(c)

Figure 4.2.8: A comparison of CV conducted on a Ni electrode immersed in H_2 saturated 0.1M KOH in the potential range from 0.0 V to 0.5 V. Different scan rates were used, without rotation. a) $\nu = 100$ mVs^{-1} b) $\nu = 20$ mVs^{-1} c) $\nu = 1$ mVs^{-1}

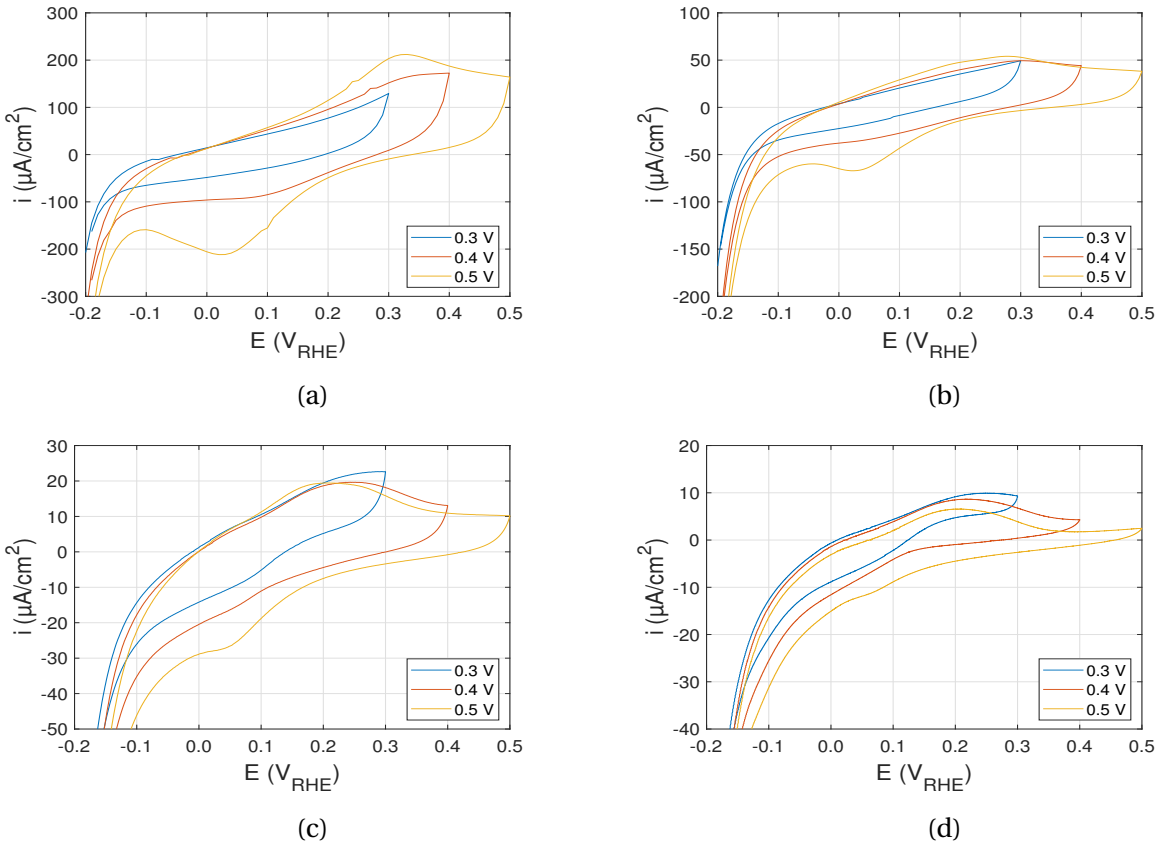

Figure 4.2.9: A comparison of CV conducted on a Ni electrode immersed in H_2 saturated 1M KOH in the potential range from 0.0 V to 0.5 V. Different scan rates were used, and the electrode was rotated at 1600rpm. a) $\nu = 100$ mVs^{-1} b) $\nu = 20$ mVs^{-1} c) $\nu = 5$ mVs^{-1} d) $\nu = 1$ mVs^{-1}

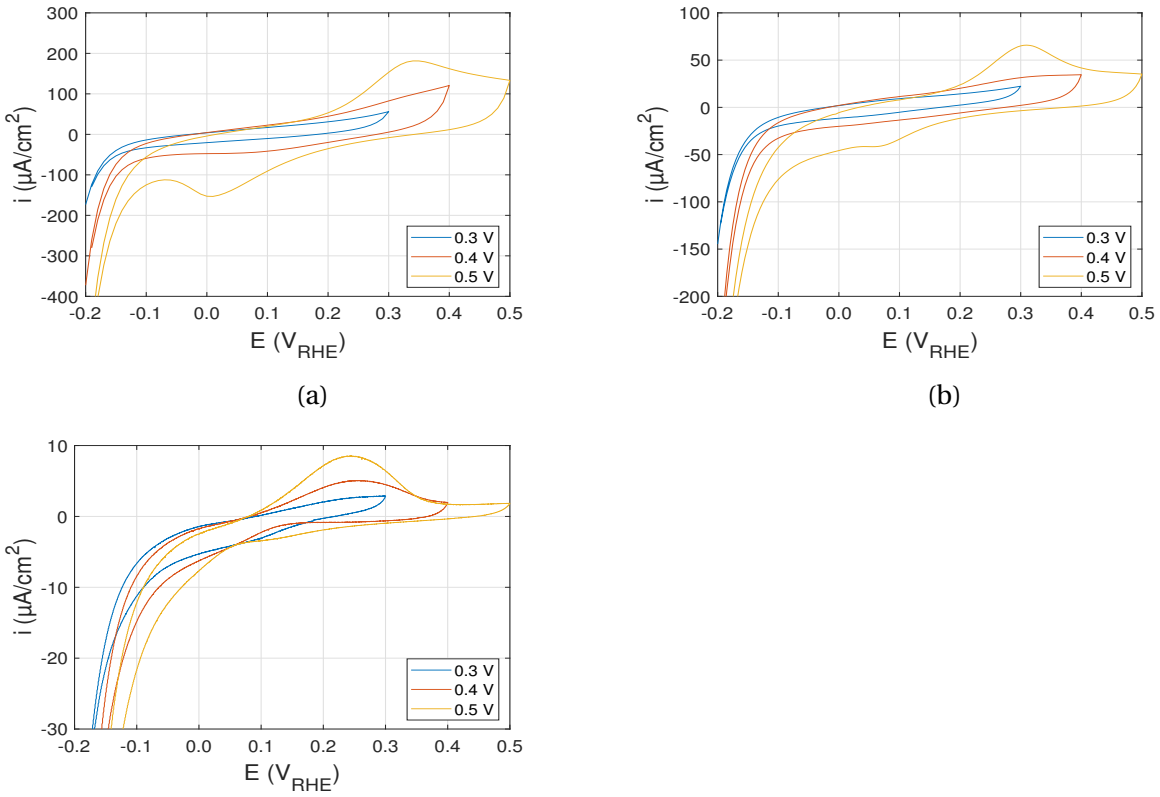

Figure 4.2.10: A comparison of CV conducted on a Ni electrode immersed in H_2 saturated 0.1M KOH in the potential range from 0.0 V to 0.5 V. Different scan rates were used, and the electrode was rotated at 1600 rpm. a) ν = 100 mVs^{-1} b) ν = 20 mVs^{-1} c) ν = 1 mVs^{-1}

The effect of rotation is evaluated in H_2 saturated atmosphere in 0.1M KOH. As noticed previously in the case of 1M KOH, at higher scan rate (100 mvs^{-1} and 20 mvs^{-1}), no significant improvement in current for the Ni in 0.1M KOH is found. But at 1 mvs^{-1} the HOR current is significantly visible in the peak at 0.1 V. Then the peak current density rises and gets stagnant at around 0.4 V. The peak reappears during the backward sweep due to the HOR on the Ni surface. Rotation has an affect in the case of 0.1M KOH when saturating the electrolyte with H_2. While rotating, a significant rise in the peak current density came about for all the three scan rates. The Ni electrode in 0.1M KOH without rotation showed the improved HOR activity.

4.2.3 Hydrogen evolution

There is always some hydrogen evolution taking place at the electrode surface even when the atmosphere is inert due to hydroxide ions reacting in the electrolyte. Conducting CV scans from different starting potentials below zero allows the investigation of HER and how it affects the resulting current. All CV scans in this section was conducted on a bulk-nickel electrode in 0.1M KOH. The scans were conducted in both Ar and H_2 atmosphere to investigate how HER is affected in different environments. Scan rate was set to be $\nu = 5$ mVs^{-1} with rotation of 1600 rpm, $\nu = 5$ mVs^{-1} without rotation, and $\nu = 1$ mVs^{-1} without rotation. The potential range was set from -0.2 V, -0.15 V, -0.10 V, -0.05 V, and 0.0 V to 0.5 V with respect to RHE. All experiments were first conducted in Ar atmosphere, then repeated in H_2 atmosphere.

A comparison of all CV scans can be viewed in figure 4.2.11. Hydrogen evolution is found in forward sweep on the interval from -0.2 V to 0.0 V, while hydrogen reduction is found in reverse sweep from on the same interval from 0.0 V to -0.2 V. Figure 4.2.11a, 4.2.11c, and 4.2.11e displays CV scans conducted in Ar atmosphere, while figure 4.2.11b, 4.2.11d, and 4.2.11f displays CV scans conducted in H_2 atmosphere. Figure 4.2.11a and 4.2.11b display CVs rotated at 1600 rpm. The remaining CV scans were measured without rotating. Hydrogen evolution decreases as the starting potential is set closer to zero. This results in a decrease in current, which is observed in all figures. There is a distinctive hydroxide peak at approximately 0.28 V in anodic direction. As the hydrogen evolution decreases, the hydroxide peak decrease as well. The peaks are also shifted to the left as there is less H_2(g) present. As the hydroxide formation is a reversible reaction, a reduction peak is found at 0.4 V. The reduction peak decrease proportionally with the formation peak as the hydrogen evolution decrease.

The hydrogen evolution seems unaffected by atmosphere on the interval -0.2 V to 0.0 V. However, when the potential is moved past 0 V, it is observed that the corresponding current is much higher in H_2 atmosphere compared to Ar atmosphere. Taking the rotation into consideration, comparing figure 4.2.11a with 4.2.11c, and figure 4.2.11b with 4.2.11d, it is observed that the CV scans conducted without rotation yields a higher current.

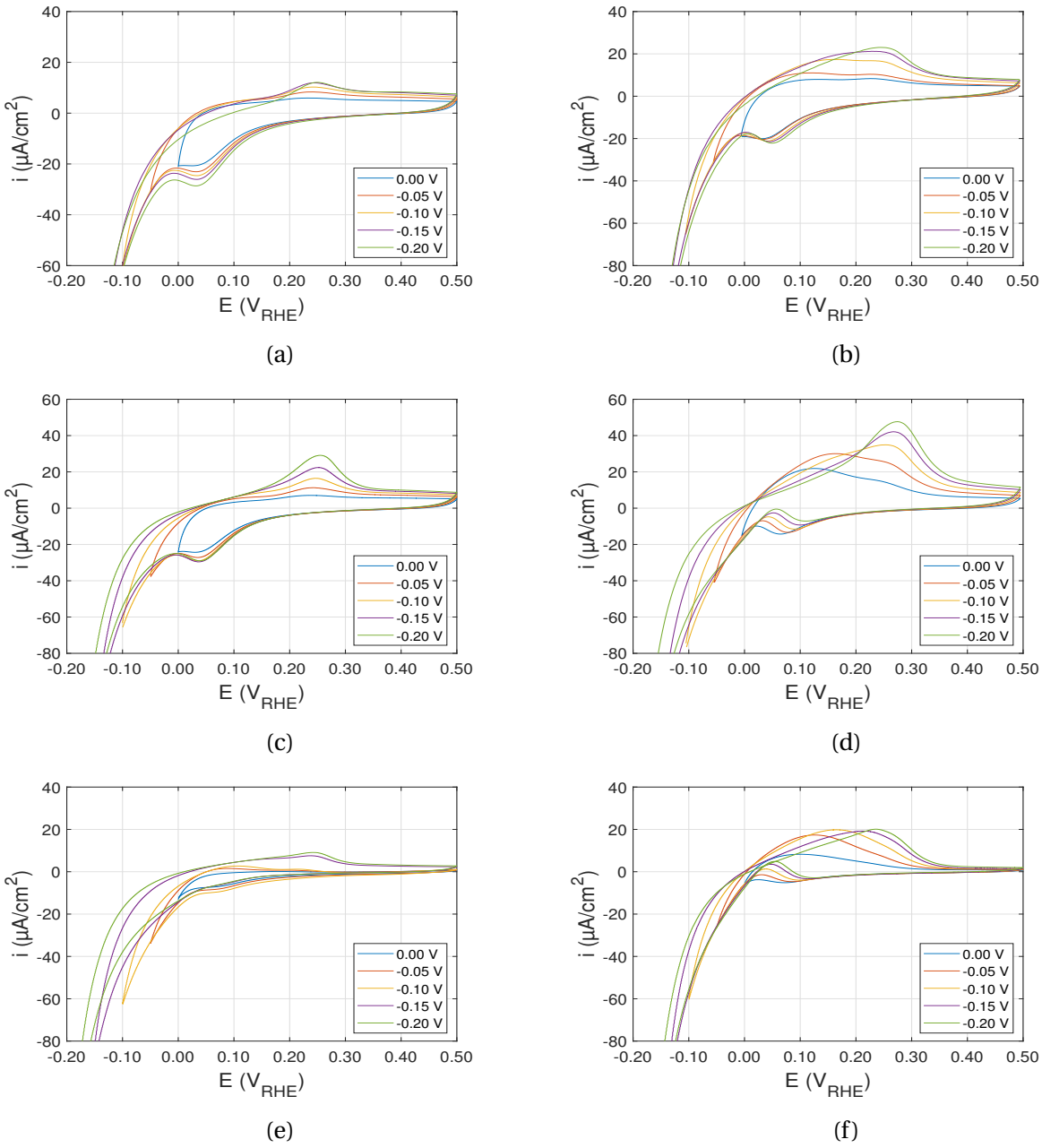

Figure 4.2.11: A comparison of CV conducted on a Ni electrode immersed in Ar(g) and H_2(g) saturated 0.1M KOH. The s were conducted from E_l = -0.2 V, -0.15 V, -0.10 V, -0.05 V, and 0 V to E_u = 0.5 V. a) Ar atmosphere, ν = 5 mVs^{-1}, rotation 1600 rpm b) H_2 atmosphere, ν = 5 mVs^{-1}, rotation 1600 rpm c) Ar atmosphere, ν = 5 mVs^{-1}, no rotation d) H_2 atmosphere, ν = 5 mVs^{-1}, no rotation e) Ar atmosphere, ν = 1 mVs^{-1}, no rotation f) H_2 atmosphere, ν = 1 mVs^{-1}, no rotation

The CV scans can be viewed separately in Appendix A.

4.2.4 Polarization of Ni electrode

A final experiment was conducted to investigate the hydrogen evolution reaction. A pre-treatment scheme was used, where the electrode was fully polarized before conducting CV scans in the potential range from 0.0 V to 0.5 V with rotation 1600 rpm.

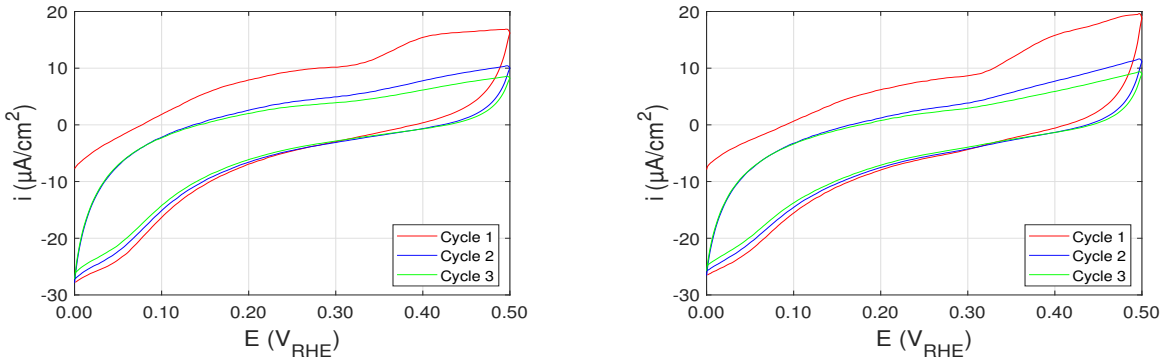

(a) (b)

Figure 4.2.12: A pre-treatment scheme was used to fully polarize the Ni electrode prior to the CV's. The electrolyte was 0.1M KOH. The pre-treatment consisted of 20 minutes sparging with H_2(g) at -0.05 V, followed by 30 minutes sparging with Ar(g) at 0.0 V. The CV was conducted in the potential range from 0.0 V to 0.5 V with scan rate $\nu = 5$ mVs^{-1}. The electrode was rotated at 1600 rpm. a) Original experiment b) Repeated experiment

The experiment is reproducible. A cathodic current is observed as the CV begins. The first cycle generates higher current density compared to the second and third cycle, and also has a more distinctive peak in the anodic direction. There is some hydrogen evolution present in the second and third cycle.

4.3 Simulation

A CV curve was simulated using MATLAB and the "Simulated annealing" algorithm. The script was coded based on a kinetic model for HOR, both made by Svein Sunde. The script and kinetic model can be viewed in appendix The simulated curve was fitted to figure 4.2.10b, which is CV conducted on bulk nickel immersed in H_2(g) saturated 0.1M KOH in the potential interval from -0.2 V to 0.5 V, with scan rate 20 mVs^{-1} and rotation 1600 rpm.

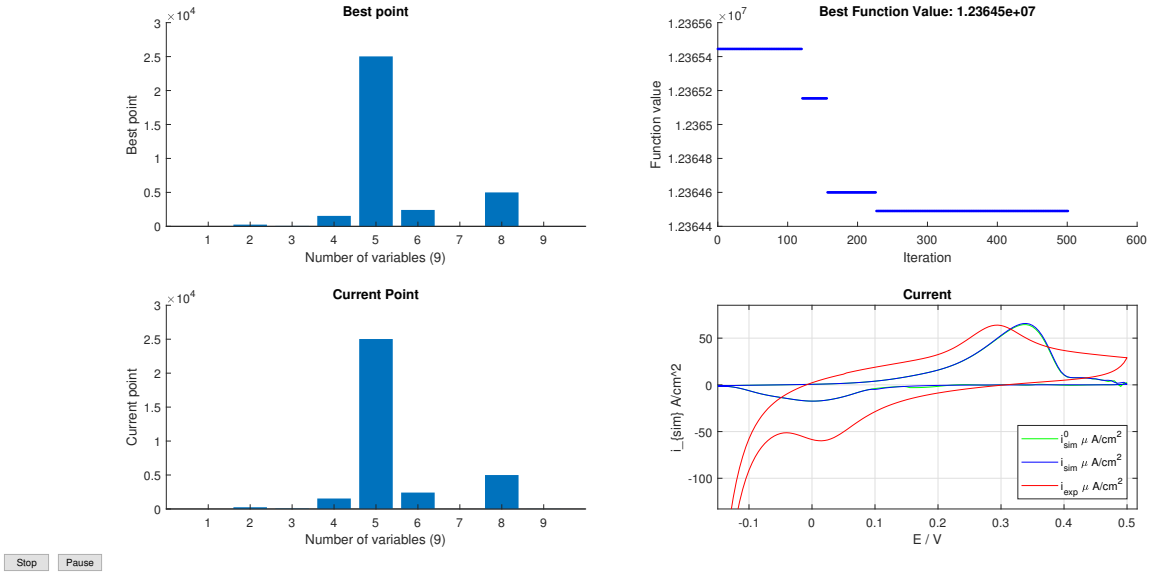

Figure 4.3.1: Simulation of CV conducted on bulk-nickel electrode immersed in H_2(g) saturated 0.1M KOH with rotation 1600 rpm in the potential range from -0.2 V to 0.5 V. The three first figures shows us the process of simulated annealing, while the forth figure in the right bottom corner is the results of the simulation. The red curve is the experimental curve from figure 4.2.10b, the green curve is the initial simulation, while the blue curve is the fitted simulation.

The simulation is not a perfect fit yet, but is getting close. The peaks in anodic and cathodic direction in the simulation occurs at almost the same potential as the experimental curve. However, there are some complications regarding the hydrogen evolution part leading to the "tale" of the voltammogram not behaving as expected.

The rate constants that were collected from this simulation are found in 4.3.1. As the simulation is not perfect, these rate constants are not valid.

k_1	k_{-1}	k_2	k_{-2}	k_3	k_{-3}	k_4	k_{-4}	k_5	k_5
1.5795e9	3.3079e6	9.4510e7	0.0402	16.7099	0.0402	6.5432e3	0.0631	0.2614	0.1306

Table 4.3.1: A summation of rate constants collected from the simulation in figure 4.3.1. These are the rate constants for the forward and backward reactions in equation C.1.7-C.1.11 from the kinetic HOR model in appendix C.1.

Chapter 5

Discussion

5.1 EIS measurements

In theory section 2.3.3, mass transfer was defined as a measure of consumption and production of reactants during a reaction. High consumption of reactants indicates high kinetics and low R_{ct}. This basically means that the overall mass transport is high as R_{ct} is low, which results in a high overpotential. Conversely, high R_{ct} yields a low mass transport in the electrochemical cell, thus low overpotential, low kinetics, and low consumption of reactants.

The same trends regarding polarization and mass transfer resistance were found for both Pt and Ni electrode. As the potential was set to below 0, the polarization increased. As the polarization was increased, the arc decreased, implying minimal R_{ct} . The opposite trends were found when looking at potential above 0 V. As the polarization increased, the arc increased as well, implying an increase in the R_{ct}.

5.2 Platinum electrode

Charge transfer resistance was higher in 1M KOH compared to 0.1M KOH. Rotation had very little effect in 1M KOH, however some changes were observed in 0.1M KOH. Not rotating the

electrode gave highest R_{ct} in H_2(g) saturated electrolyte compared to rotation. Conversely, rotating the electrode at 1600 rpm in Ar(g) saturated electrolyte gave higher R_{ct} compared to no rotation. During the investigation whether the rotation had an actual effect or not, it was found that it did not affect R_{ct}. These observation contradicts one-another, and the rotational effect should be further investigated as no proper solution has been found. It could be due to disturbances in the cell, or that the cell was not in a steady-state because of changes in potential during the experiments. The charge transfer resistance was found to increase with increasing potential before it stagnated.

Having R_{ct} as low as possible results in better kinetics and a higher overpotential. The best conditions for Pt was found when conducting EIS in 0.1M KOH saturated with H_2(g) and rotation 1600 rpm.

5.2.1 Nickel electrode

The charge transfer resistance is highest in 0.1M KOH, which is opposite of what was found at the Pt electrode. The rotation seems to have some effect, especially at the lower potentials. This trend is consistent in both 0.1M and 1M KOH. H_2(g) promotes R_{ct}. The lowest R_{ct} was found in Ar(g) saturated 1M KOH with rotation 1600 rpm.

The R_{ct} has much higher values while conducting EIS on the Ni electrode compared to Pt electrode. This is as expected, as Pt has better catalytic properties compared to Ni. The R_{ct} stabilizes at higher potentials for the Pt catalyst compared to Ni. ¨

Further investigation and interpretation of the results must be conducted as this thesis barely scratched the surface. A suggestion is put in further work.

5.3 CV and pH dependence

5.3.1 Platinum

Figure 4.2.1 showed the CV's carried out for a Pt electrode in an Ar atmosphere in both 1M and 0.1M KOH with and without rotation. The CV with and without rotation at both 1M and 0.1M KOH concentration looks like a typical CV of Pt electrode in alkaline condition. A clear H_2 adsorption in the H_2 region followed by the Pt-OH formation in the O_2 regions was seen during the forward scan. In the same way, the reduction of Pt-OH and the desorption of H_{ads} from the Pt surface appeared as distinct peaks in the backward scan. One could see three distinct H_{ads} peaks in both electrolyte concentrations without rotation. But when the electrode was rotated, the first H_{ads} peak is suppressed in both the electrolyte concentration. It is direct evidence that the H_2 evolution is occurring at 0 V vs RHE and this evoluted H_2 being weakly adsorbed on the Pt electrode surface. A rotation is sufficient enough to remove those weakly adsorbed H_{ads} molecules preventing it from participating in reactions, and thus generating no current at this stage. The remaining H_{ads} peaks could be from two different crystallographic planes of Pt[55].

When comparing the oxygen region, the CV's in 1M KOH showed the higher magnitude of Pt-OH peak, probably due to the increase in the concentration of the OH_{ads} on the surface. Less H_{ads} is found in 1M KOH compared to 0.1M KOH, leaving more vacant sites at the electrode surface. It is possible that the larger number of vacant sites from the hydrogen region enables more OH_{ads} in the oxygen region. This could explain the why the Pt-OH formation is slightly intensified when electrolyte concentration increases, which is seen in fig. 4.2.1c and 4.2.1a [56].

When the same CV scans were conducted in the H_2(g) saturated electrolyte, the only process taking place at the surface of the Pt electrode was the oxidation of H_2. The oxygen region in the CV is suppressed, as no Pt-OH formation took place after 0.8 V. When the electrode is rotated, it becomes evident that the only two reactions taking place are HOR and HER. The 0.1M KOH still generates higher current compared to 1M KOH, and an explanation to this could be hydrogen binding energy. In earlier research, it was found that HBE is a dominating factor in HOR/HER activity and kinetics [24]. HBE is modified by changing the pH, proving that the pH has an effect

on the kinetics. Fast kinetics are connected with low HBE, and a low HBE is achieved in low pH. HBE is known for suppressing any catalytic properties, which could be the causes of the slow kinetics in electrolytes of high pH. However, a more thorough evaluation is required to confirm this, which will be conducted in further works.

5.3.2 Nickel

Conducting CV on nickel electrodes is not always easy, as there are many factors that could affect the scans. Achieving perfect results is therefore very difficult, especially when performed in a PTFE-cell that is not see-through. Achieving an even current distribution throughout the cell is difficult, and presence of dissolved H_2(g) would have a significant impact on the CV profiles[5]. The presence of H_2 would shift the current density towards different values, which could be an explanation to behavior like the 0.3 V measurements in figure 4.2.3. As stated in theory section **??**, Ni is easily oxidized, meaning that exposure in air could lead to forming of oxide layers at the surface.

When conducting CV's on the Ni electrode, it was found that the formation of α-Ni$(OH)_2$ was completely reversible. The highest current densities and the most distinctive α-Ni$(OH)_2$ formation and reduction peaks was found in 0.1M KOH compared to 1M KOH. Scan rates seemed to influence the peak position as they were shifted towards more positive potentials as the scan rates increased. The rotation proved to have an impact in 0.1M KOH, as the α-Ni$(OH)_2$ formation peak became insignificant. Conversely, it did not seem to have any affect in 1M KOH. Rotation is applied to remove adsorbed species and oxide layers at the electrode surface. Earlier work by Zheng et.al indicates that HBE could explain the why rotation does have any effect in 1M KOH. In theory section 2.4 HBE was said to be low in low pH. This could mean that the HBE is so high in 1M KOH that the rotation of the electrode alone is not enough to remove adsorbed species from the electrode surface due to strong binding, causing a decrease in current. It is also possible that the α-Ni$(OH)_2$ formation was not fully reversed in the reverse sweep in 1M KOH, promoting OH_{ads} at the surface. OH_{ads} could block the surface, thus lowering the current. Another explanation to the lower current in 1M KOH could be the electrolyte concentration. There could be more resistance in 1M KOH, thus lowering the kinetics of the reactions taking place in

the electrolyte. These results are found in earlier work by Floner et.al which showed that current density decreases as pH increases [54].

While investigating the HOR activity, some effect at low scan rates (1 mVs^{-1}) was found. The effect was confirmed while comparing CV's conducted with scan rate 1 mVs^{-1} in H_2 to Ar. However, an overall observation was that HOR activity is negligible. This could be explained by a too small surface area of the electrode.

When comparing the effect of Ar(g) vs H_2(g) atmosphere in 1M KOH, Ar(g) proved to produce highest current at high scan rate (100 mVs^{-1}). However, H_2(g) proved to be the best environment at low scan rate (1 mVs^{-1}). Hydrogen is a very small and light element with low solubility in the electrolyte. Low scan rate means a more time-consuming voltammetry, allowing more H_2(g) to react at the electrode surface. This is independent of rotation, and the same trends were found for 0.1M KOH, which shows consistency. The CV scans conducted in 0.1M KOH without rotation in H_2(g) saturated atmosphere showed improvement in HOR.

There is a lack of research regarding pH-dependence and HOR/HER on Ni electrodes in alkaline electrolytes, thus very little literature to support this discussion on. The effect of HBE has not yet been validated and a more thorough investigation is needed to fully understand the kinetics and behavior of HOR/HER in alkaline media, and the effect of pH.

5.3.3 Hydrogen evolution

Hydrogen evolution takes place in potential ranges below zero and increases as the initial potential is set to more negative values. This can be viewed in figure 4.2.11. The increase in hydrogen evolution results in an increase in current. This trend has been observed in previous work by A.Seghiour et al. [57]. This can be explained by taking the hydrogen content in the electrolyte into consideration. More hydrogen evolution yields a higher hydrogen content, thus enhancing hydrogen adsorption at the electrode surface. There are less vacant sited available and the hydrogen coverage increases, yielding an increase in current as well.

Saturating the electrochemical cell with hydrogen promotes the current as there is a constant flow of hydrogen to the electrode surface, promoting hydrogen adsorption. However, the ad-

sorbed hydrogen can be removed from the surface by rotating the electrode, which justifies why CV scans with rotation generates lower current. A second anodic peak is taking form in the hydrogen atmosphere as the starting potential gets close to 0 V and the hydrogen content is decreased. These can be viewed in figures 4.2.11b, 4.2.11d, and 4.2.11f. The same behavior has been observed in previous work [46, 54, 58, 59], and is believed to be the result of oxidation of H_{ad} from nickel hydride (NiH_x) in the cathodic direction. The second anodic peak could also be a result of α-$Ni(OH)_2$ not being completely reduced back to metallic nickel. There could be oxides in the electrolyte passivating the electrode surface, decreasing the active electrochemical surface area. The amount of available sites for the cathodic reduction of α-$Ni(OH)_2$ is decreased, resulting in an incomplete reduction in cathodic direction.

A better understanding of the HER can be achieved by simulating the CV curves, looking into the kinetics and velocity of the reactions occuring at the electrode surface.

5.3.4 Effect of polarization

A polarization scheme was used prior to CV measurements to fully reduce the electrode back to metallic nickel from α-$Ni(OH)_2$, making sure there was no oxide layers at the electrode surface [57]. The polarization potential (E_p) was chosen from the Ni-H_2O pourbaix diagram at pH 13 to make sure that a potential within the Ni section was chosen. The pourbaix diagram can be viewed in appendix E. The pre-treated CV scans can be viewed in figure 4.2.12.

The results were not quite as expected, and was therefore repeated to see if the they were reproducible. They were, but are not comparable to earlier work like in Alsabet et al.[5]. The current is cathodic in the beginning of the scans, and the first cycle has a higher current, most likely due to a larger amount of dissolved hydrogen in the electrolyte from formation nickel hydride (NiH_x) as a result of prolonged cathodic polarization [6].

The characteristic peaks of α-$Ni(OH)_2$ are suppressed when comparing them to the same scan conducted without the pre-treatment in figure 4.2.6b, and the resulting current density is considerably lower when the electrode was fully polarized prior to the cycling. It is possible that the formation of α-$Ni(OH)_2$ was not a fully reversed, leaving oxide layers at the electrode surface,

limiting vacant surface sites, preventing reactions and thus causing the suppressed curves. In previous studies on polarization time it was found that holding the polarization for longer than 600 seconds lead to change in the anodic current density. The current decreases as the polarization time increases. This phenomenon is called aging, and it leads to less pronounced and more diffusive peaks, as well as lower current [60, 57]. The total polarization time during these experiments were 3000 seconds, which could explain the low current density.

5.4 Simulation

By developing a kinetic model for HOR and implementing it in MATLAB to fit CV curves, the rate constants for reactions C.1.7-C.1.11 was found, however these are not valid as the simulation does not have the preferred quality. Many more simulations were performed, but due to the quality of the simulations they were not included in this thesis. In theory, this simulation is a great tool for investigating the kinetics of HOR as it is possible to observe how the hydrogen acts when the reactions are too slow or too fast, what happens if a peak is missing, and so on. The velocity plot in figure B.2.1 gives an indication of whether the reactions are too fast or too slow and is how the parameters for each simulation are adjusted, while the coverage in figure B.1.1 shows the site occupation of the electrode surface during the reactions. The green line in the coverage plot is the sum of available sites. A high number of occupied sites corresponds to a high amount of $OH-_{ads}$ which enhances current generation. This trend of occupied sites was observed earlier when the effect of rotation was discussed.

The parameters collected from the simulation are dimensionless, as the mathematics and simulation became very complex when units were included. Achieving a perfect simulation has proven to be difficult. The simulation does not respond to the hydrogen evolution in the potential range from 0 V to -0.2 V. Another approach to achieve a better simulated curve is discussed in section 7. It is also worth mentioning that the the "Simulated Annealing" algorithm runs by generating a random point and then continue with iteration of more randomly generated points. This means that the results will always differ to a certain extent.

Chapter 6

Conclusion

The behavior of HOR using Pt and Ni as electrodes was investigated in 0.1M and 1M KOH in Ar (g) and H_2(g) atmosphere, conducting EIS and CV.

Conducting EIS showed a decrease in R_{ct} as the polarization was increased below 0 V and an increase in R_{ct} as the polarization was increased above 0 V. The effect of rotation was investigated, but it gave somewhat contradicting results. This could be due to cell disturbances if the system did not achieve a steady state. Further investigation must be conducting regarding rotation. Low R_{ct} is desired to achieve better kinetics for HOR. The best conditions for Pt was found when conducting EIS in 0.1M KOH saturated with H_2(g) and rotation 1600 rpm, while for Ni Ar (g) saturated 1M KOH with rotation 1600 rpm gave best results. Pt has generally much lower R_{ct} compared to Ni, which is justified as the catalytic properties of Pt are better than Ni. Further inspection of the results must be conducted, and a suggestion has been put in Further Works.

CV's conducted on Pt provided proof of H_2(g) evolution at 0 V, as the H_{ads} peak was suppressed during rotation. The suppression is a result of H_{ads} being removed, thus preventing current from being generated in this area. Less hydrogen adsorption and more oxygen adsorption were observed in 1M KOH, which are the opposite trends found in 0.1M KOH. The availability of surface sites could be an explanation to these trends, however this needs a more thorough investigation to be justified. There was no Pt-OH formation after 0.8 V when conducting CV's in H_2(g) saturated electrolytes, and by rotating the electrode it was clear that HOR and HER were the only

two reactions taking place at the electrode.

The effect of HOR activity was observed on the Ni electrode when comparing scan rate 1 mVs^{-1} conducted in Ar and H_2 saturated atmosmphere. However, it was found that the overall HOR activity on Ni could be negligible. The rotational effect was investigated on the Ni electrode immersed in 0.1M and 1M KOH. A significant modification of the current was found in 0.1M KOH, however, it did not seem to have any effect in 1M KOH. HBE is proposed as an explanation, and suggests that the binding energy increases with increasing pH, causing stronger binding of the adsorbed species at the electrode surface. This could explain why CV's remains unaffected by rotation in 1M KOH, as rotation alone is not enough to remove the adsorbed species. A comparison of atmosphere showed that Ar(g) gave best results for high scan rates while H_2(g) was better suited at low scan rates, which was justified by hydrogen properties. In conclusion, it was found that H_2-saturated 0.1M KOH without rotation promoted the HOR at low scan rates.

It is commonly known that oxide layers starts forming at the electrode surface of the Ni electrode when conducting CV over a longer period of time, reducing the active surface area. Due to unexpected results of the polarization regime of this experiment, it was not possible to see the effect of polarization. Consistent trends regarding hydrogen evolution were found when conducting CV's from different starting potentials below 0 V. The hydrogen evolution increased as the starting potential was set to more negative values. As the starting potential approached 0 V, a second peak was observed in the forward sweep in H_2(g) saturated atmosphere. This could be due to oxidation of H_{ads} fromNiH_x in the reverse sweep or incomplete reduction of α-$Ni(OH)_2$

Despite many years of research on the HOR mechanism, many properties remains unknown. By developing a kinetic model for HOR and using a software to make a simulation that fits the experimental data, important information like rate constants, coverage and reaction velocity can be collected. An attempt to make such a simulation was made in this paper, however some work still remains until a perfect fit is achieved. The constants collected in this paper does not give any information of value.

A final conclusion based on the results and discussion is that H_2(g) saturated 0.1M KOH without rotation at low scan rates promotes HOR activity, and that atmosphere should chosen based on scan rate. H_2 evolution increases as the starting potential becomes more negative, resulting

in more distinctive formation and reduction peaks due to hydrogen adsorption at the surface. Further investigation of HBE is needed in order to anticipate the effect of pH dependence on HOR. A proper simulation of CV scans gives the opportunity to collect valuable information like rate constants, velocity, and coverage of the Ni catalyst. A proposition of how to improve the simulation is found in section 7

Chapter 7

Further work

7.1 Impedance

Plotting the impedance data in Tafel and Bode diagrams, and Armstrong and Henderson Equivalent Circuit (AHEC) would give more information on the capacitance and charge transfer resistance. Investigating the adsorption isotherm and possible changes would give an indication of any changes arising in HOR. This has been conducted by Franceschini et al. in previous work, and shows promising results [47]. A more thorough impedance analysis could also be conducted according to the kinetic HOR model in section C.1 developed by Svein Sunde, implementing equations in a software and run simulations.

7.2 CV and Hydrogen Binding Energy

The effect of pH dependence remains unsolved. A proper investigation of HBE is needed to justify the assumptions and explanations made in the discussion part. Consistency of HBE can be investigated by conducting CV and EIS in a wider pH-range, with different catalysts. The activity and its pH dependence in HOR/HER should be investigated. Zheng et al. provides an idea of further research, where they used density functional theory (DFT) calculations and volcano plots to show correlations to the exchange current density [24, 61].

7.3 Simulation

There are several ways to improve the simulations in MATLAB. One is to create a Tafel plot and find what mechanism runs the rds in equations C.1.2-C.1.6. Tafel plot is created by plotting the logarithm of current density vs potential. Then, the Tafel slope can be found, which is given in mV/decade. By extrapolating the linear part of the Tafel plot to the y-axis, the exchange current density (i_0) is found.

The Tafel slope will most likely indicate the rds to be a Volmer mechanism, which has been found in earlier work [47]. This makes the reaction in equation C.1.4 the rate determining step in the HOR mechanism. The rate constant k^0_{-3} can be calculated from i_0 by assuming the coverage θ_1 moves towards zero due to slow kinetics, and that $\theta_2 = \theta_3 = 0$;

$$i_0 = 2F\Gamma k^0_{-3} exp\Big(-\alpha\frac{FE}{RT}\Big) \tag{7.3.1}$$

$$k^0_{-3} = \frac{i_0}{2F\Gamma exp\Big(-\alpha\frac{FE}{RT}\Big)} = \frac{i_0}{2F\Gamma} \tag{7.3.2}$$

F is Faraday's constant, Γ is the surface excess, α is the charge transfer coefficient, E is the potential, R is the gas constant and T is temperature. The potential was assumed to be zero, and k^0_{-3} was rewritten according to equations C.1.13

An expression for θ_1 can be found from equation C.1.9:

$$\Gamma k_3 c_{OH^-}\theta_1 - \Gamma k_{-3}(1-\theta_1) = 0 \tag{7.3.3}$$

$$(k_3 c_{OH^-} + k_{-3})\theta_1 = k_{-3} \tag{7.3.4}$$

$$\theta_1 = \frac{k_{-3}}{k_3 c_{OH^-} + k_{-3}} \tag{7.3.5}$$

$$\theta_1 = \frac{1}{1 + \frac{k_3}{k_{-3}} c_{OH^-}} \tag{7.3.6}$$

$$\theta_1 = \frac{1}{1 + c_{OH^-}\frac{k_3^0}{k_{-3}^0} exp\left(\frac{FE}{RT}\right)} \tag{7.3.7}$$

Since the rds is determined, it is fair to assume that the prior reactions in equation C.1.8 is much faster. The coverages θ_2 and θ_3 are assumed to be zero, and a second expression for θ_1 can be found rearranging equation C.1.8:

$$\Gamma k_2 c_{H_2} c_{OH^-}(1-\theta_1) - \Gamma k_{-2}\theta_1 = 0 \tag{7.3.8}$$

$$-(k_2 c_{H_2} c_{OH^-} + k_{-2})\theta_1 = -k_2 c_{H_2} c_{OH^-} \tag{7.3.9}$$

$$\theta_1 = \frac{k_2 c_{H_2} c_{OH^-}}{k_2 c_{H_2} c_{OH^-} + k_{-2}} \tag{7.3.10}$$

$$\theta_1 = \frac{c_{H_2} c_{OH^-}}{c_{H_2} c_{OH^-} + \frac{k_{-2}}{k_2}} \tag{7.3.11}$$

$$\theta_1 = \frac{c_{H_2} c_{OH^-}}{c_{H_2} c_{OH^-} + \frac{k_{-2}^0}{k_2^0} exp\left(-\frac{FE}{RT}\right)} \tag{7.3.12}$$

The two expressions for θ_1 can now be set equal, which gives equation 7.3.13.

$$\frac{1}{1 + c_{OH^-}}\frac{k_3^0}{k_{-3}^0} exp\left(\frac{FE}{RT}\right) = \frac{c_{H_2} c_{OH^-}}{c_{H_2}} c_{OH^-} + \frac{k_{-2}^0}{k_2^0} exp\left(-\frac{FE}{RT}\right) \tag{7.3.13}$$

The parameter k_{-3} is already known. By choosing values for two of the three remaining parameters, k_{-2} and k_3 for example, the last unknown parameter (k_2) can be calculated. These expressions have to be implemented in the MATLAB code. Hopefully, by repeating this procedure for

the other rate constants with more assumptions, the MATLAB code will be able to make a perfect simulation, making it possible to proceed and collect valuable information. Unfortunately, there was no time to implement this method and see if it worked.

Bibliography

[1] Sadia Kabir, Kenneth Lemire, Kateryna Artyushkova, Aaron Roy, Madeleine Odgaard, Debbie Schlueter, Alexandr Oshchepkov, Antoine Bonnefont, Elena Savinova, Dinesh C. Sabarirajan, Pratiti Mandal, Ethan J. Crumlin, Iryna[space]V. Zenyuk, Plamen Atanassov, and Alexey Serov. Platinum group metal-free nimo hydrogen oxidation catalysts: high performance and durability in alkaline exchange membrane fuel cells. *J. Mater. Chem. A*, 5:24433–24443, 2017.

[2] Omar Z. Sharaf and Mehmet F. Orhan. An overview of fuel cell technology: Fundamentals and applications. *Renewable and Sustainable Energy Reviews*, 32:810 – 853, 2014.

[3] Yangxin Pan, Gaohe Hu, Juntao Lu, Li Xiao, and Lin Zhuang. Interfacial water reorganization as a ph-dependent descriptor of the hydrogen evolution rate on platinum electrodes. *Journal of Energy Chemistry*, 2018.

[4] P. J. Rheinlander, J. Herranz, J. Durst, and H. A. Gasteiger. Kinetics of the hydrogen oxidation/evolution reaction on polycrystalline platinum in alkaline electrolyte reaction order with respect to hydrogen pressure. *Journal of the Electrochemical Society*, 161(14):F1448–F1457, oct 2014.

[5] M Grden M Alsabet and G Jerkiewicz. Electrochemical growth of surface oxides on nickel. part 1: Formation of α-ni(oh)2 in relation to the polarization potential, polarization time, and temperature. *Electrocatalysis*, 2(4):317 – 330, 2011.

[6] Alexandr G. Oshchepkov, Antoine Bonnefont, Valentin N. Parmon, and Elena R. Savinova. On the effect of temperature and surface oxidation on the kinetics of hydrogen electrode reactions on nickel in alkaline media. *Electrochimica Acta*, 269:111 – 118, 2018.

[7] Lijun Bai, D.A. Harrington, and B.E. Conway. Behavior of overpotentialâ€"deposited species in faradaic reactionsâ€"ii. ac impedance measurements on h2 evolution kinetics at activated and unactivated pt cathodes. *Electrochimica Acta*, 32(12):1713 – 1731, 1987.

[8] Strand Sigrid. *Electrochemical Analysis of Nickel for the Alkaline Fuel Cell. Project thesis, Department of Material Science and Engineering, Norwegian University of Science and Technology*. 2018.

[9] United Nations Department of Economic and Social Affairs. World population prospects 2017, 2018.

[10] Shaojun Guo, Sen Zhang, and Shouheng Sun. Tuning nanoparticle catalysis for the oxygen reduction reaction. *Angewandte Chemie International Edition*, 52(33):8526–8544.

[11] Magdalena Momirlan and T.N. Veziroglu. The properties of hydrogen as fuel tomorrow in sustainable energy system for a cleaner planet. *International Journal of Hydrogen Energy*, 30(7):795 – 802, 2005.

[12] P.P. Edwards, V.L. Kuznetsov, W.I.F. David, and N.P. Brandon. Hydrogen and fuel cells: Towards a sustainable energy future. *Energy Policy*, 36(12):4356 – 4362, 2008. Foresight Sustainable Energy Management and the Built Environment Project.

[13] Yuanyuan Cong, Baolian Yi, and Yujiang Song. Hydrogen oxidation reaction in alkaline media: From mechanism to recent electrocatalysts. *Nano Energy*, 44:288 – 303, 2018.

[14] Shaun Alia and Bryan S. Pivovar. Evaluating hydrogen evolution and oxidation in alkaline media to establish baselines. *Journal of The Electrochemical Society*, 165:F441–F455, 01 2018.

[15] J. Durst, A. Siebel, C. Simon, F. Hasche, J. Herranz, and H. A. Gasteiger. New insights into the electrochemical hydrogen oxidation and evolution reaction mechanism. *Energy Environ. Sci.*, 7:2255–2260, 2014.

[16] Larminie James and Andrew Dicks. *Fuel cell systems explained*. Wiley, 2009.

[17] G.F. McLean, T. Niet, S. Prince-Richard, and N. Djilali. An assessment of alkaline fuel cell technology. *International Journal of Hydrogen Energy*, 27(5):507 – 526, 2002.

[18] Dario R. Dekel. Review of cell performance in anion exchange membrane fuel cells. *Journal of Power Sources*, 375:158 – 169, 2018.

[19] Wenchao Sheng, MyatNoeZin Myint, Jingguang G. Chen, and Yushan Yan. Correlating the hydrogen evolution reaction activity in alkaline electrolytes with the hydrogen binding energy on monometallic surfaces. *Energy Environ. Sci.*, 6:1509–1512, 2013.

[20] Hao Wang and Lijun Gao. Recent developments in electrochemical hydrogen evolution reaction. *Current Opinion in Electrochemistry*, 7:7 – 14, 2018.

[21] Ali Eftekhari. Electrocatalysts for hydrogen evolution reaction. *International Journal of Hydrogen Energy*, 42(16):11053 – 11077, 2017.

[22] Mary Helen McCay. Chapter 23 - hydrogen: An energy carrier. In Trevor M. Letcher, editor, *Future Energy (Second Edition)*, pages 495 – 510. Elsevier, Boston, second edition edition, 2014.

[23] Isis Ledezma-Yanez, W. David Z Wallace, Paula Sebastián-Pascual, Victor Climent, Juan M. Feliu, and Marc T. M. Koper. Ni(oh)2-ni/c for hydrogen oxidation reaction in alkaline media. *Nature Energy*, 2017.

[24] Jie Zheng, Wenchao Sheng, Zhongbin Zhuang, Bingjun Xu, and Yushan Yan. Universal dependence of hydrogen oxidation and evolution reaction activity of platinum-group metals on ph and hydrogen binding energy. *Science Advances*, 2:e1501602–e1501602, 03 2016.

[25] Nagappan Ramaswamy, Shraboni Ghoshal, Michael K. Bates, Qingying Jia, Jingkun Li, and Sanjeev Mukerjee. Hydrogen oxidation reaction in alkaline media: Relationship between electrocatalysis and electrochemical double-layer structure. *Nano Energy*, 41:765 – 771, 2017.

[26] Mukesh Bhardwaj and R. Balasubramaniam. Uncoupled non-linear equations method for determining kinetic parameters in case of hydrogen evolution reaction following

volmerâ€“heyrovskyâ€“tafel mechanism and volmerâ€“heyrovsky mechanism. *International Journal of Hydrogen Energy*, 33(9):2178 – 2188, 2008.

[27] W.Sheng, H.A Gasteiger, and Y. Shao-Horn. Hydrogen oxidation and evolution reaction kinetics on platinum: Acid vs alkaline electrolytes. *Electrochemical Society*, 157(11):317 – 330, 2010.

[28] P.J Rheinländer, S. Henning, J. Herranz, and H. A. Gasteiger. Comparing hydrogen oxidation and evolution reaction kinetics on polycrystalline platinum in 0.1 m and 1 m koh. *Journal of The Electrochemical Society*, 50(2), 2013.

[29] Andrzej Lasia. Hydrogen evolution reaction. *Handbook of Fuel Cell Technology*, 2:414–440, 06 2003.

[30] Yao Zheng, Yan Jiao, Anthony Vasileff, and Shi-Zhang Qiao. The hydrogen evolution reaction in alkaline solution: From theory, single crystal models, to practical electrocatalysts. *Angewandte Chemie International Edition*, 10 2017.

[31] Alan M.Bond Oldham Keith, Jan C. Myland. *Electrochemical Science and Technology: Fundamentals and Applications*. Wiley, 2012.

[32] Bamford C.H and Compton R.G. *Electrode Kinetics: Principles and Methodology*. Elsevier, 1986.

[33] Electrochemical University of Cambridge and Micro Engineering group. Linear sweep and cyclic voltametry: The principles, 2017.

[34] Andrew Hamnett Hamann Carl H. and Wolf Vielstich. *Electrochemistry*. Wiley, 2007.

[35] Noémie Elgrishi, Kelley J. Rountree, Brian D. McCarthy, Eric S. Rountree, Thomas T. Eisenhart, and Jillian L. Dempsey. A practical beginner's guide to cyclic voltammetry. *Journal of Chemical Education*, 95(2):197–206, 2018.

[36] Gamry Instruments. Basics of electrochemical impedance spectroscopy, 2018.

[37] Utz Retter and Heinz Lohse. *Electrochemical Impedance Spectroscopy*. Springer Berlin Heidelberg, Berlin, Heidelberg, 2010.

[38] Byoung-Yong Chang and Su-Moon Park. Electrochemical impedance spectroscopy. *Annual Review of Analytical Chemistry*, 3(1):207–229, 2010. PMID: 20636040.

[39] Parthasarathy M. Gomadam and John W. Weidner. Analysis of electrochemical impedance spectroscopy in proton exchange membrane fuel cells. *International Journal of Energy Research*, 29(12):1133–1151, 10 2005.

[40] Adriano Sacco. Electrochemical impedance spectroscopy: Fundamentals and application in dye-sensitized solar cells. *Renewable and Sustainable Energy Reviews*, 79:814 – 829, 2017.

[41] Fariba Safizadeh, Edward Ghali, and Georges Houlachi. Electrocatalysis developments for hydrogen evolution reaction in alkaline solutions â€“ a review. *International Journal of Hydrogen Energy*, 40(1):256 – 274, 2015.

[42] Aicheng Chen and Peter Holt-Hindle. Platinum-based nanostructured materials: Synthesis, properties, and applications. *Chemical Reviews*, 110(6):3767–3804, 2010. PMID: 20170127.

[43] Yao Zheng, Yan Jiao, Mietek Jaroniec, and Shi Zhang Qiao. Advancing the electrochemistry of the hydrogen-evolution reaction through combining experiment and theory. *Angewandte Chemie International Edition*, 54(1):52–65.

[44] Fatemeh Davar, Zeinab Fereshteh, and Masoud Salavati-Niasari. Nanoparticles ni and nio: Synthesis, characterization and magnetic properties. *Journal of Alloys and Compounds*, 476(1):797 – 801, 2009.

[45] Ming Gong, Wu Zhou, Mon-Che Tsai, Jigang Zhou, Mingyun Guan, Meng-Chang Lin, Bo Zhang, Yongfeng Hu, Di-Yan Wang, Jiang Yang, Stephen J Pennycook, Bing Joe Hwang, and Hongjie Dai. Nanoscale nickel oxide/nickel heterostructures for active hydrogen evolution electrocatalysis. *Nature communications*, 5:4695, 08 2014.

[46] Alexandr G. Oshchepkov, Antoine Bonnefont, Viktoriia A. Saveleva, Vasiliki Papaefthimiou, Spyridon Zafeiratos, Sergey N. Pronkin, Valentin N. Parmon, and Elena R. Savinova. Exploring the influence of the nickel oxide species on the kinetics of hydrogen electrode reactions in alkaline media. *Topics in Catalysis*, 59(15):1319–1331, Sep 2016.

[47] Esteban A. Franceschini, Gabriela I. Lacconi, and Horacio R. Corti. Kinetics of the hydrogen evolution on nickel in alkaline solution: new insight from rotating disk electrode and impedance spectroscopy analysis. *Electrochimica Acta*, 159:210 – 218, 2015.

[48] M.M. Kashani Motlagh, A.A. Youzbashi, F. Hashemzadeh, and L. Sabaghzadeh. Structural properties of nickel hydroxide/oxyhydroxide and oxide nanoparticles obtained by microwave-assisted oxidation technique. *Powder Technology*, 237:562 – 568, 2013.

[49] M Grden M Alsabet and G Jerkiewicz. Electrochemical growth of surface oxides on nickel. part 2: Formation of β-ni(oh)2 and nio in relation to the polarization potential, polarization time, and temperature. *Electrocatalysis*, 5(2):136–147, 2014.

[50] Xianyou Wang, Hean Luo, P.V Parkhutik, Ari-Carman Millan, and E Matveeva. Studies of the performance of nanostructural multiphase nickel hydroxide. *Journal of Power Sources*, 115(1):153 – 160, 2003.

[51] inc The Mathworks. What is simulated annealing?, 2018.

[52] inc The Mathworks. How simulated annealing works, 2018.

[53] inc The Mathworks. Simulated annealing terminology, 2018.

[54] D. Floner, C. Lamy, and J.-M. Leger. Electrocatalytic oxidation of hydrogen on polycrystal and single-crystal nickel electrodes. *Surface Science*, 234(1):87 – 97, 1990.

[55] Amal Suleiman, Christian L. MenÃ©ndez, RamÃ³n Polanco, Esteban Rosim Fachini, Yaritza HernÃ¡ndez-LebrÃ³n, Maxime J.-F. Guinel, Rolando Roque-Malherbe, and Carlos R. Cabrera. Rotating disk slurry electrodeposition of platinum at y-zeolite/carbon vulcan xc-72r for methanol oxidation in alkaline media. *RSC Adv.*, 5:7637–7646, 2015.

[56] Wei Jin, Hao Du, Shili Zheng, Hongbin Xu, and Yi Zhang. Comparison of the oxygen reduction reaction between naoh and koh solutions on a pt electrode: The electrolyte-dependent effect. *The Journal of Physical Chemistry B*, 114(19):6542–6548, 2010.

[57] A. Seghiouer, J. Chevalet, A. Barhoun, and F. Lantelme. Electrochemical oxidation of nickel in alkaline solutions: a voltammetric study and modelling. *Journal of Electroanalytical Chemistry*, 442(1):113 – 123, 1998.

[58] S.A.S. Machado and L.A. Avaca. The hydrogen evolution reaction on nickel surfaces stabilized by h-absorption. *Electrochimica Acta*, 39(10):1385 – 1391, 1994.

[59] W. Visscher and E. Barendrecht. Absorption of hydrogen in reduced nickel oxide. *Journal of Applied Electrochemistry*, 10(2):269–274, Mar 1980.

[60] David S. Hall, Christina Bock, and Barry R. Macdougall. The electrochemistry of metallic nickel: oxides, hydroxides, hydrides and alkaline hydrogen evolution. *Journal of the Electrochemical Society*, 2013.

[61] Wenchao Sheng, Zhongbin Zhuang, Minrui, Jie Zheng, Jingguang G. Chen, and Yushan Yan. Correlating hydrogen oxidation and evolution activity on platinum at different ph with measured hydrogen binding energy. *Nature Communications*, 6, 2017.

Appendix A

Hydrogen evolution

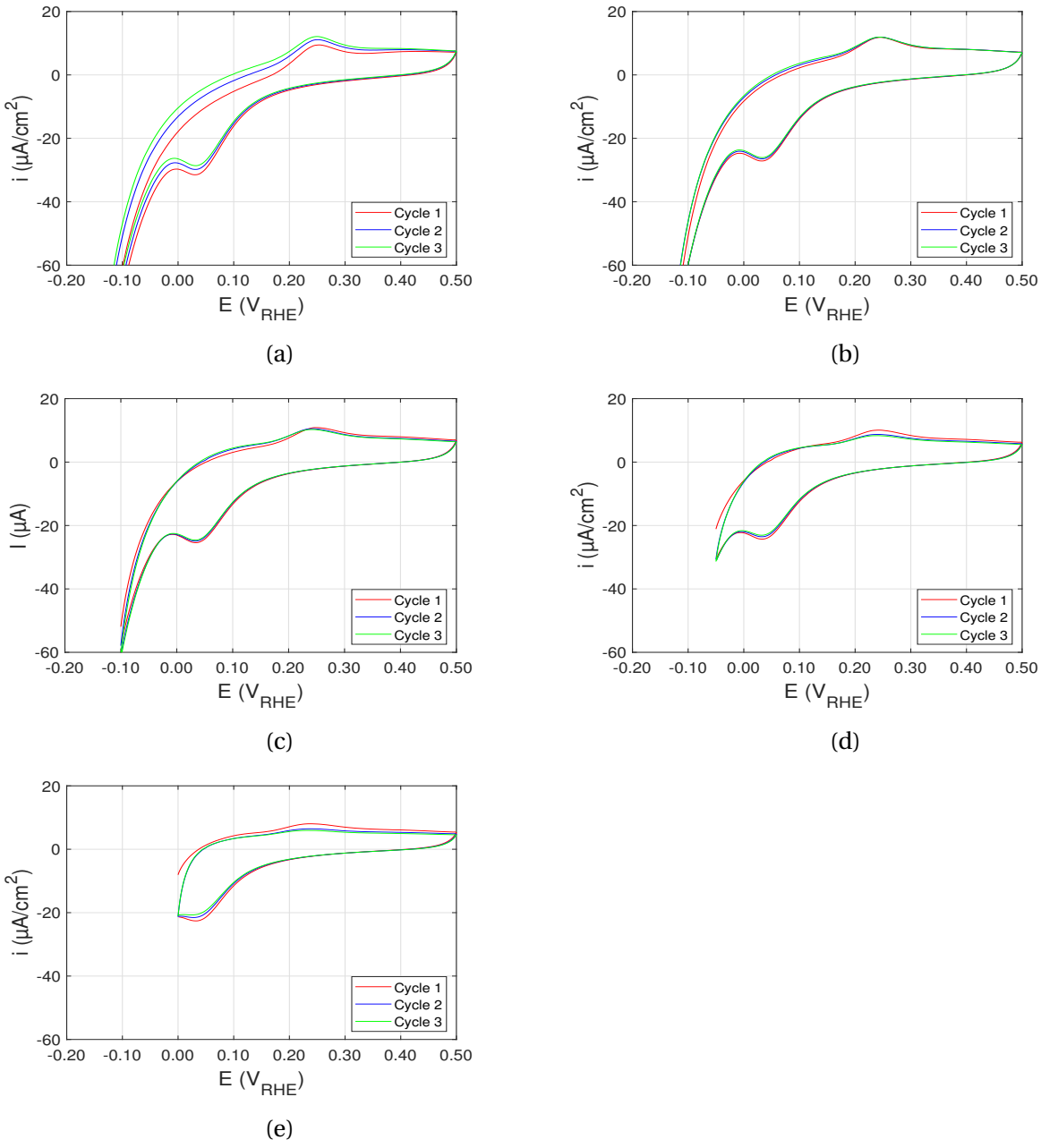

Figure A.0.1: A comparison of CV scans conducted in 0.1M KOH and Ar atmosphere with scan rate ν= 5mVs^{-1} and rotation 1600 rpm. Different potential intervals was used to investigate the hydrogen evolution. The electrode was rotated. a) from -0.2 V to 0.5 V b) from -0.15 V to 0.5 V c) from -0.1 V to 0.5 V d) from -0.05 V to 0.5 V e) from 0 V to 0.5 V

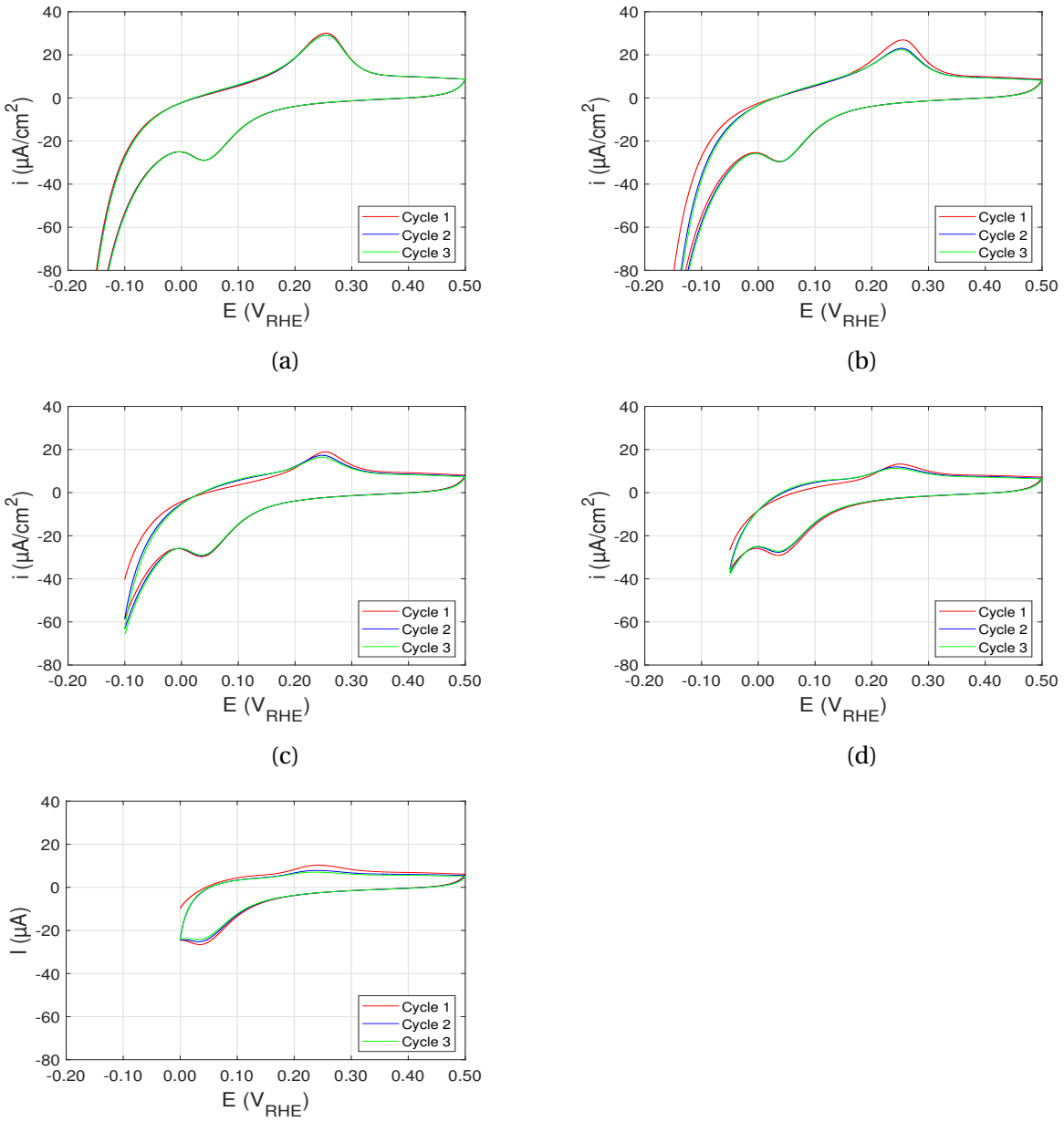

Figure A.0.2: A comparison of CV scans conducted in 0.1M KOH and Ar atmosphere with scan rate ν= 5mVs^{-1}, no rotation. Different potential intervals was used to investigate the hydrogen evolution. a) from -0.2 V to 0.5 V b) from -0.15 V to 0.5 V c) from -0.1 V to 0.5 V d) from -0.05 V to 0.5 V e) from 0 V to 0.5 V

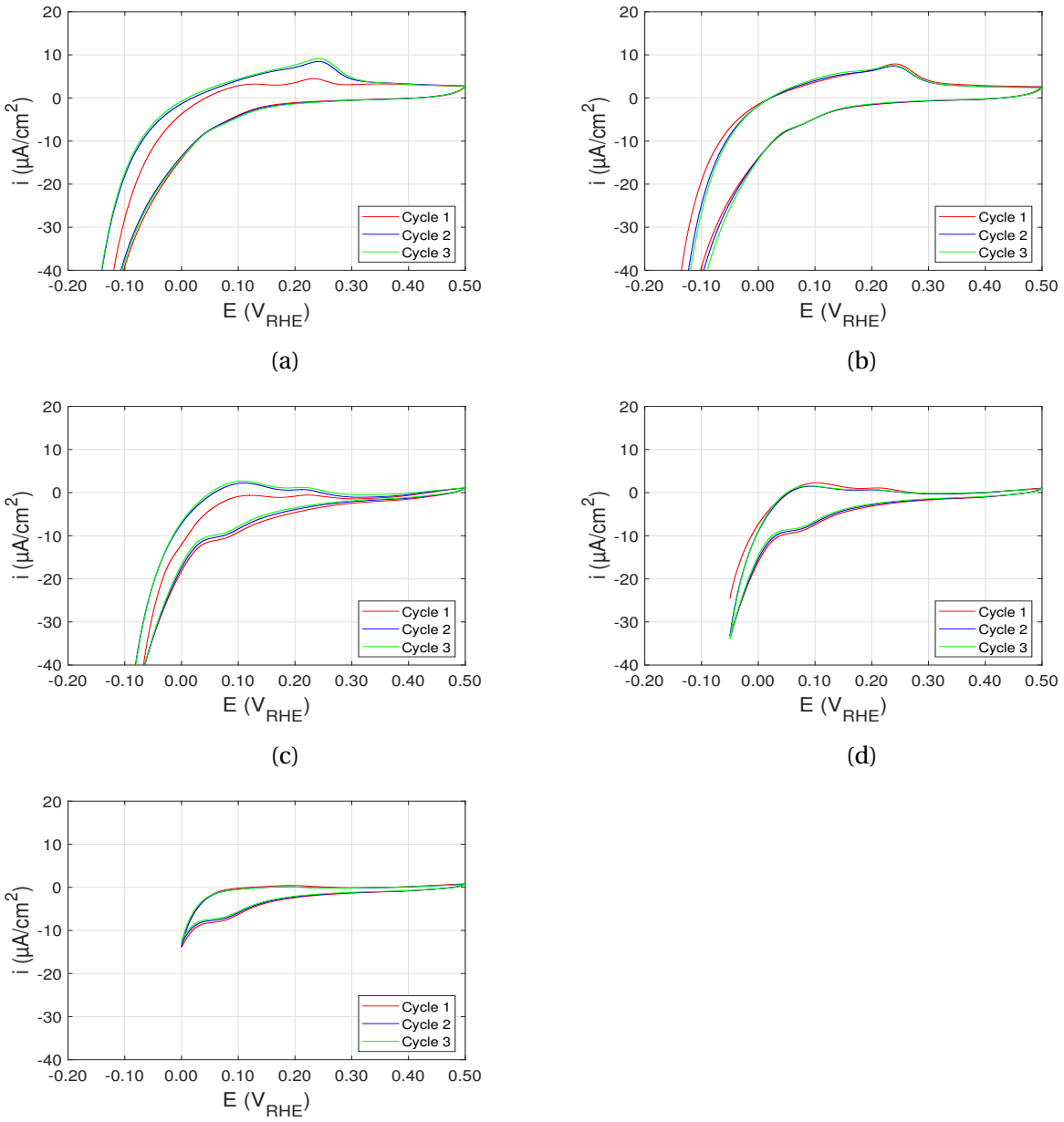

Figure A.0.3: A comparison of CV scans conducted in 0.1M KOH and Ar atmosphere with scan rate ν= 1 mVs^{-1}, no rotation. Different potential intervals was used to investigate the hydrogen evolution. The electrode was rotated. a) from -0.2 V to 0.5 V b) from -0.15 V to 0.5 V c) from -0.1 V to 0.5 V d) from -0.05 V to 0.5 V e) from 0 V to 0.5 V

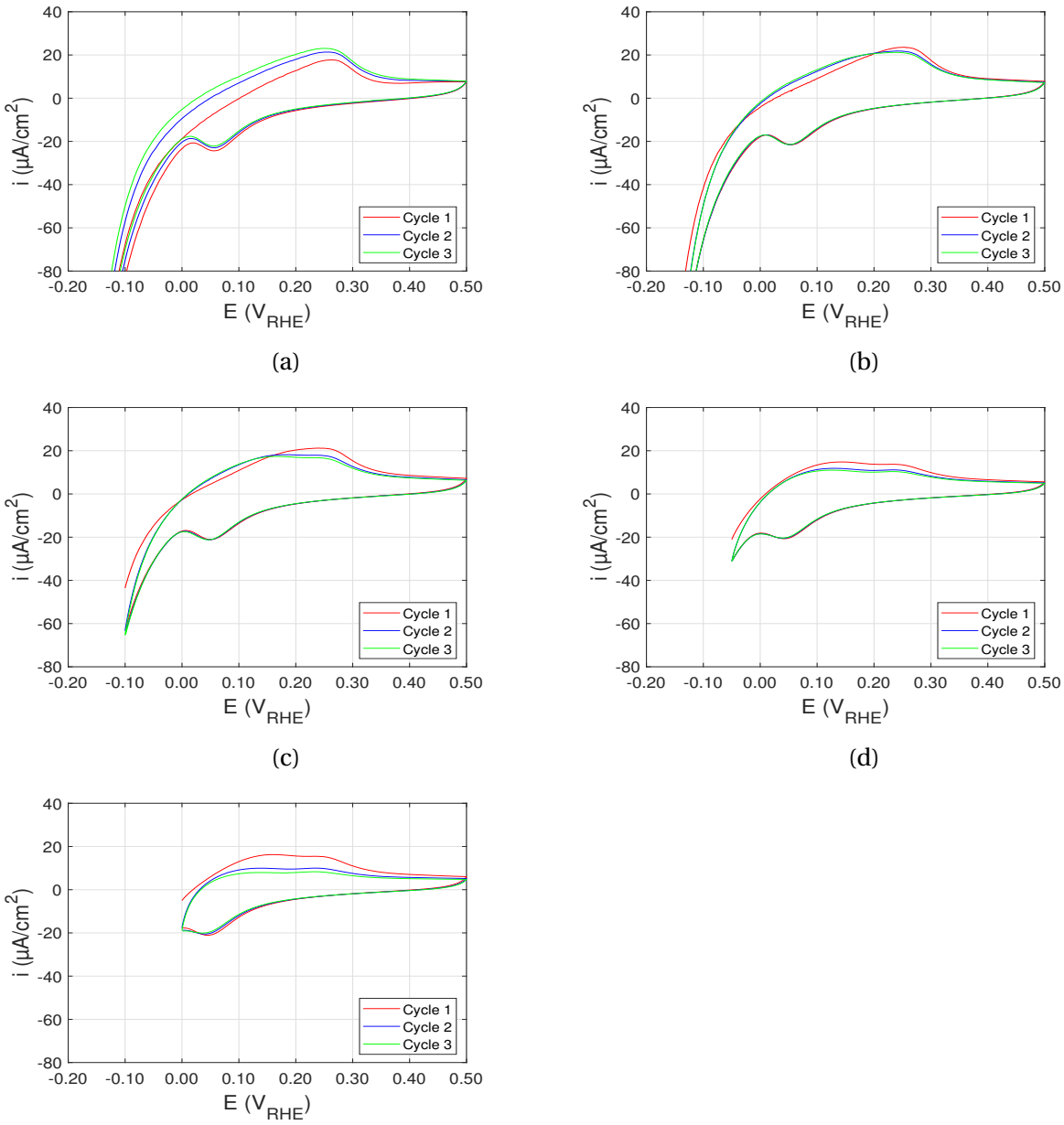

Figure A.0.4: A comparison of CV scans conducted in 0.1M KOH and H_2 atmosphere with scan rate ν= 5mVs^{-1} and rotation 1600 rpm. Different potential intervals was used to investigate the hydrogen evolution. The electrode was rotated. a) from -0.2 V to 0.5 V b) from -0.15 V to 0.5 V c) from -0.1 V to 0.5 V d) from -0.05 V to 0.5 V e) from 0 V to 0.5 V

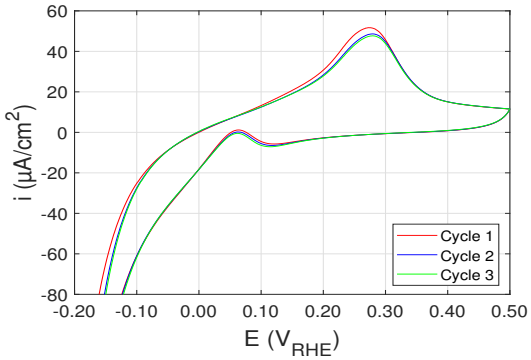

(a)

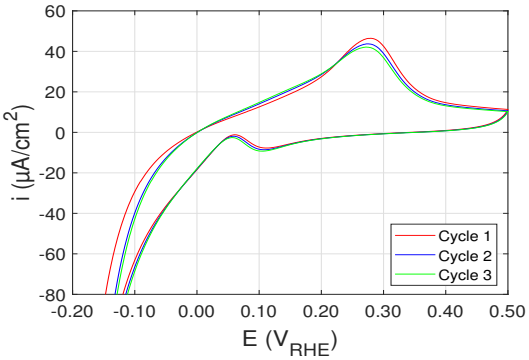

(b)

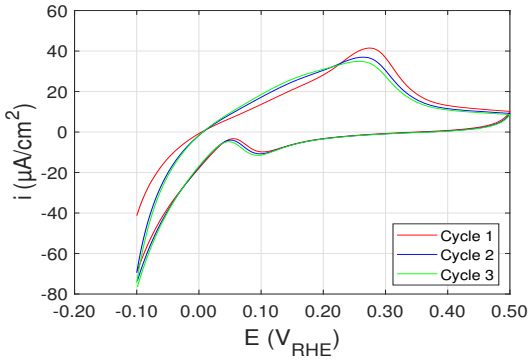

(c)

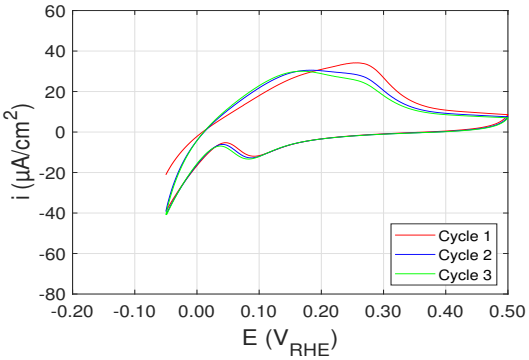

(d)

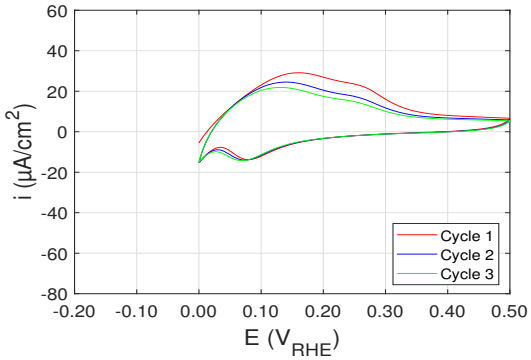

(e)

Figure A.0.5: A comparison of CV scans conducted in 0.1M KOH and H_2 atmosphere with scan rate ν= 5mVs^{-1}, no rotation. Different potential intervals was used to investigate the hydrogen evolution. a) from -0.2 V to 0.5 V b) from -0.15 V to 0.5 V c) from -0.1 V to 0.5 V d) from -0.05 V to 0.5 V e) from 0 V to 0.5 V

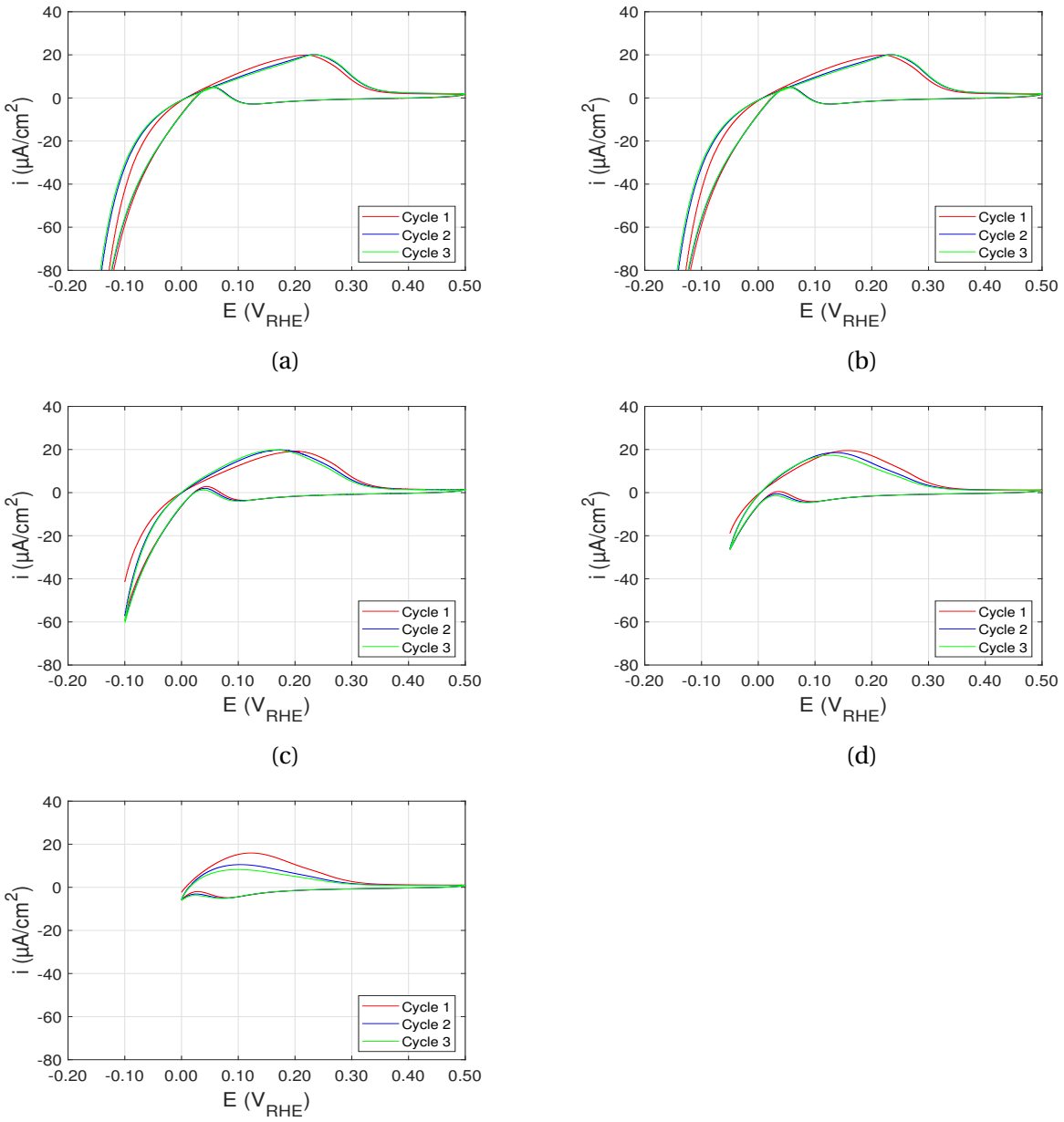

Figure A.0.6: A comparison of CV scans conducted in 0.1M KOH and H_2 atmosphere with scan rate ν= 1mVs^{-1}, no rotation. Different potential intervals was used to investigate the hydrogen evolution. The electrode was rotated. a) from -0.2 V to 0.5 V b) from -0.15 V to 0.5 V c) from -0.1 V to 0.5 V d) from -0.05 V to 0.5 V e) from 0 V to 0.5 V

Appendix B

Simulation

B.1 Coverage

During simulation, the coverage of the species participating in the HOR reaction, equation C.1.7-C.1.11, is investigated. It displays which species has the highest coverage during the forward and backward reaction in the potential range from -0.2 V to 0.5 V, and the green curve is the total coverage. Since a proper simulation has not yet been achieved, figure B.1.1 is not representative of how the coverage behaves.

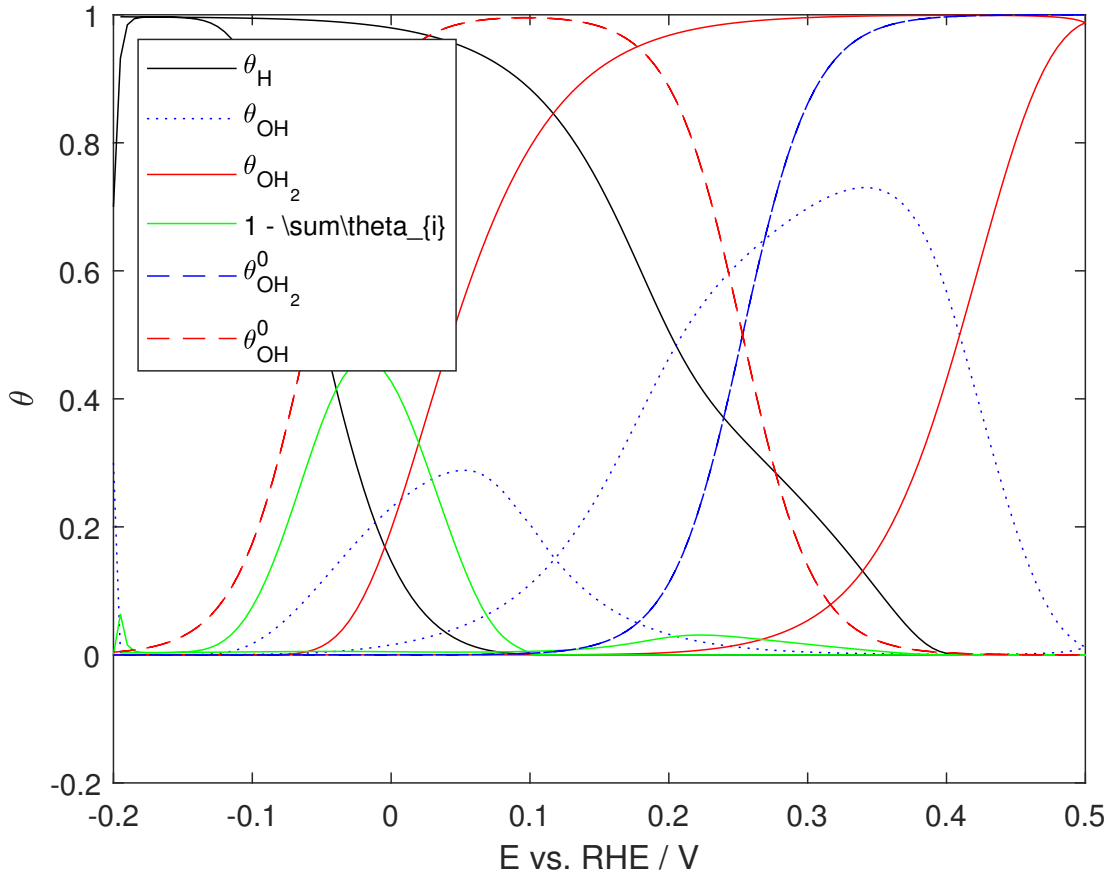

Figure B.1.1: Coverage of participating species in HOR reactions, found in equation C.1.7-C.1.11. This figure gives the relationship of species occupying sites at the electrode surface in the potential range from -0.2 V to 0.5 V. The green line is the total coverage.

B.2 Velocity

Adjusting equilibrium constants, predicting fast and slow reactions, is the key to improve the simulation. By investigating figure B.2.1, it is possible to anticipate whether the forward and backward reactions in equations C.1.2-C.1.6 needs a faster or slower velocity. Figure B.2.1 shows the dimensionless velocities of the HOR, defined in equation C.1.16-C.1.20. There are some issues finding the correct velocities for hydrogen evolution in the potential range form 0.0 V to -0.2 V to achieve a perfect fit in figure 4.3.1. A way of solving this issue is described in section 7 "Further Work".

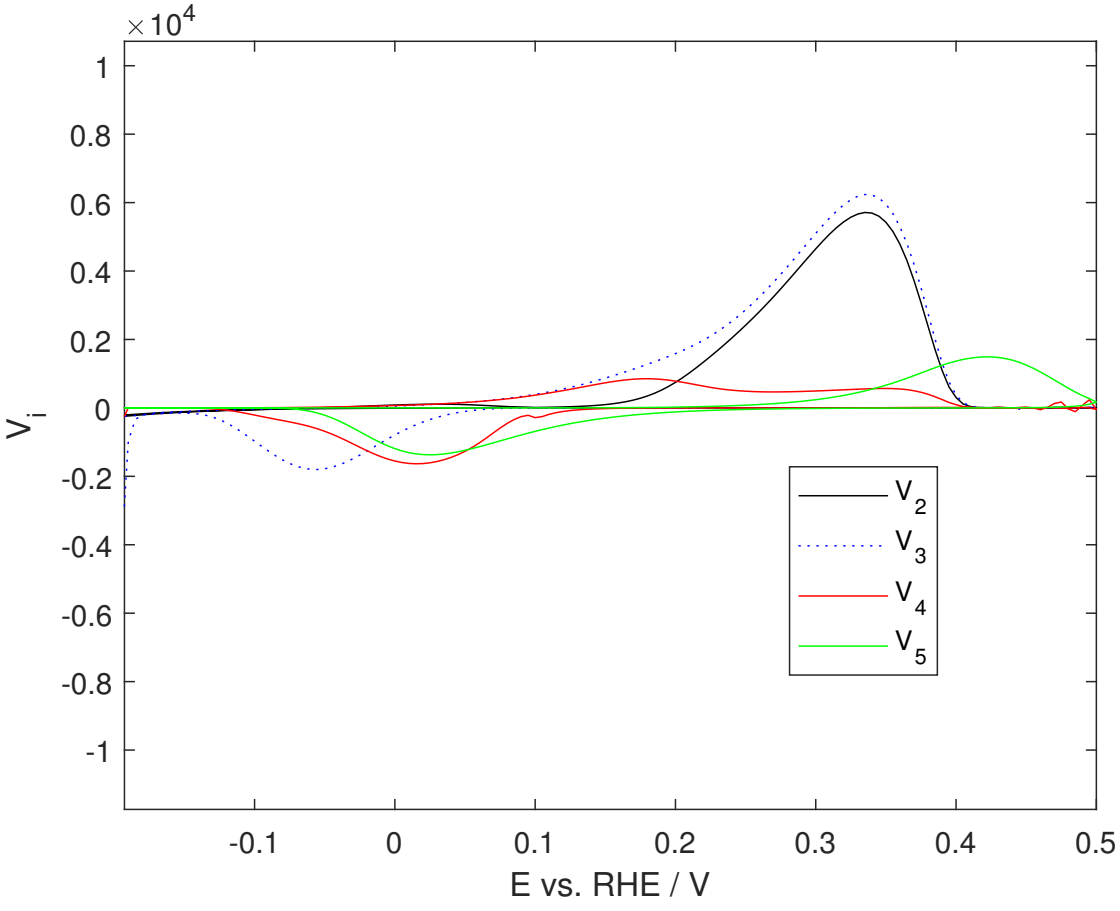

Figure B.2.1

Appendix C

KineticHOR

This section was provided by Professor Svein Sunde[1]

C.1 Model for the HOR at Nickel according to Ref. [1]

C.1.1 Reaction mechanism

$$\mathrm{H_2(aq, y=\infty)} \overset{D_{\mathrm{H_2}}, c_{\mathrm{H_2}}(aq, y=\infty), \Omega}{\rightarrow} \mathrm{H_2(ad)} \tag{C.1.1}$$

where $c_{\mathrm{H_2}}(aq, y=\infty)$ is the bulk concentration of hydrogen, for which we will use the symbol $c^*_{\mathrm{H_2}}$ below.

$$\mathrm{H_2(ad)} \underset{k^0_{-1}}{\overset{k^0_1}{\rightleftharpoons}} \mathrm{2H(ad)} \tag{C.1.2}$$

$$\mathrm{H_2(aq) + OH^-(aq)} \underset{k_{-2}}{\overset{k_2}{\rightleftharpoons}} \mathrm{H(ad) + H_2O(\ell) + e^-} \tag{C.1.3}$$

$$\mathrm{H(ad) + OH^-(aq)} \underset{k_{-3}}{\overset{k_3}{\rightleftharpoons}} \mathrm{H_2O(\ell) + e^-} \tag{C.1.4}$$

[1] The Department of Materials Science and Engineering, NTNU, Trondheim

$$\mathrm{OH^-(aq)} \underset{k_{-4}}{\overset{k_4}{\rightleftharpoons}} \mathrm{OH_{ad} + e^-} \tag{C.1.5}$$

$$\mathrm{OH(ad) + OH^-(aq)} \underset{k_{-5}}{\overset{k_5}{\rightleftharpoons}} \mathrm{(OH)_2\,(ad) + e^-} \tag{C.1.6}$$

C.1.2 Governing equations

We label the coverages, i.e. the number of sites occupied (surface excess) by an adsorbate divided by the total number of available adsorption sites, of H, OH^-, and $(OH)_2$ as θ_1, θ_2, and θ_3, respectively. Thus

$$\begin{aligned}
v_1 &= \Gamma^2 k_1^0 c_{\mathrm{H_2}} (1-\theta_1-\theta_2-\theta_3)^2 - \Gamma^2 k_{-1}^0 \theta_1^2 && \text{(C.1.7)}\\
v_2 &= \Gamma k_2 c_{\mathrm{H_2}} c_{\mathrm{OH^-}} (1-\theta_1-\theta_2-\theta_3) - \Gamma k_{-2}\theta_1 && \text{(C.1.8)}\\
v_3 &= \Gamma k_3 c_{\mathrm{OH^-}} \theta_1 - \Gamma k_{-3} (1-\theta_1-\theta_2-\theta_3) && \text{(C.1.9)}\\
v_4 &= \Gamma k_4 c_{\mathrm{OH^-}} (1-\theta_1-\theta_2-\theta_3) - \Gamma k_{-4}\theta_2 && \text{(C.1.10)}\\
v_5 &= \Gamma k_5 c_{\mathrm{OH^-}} \theta_2 - \Gamma k_{-5}\theta_3 && \text{(C.1.11)}
\end{aligned}$$

where Γ is then the surface excess corresponding to $\theta_\mathrm{i} = 1$. The rate constants are

$$\begin{aligned}
k_\mathrm{i} &= k_\mathrm{i}^0 \exp\left[(1-\alpha_\mathrm{i}) FE/RT\right] \; i = 2\ldots3,5 && \text{(C.1.12)}\\
k_{-\mathrm{i}} &= k_{-\mathrm{i}}^0 \exp\left(-\alpha_\mathrm{i} FE/RT\right) \; i = 2\ldots3,5 && \text{(C.1.13)}
\end{aligned}$$

and

$$\begin{aligned}
k_4 &= k_4^0 \exp\left[\left(1-\alpha_\mathrm{i} FE/RT - \gamma\theta_2/2\right)\right] && \text{(C.1.14)}\\
k_{-4} &= k_{-4}^0 \exp\left(-\alpha_\mathrm{i} FE/RT + \gamma\theta_2/2\right) && \text{(C.1.15)}
\end{aligned}$$

We introduce dimensionless reaction rates

$$V_1 = \frac{v_1}{\Gamma k_5^0 c_{OH^-}} = K_1 (1-\theta_1-\theta_2-\theta_3)^2 - K_{-1}\theta_1^2 \quad \text{(C.1.16)}$$

$$V_2 = \frac{v_2}{\Gamma k_5^0 c_{OH^-}} = K_2 (1-\theta_1-\theta_2-\theta_3) - K_{-2}\theta_1 \quad \text{(C.1.17)}$$

$$V_3 = \frac{v_5}{\Gamma k_5^0 c_{OH^-}} = K_3\theta_1 - K_{-3} (1-\theta_1-\theta_2-\theta_3) \quad \text{(C.1.18)}$$

$$V_4 = \frac{v_4}{\Gamma k_5^0 c_{OH^-}} = K_4 (1-\theta_1-\theta_2-\theta_3) - K_{-4}\theta_2 \quad \text{(C.1.19)}$$

$$V_5 = \frac{v_5}{\Gamma k_5^0 c_{OH^-}} = K_5\theta_2 - K_{-5}\theta_3 \quad \text{(C.1.20)}$$

where

$$K_1 = \frac{\Gamma k_1^0 c_{H_2}}{k_5^0 c_{OH^-}} \tag{C.1.21}$$

$$K_{-1} = \frac{\Gamma k_{-1}^0}{k_5^0 c_{OH^-}} \tag{C.1.22}$$

$$\begin{aligned} K_2 &= \left(\frac{k_2^0 c_{H_2}}{k_5^0}\right) \exp\left[(1-\alpha_2)\,\Delta\right] \\ &= K_2^0 \exp\left[(1-\alpha_2)\,\Delta\right] \end{aligned} \tag{C.1.23}$$

$$K_{-2} = \frac{k_{-2}^0}{k_5^0 c_{OH^-}} \exp\left(-\alpha_2 \Delta\right) = K_{-2}^0 \exp\left(-\alpha_2 \Delta\right) \tag{C.1.24}$$

$$\begin{aligned} K_3 &= \left(\frac{k_3^0}{k_5^0}\right) \exp\left[(1-\alpha_3)\,\Delta\right] \\ &= K_3^0 \exp\left[(1-\alpha_3)\,\Delta\right] \end{aligned} \tag{C.1.25}$$

$$K_{-3} = \frac{k_{-3}^0}{k_5^0 c_{OH^-}} \exp\left(-\alpha_3 \Delta\right) = K_{-3}^0 \exp\left(-\alpha_3 \Delta\right) \tag{C.1.26}$$

$$\begin{aligned} K_4 &= \left(\frac{k_4^0}{k_5^0}\right) \exp\left[(1-\alpha_4)\,\Delta - \left(\gamma/2\right)\theta_2\right] \\ &= K_4^0 \exp\left[(1-\alpha_4)\,\Delta\right. \\ &\quad \left. -\left(\gamma/2\right)\theta_2\right] \end{aligned} \tag{C.1.27}$$

$$\begin{aligned} K_{-4} = \frac{k_{-4}}{k_5^0 c_{OH^-}} = \frac{k_{-4}^0}{k_5^0 c_{OH^-}} \exp\left[-\alpha_4 \Delta + \left(\gamma/2\right)\theta_2\right] &= K_{-4}^0 \\ &\quad \times \exp\left[-\alpha_4 \Delta + \left(\gamma/2\right)\theta_2\right] \end{aligned} \tag{C.1.28}$$

$$K_5 = \exp\left[(1-\alpha_5)\,\Delta\right] \tag{C.1.29}$$

$$K_{-5} = \frac{k_{-5}^0}{k_5^0 c_{OH^-}} \exp\left(-\alpha_5 \Delta\right) = K_{-5}^0 \exp\left(-\alpha_5 \Delta\right) \tag{C.1.30}$$

with $\Delta = FE/RT$.

Note that at the equilibrium potential for the hydrogen evolution and oxidation reaction the rates of reactions (C.1.2) through (C.1.4) implies that $V_1 = 0$, $V_2 = 0$, and $V_3 = 0$. Combining Eqs. (C.1.7), (C.1.8), and (C.1.9) gives

$$\frac{K_{-3}^0}{K_3^0} \exp\left(-\Delta_H\right) = \frac{K_2^0}{K_{-2}^0} \exp\left(\Delta_H\right) = \sqrt{\frac{K_1}{K_{-1}}} \tag{C.1.31}$$

where Δ_{H} is the null potential for the hydrogen reaction.

Similarly, if $\Delta^0_{\mathrm{OH}_2}$ is the *standard* electrode potential for the sum of reaction (C.1.5) and (C.1.6)

$$2\mathrm{OH}^-(\mathrm{aq}) \rightleftharpoons (\mathrm{OH})_2\,(\mathrm{ad}) + 2\mathrm{e}^- \tag{C.1.32}$$

then if $\theta_3 = 1$ rates of reactions (C.1.5) and (C.1.6) are equal to zero at $\Delta^0_{\mathrm{OH}_2}$ (at steady state). From Eq. (C.1.10) and Eq. (C.1.11) we may then obtain

$$1-\theta_3 = \left(\frac{K_{-4}}{K_4}+1\right)\theta_2 \tag{C.1.33}$$

$$\frac{K_5}{K_{-5}} = \frac{\theta_3}{\theta_2} \tag{C.1.34}$$

and

$$\theta_2 = \frac{K_{-5}}{K_5}\theta_3 \tag{C.1.35}$$

$$1 = \left(\frac{K_{-4}}{K_4}+1\right)\frac{K_{-5}}{K_5}\theta_3 + \theta_3 \tag{C.1.36}$$

$$\theta_3 = \frac{1}{\left(\frac{K_{-4}}{K_4}+1\right)\frac{K_{-5}}{K_5}+1} \tag{C.1.37}$$

$$\theta_3 = \frac{1}{\left(\frac{K^0_{-4}}{K^0_4}+1\right)\frac{K^0_{-5}}{K^0_5}+1} \tag{C.1.38}$$

$$\theta_3 = \frac{1}{\left[\frac{K^0_{-4}}{K^0_4}\exp\left(-\Delta+\gamma\theta_2\right)+1\right]\frac{K^0_{-5}}{K^0_5}\exp\left(-\Delta\right)+1} \tag{C.1.39}$$

or since $\theta_3 = 1$ and $\theta_2 = 0$ at $\Delta^0_{\mathrm{OH}_2}$

$$\left[\frac{K^0_{-4}}{K^0_4}\exp\left(-\Delta^0_{\mathrm{OH}_2}\right)+1\right]\frac{K^0_{-5}}{K^0_5}\exp\left(-\Delta^0_{\mathrm{OH}_2}\right) = 0 \tag{C.1.40}$$

and

$$K^0_{-4} = K^0_4\exp\left(\Delta^0_{\mathrm{OH}_2}\right) \tag{C.1.41}$$

For the coverage θ_i we may write

$$\Gamma \frac{d\theta_1}{dt} = 2v_1 + v_2 - v_3 \tag{C.1.42}$$
$$\Gamma \frac{d\theta_2}{dt} = v_4 - v_5 \tag{C.1.43}$$
$$\Gamma \frac{d\theta_3}{dt} = v_5 \tag{C.1.44}$$

or

$$\frac{d\theta_1}{d\tau} = 2V_1 + V_2 - V_3 \tag{C.1.45}$$
$$\frac{d\theta_2}{d\tau} = V_4 - V_5 \tag{C.1.46}$$
$$\frac{d\theta_3}{d\tau} = V_5 \tag{C.1.47}$$

where we have introduced the dimensionless time

$$\tau = t k_5^0 c_{OH^-} \tag{C.1.48}$$

where t is time. A dimensionless sweep rate is thus

$$\nu = \frac{d\Delta}{d\tau} = \frac{F}{k_5^0 c_{OH^-} RT} \frac{dE}{dt} \tag{C.1.49}$$

C.2 Voltammograms in hydrogen-sparged solutions

C.2.1 Current

In the absence of transport limitations the current becomes

$$I = F(v_2 + v_3 + v_4 + v_5) \tag{C.2.1}$$

or

$$\iota = \frac{I}{AF\Gamma k_5^0 c_{\mathrm{OH}}} = V_2 + V_3 + V_4 + V_5 \tag{C.2.2}$$

where we have used Eqs. (C.1.16) through Eq. (C.1.20).

C.3 Voltammograms in argon-sparged solutions

C.3.1 Current

In the absence of transport limitations the current becomes

$$I = F\left(v_4 + v_5\right) \tag{C.3.1}$$

or in the absence of hydrogen

$$\iota = \frac{I}{AF\Gamma k_5^0 c_{\mathrm{OH}}} = \frac{d\theta_2}{d\tau} + 2\frac{d\theta_3}{d\tau} \tag{C.3.2}$$

C.4 Irreversible adsorption of OH

We consider now reaction (C.1.5) to be dominating, such as will be the case in the absence of hydrogen and in the low potential range

$$v_4 \approx \Gamma k_4 c_{\mathrm{OH^-}} \left(1 - \theta_2\right) \tag{C.4.1}$$

where we have also neglected the reverse reaction. We assume the current to stem from this reaction alone, so that

$$\iota_4 \approx K_4 \left[1 - \theta_2\left(\tau\right)\right] \tag{C.4.2}$$

in dimensionless form.

Starting the positive-going sweep at the initial potential Δ_i

$$\frac{d\theta_2}{d\tau} \approx K_4 \left[1-\theta_2(\tau)\right] \tag{C.4.3}$$

$$\int_{1-\theta_2(0)}^{1-\theta_2(\tau)} \frac{d(1-\theta_2)}{(1-\theta_2)} \approx -\int_0^{\tau} K_4^0 \exp\left\{(1-\alpha_4)(\Delta_i+\nu\tau)\right\} d\tau \tag{C.4.4}$$

$$\ln\left[1-\theta_2(\tau)\right]-\ln\left[1-\theta_2(0)\right] \approx -\frac{1}{(1-\alpha_4)\nu} K_4^0 \exp\left\{(1-\alpha_4)(\Delta_i+\nu\tau)\right\}+\frac{1}{(1-\alpha_4)\nu} K_4^0 \exp\left\{(1-\alpha_4)(\Delta_i)\right\} \tag{C.4.5}$$

$$\ln\left[1-\theta_2(\tau)\right] \approx -\frac{K_4(\tau)}{(1-\alpha_4)\nu}+\frac{1}{(1-\alpha_4)\nu} K_4^0 \exp\left\{(1-\alpha_4)(\Delta_i)\right\} \tag{C.4.6}$$

$$\ln\left[1-\theta_2(\tau)\right] \approx -\frac{K_4(\tau)}{(1-\alpha_4)\nu}+\frac{K_4(0)}{(1-\alpha_4)\nu} \tag{C.4.7}$$

$$\left[1-\theta_2(\tau)\right] \approx \exp\left[-\frac{K_4(\tau)}{(1-\alpha_4)\nu}+\frac{K_4(0)}{(1-\alpha_4)\nu}\right] \tag{C.4.8}$$

Then, with Eq. (C.4.2)

$$\iota_4 \approx K_4(\tau) \exp\left[-\frac{K_4(\tau)-K_4(0)}{(1-\alpha_4)\nu}\right] \tag{C.4.9}$$

where we have assumed that $1-\theta_2(0)=1$ (at $\Delta=\Delta_i$).

The current is maximum at

$$\frac{\partial \iota_4}{\partial \tau} \approx \frac{\partial K_4(\tau)}{\partial \tau} \exp\left[-\frac{K_4(\tau)-K_4(0)}{(1-\alpha_4)\nu}\right] - \frac{1}{(1-\alpha_4)\nu} K_4(\tau) \frac{\partial K_4(\tau)}{\partial \tau} \exp\left[-\frac{K_4(\tau)-K_4(0)}{(1-\alpha_4)\nu}\right] = 0 \tag{C.4.10}$$

or

$$K_4(\tau) = (1-\alpha_4)\nu \tag{C.4.11}$$

and

$$K_4^0 \approx (1-\alpha_4)\,\nu \exp\left\{-(1-\alpha_4)\,\Delta_{\mathrm{p4}}\right\} \tag{C.4.12}$$

Starting the negative-going sweep at the vertex potential Δ_{v}

$$\frac{d\theta_2}{d\tau} \approx -K_{-4}\theta_2 \tag{C.4.13}$$

$$\int_{\theta_2(\tau_{\mathrm{v}})}^{\theta_2(\tau)} \frac{d\theta_2}{\theta_2} \approx -\int_{\tau_{\mathrm{v}}}^{\tau} K_{-4}^0 \exp\left\{-\alpha_4\left(\Delta_{\mathrm{v}}-\nu\tau\right)\right\} d\tau \tag{C.4.14}$$

$$\ln\theta_2(\tau) - \ln\theta_2(\tau_{\mathrm{v}}) \approx -\frac{1}{\alpha_4\nu}K_{-4}^0 \exp\left\{-\alpha_4\left(\Delta_{\mathrm{i}}+2\nu\tau_{\mathrm{v}}-\nu\tau\right)\right\} + \frac{1}{\alpha_4\nu}K_{-4}^0 \exp\left\{-\alpha_4\left(\Delta_{\mathrm{v}}\right)\right\} \tag{C.4.15}$$

$$\ln\theta_2(\tau) \approx -\frac{K_{-4}}{\alpha_4\nu} + \frac{1}{\alpha_4\nu}K_{-4}^0 \exp\left\{-\alpha_4\left(\Delta_{\mathrm{v}}\right)\right\} \tag{C.4.16}$$

$$\ln\theta_2(\tau) \approx -\frac{K_{-4}(\tau) - K_{-4}(\tau_{\mathrm{v}})}{\alpha_4\nu} \tag{C.4.17}$$

$$\iota_{-4} = -K_{-4}\theta_2(\tau) \approx -K_{-4}\exp\left\{-\frac{K_{-4}(\tau)-K_{-4}(\tau_{\mathrm{v}})}{\alpha_4\nu}\right\} \tag{C.4.18}$$

where we have assumed that $\theta_2(\tau_{\mathrm{v}}) = 1$ (at $\Delta = \Delta_{\mathrm{v}} = \Delta_{\mathrm{i}} + \nu\tau_{\mathrm{v}}$).

The current in Eq. (C.4.18) peaks at

$$\frac{\partial K_{-4}(\tau)}{\partial\tau}\exp\left\{-\frac{K_{-4}(\tau)-K_{-4}(\tau_{\mathrm{v}})}{\alpha_4\nu}\right\} - \frac{1}{\alpha_4\nu}K_{-4}\frac{\partial K_{-4}(\tau)}{\partial\tau}\exp\left\{-\frac{K_{-4}(\tau)-K_{-4}(\tau_{\mathrm{v}})}{\alpha_4\nu}\right\} = 0 \tag{C.4.19}$$

$$K_{-4}^0 = \alpha_4\nu\exp\left(\alpha_4\Delta_{-\mathrm{p4}}\right) \tag{C.4.20}$$

C.5 Irreversible adsorption of $(OH)_2$

For the positive-going sweep and with Eq. (C.4.8),

$$\frac{d\theta_3}{d\tau} = V_5 \approx K_5\theta_2 \approx K_5\left\{1-\exp\left[-\frac{K_4(\tau)}{(1-\alpha_4)\nu}+\frac{K_4(0)}{(1-\alpha_4)\nu}\right]\right\} \tag{C.5.1}$$

For the negative-going sweep, in analogy with Eq. (C.4.18)

$$\iota_{-5} = -K_{-5}\theta_3(\tau) \approx -K_{-5}\exp\left\{-\frac{K_{-5}(\tau)-K_{-5}(\tau_v)}{\alpha_5\nu}\right\} \tag{C.5.2}$$

This current peaks at Δ_{-p5} and

$$\frac{\partial K_{-5}(\tau)}{\partial\tau}\exp\left\{-\frac{K_{-5}(\tau)-K_{-5}(\tau_v)}{\alpha_5\nu}\right\}-\frac{1}{\alpha_5\nu}\frac{\partial K_{-5}(\tau)}{\partial\tau}\exp\left\{-\frac{K_{-5}(\tau)-K_{-5}(\tau_v)}{\alpha_5\nu}\right\}=0 \tag{C.5.3}$$

$$1-\frac{K_{-5}}{\alpha_5\nu}=0 \tag{C.5.4}$$

$$K_{-5}=\alpha_5\nu \tag{C.5.5}$$

$$\alpha_5\nu = \frac{k^0_{-5}}{k^0_5 c_{OH^-}}\exp\left(-\alpha_5\Delta_{-p5}\right) \tag{C.5.6}$$

$$k^0_{-5} = k^0_5 c_{OH^-}\alpha_5\nu\exp\left(\alpha_5\Delta_{-p5}\right) \tag{C.5.7}$$

C.6 Irreversible adsorption of OH and OH_2

We now assume the simultaneous, irreversible adsorption of both species OH and OH_2 at the surface. The relevant reactions rates are

$$V_4 = \frac{\upsilon_4}{\Gamma k_5^0 c_{OH^-}} \approx K_4 (1-\theta_2-\theta_3) \tag{C.6.1}$$

$$V_5 = \frac{\upsilon_5}{\Gamma k_5^0 c_{OH^-}} \approx K_5 \theta_2 \tag{C.6.2}$$

For the coverage θ_i we obtain

$$\frac{d\theta_2}{d\tau} \approx K_4 (1-\theta_2-\theta_3) \tag{C.6.3}$$

$$\frac{d\theta_3}{d\tau} \approx K_5 \theta_2 \tag{C.6.4}$$

Differentiating Eq. (C.6.3) and inserting Eq. (C.6.4) for $d\theta_3/d\tau$ gives

$$\frac{d^2\theta_2}{d\tau^2} \approx -K_4 \frac{d\theta_2}{d\tau} + K_4 K_5 \theta_2 \tag{C.6.5}$$

and use of Eq. (C.1.27) and (C.1.29) gives

$$\frac{d^2\theta_2}{d\tau^2} \approx -K_4^0 \exp\left[(1-\alpha_4)\Delta\right] \frac{d\theta_2}{d\tau} + K_4 \exp\left[(1-\alpha_5)\Delta\right] \theta_2 \tag{C.6.6}$$

$$\frac{d^2\theta_2}{d\tau^2} \approx -K_4^0 \exp\left[(1-\alpha_4)(\Delta_i+\nu\tau)\right] \frac{d\theta_2}{d\tau} + \\ + K_4^0 \exp\left[(1-\alpha_4)(\Delta_i+\nu\tau)\right] \exp\left[(1-\alpha_5)(\Delta_i+\nu\tau)\right] \theta_2 \tag{C.6.7}$$

$$\frac{d^2\theta_2}{d\tau^2} \approx -a' \exp\left[(1-\alpha_4)\nu\tau\right] \frac{d\theta_2}{d\tau} + b' \exp\left[(2-\alpha_4-\alpha_5)\nu\tau\right] \theta_2 \tag{C.6.8}$$

where we have set γ to zero as an approximation in order to achieve an analytical solution. Δ_i is the initial potential before the sweep commences. The constants a' and b' are implicitly defined by Eqs. (C.6.7) and (C.6.8).

Laplace-transforming Eq. (C.6.8) gives

$$s^2 \mathscr{L}\{\theta_2\}(s) - s\theta_2(0) - \frac{d\theta_2}{d\tau}(0) = -a'\left[s\mathscr{L}\{\theta_2\}(s-[1-\alpha_4]) - \theta_2(0)\right] + b'\mathscr{L}\{\theta_2\}(s-[1-\alpha_4-\alpha_5]) \tag{C.6.9}$$

where we have replaced the approximation sign with an equality sign to simplify notation.

C.7 Charge-transfer resistance in hydrogen-sparge solutions

We neglect the contribution to the current from Eq. (C.1.7), and at the equilibrium potential $\upsilon_2 = \upsilon_3 = 0$. Then

$$\frac{\upsilon_2(E_\mathrm{n})}{\Gamma} = k_2^0 \exp\left[(1-\alpha_\mathrm{i})FE_\mathrm{n}/RT\right] c_{\mathrm{H_2}} c_{\mathrm{OH^-}} (1-\theta_1) - k_{-2}^0 \exp\left(-\alpha_\mathrm{i} FE_\mathrm{n}/RT\right)\theta_1 = 0 \tag{C.7.1}$$

$$\frac{\upsilon_3(E_\mathrm{n})}{\Gamma} = k_3 c_{\mathrm{OH^-}}\theta_1 - k_{-3}(1-\theta_1) \tag{C.7.2}$$

where

$$E_\mathrm{n} = -\frac{RT}{2F}\ln\left\{\frac{1}{c_{\mathrm{H_2}} c_{\mathrm{OH^-}}^2}\right\} \tag{C.7.3}$$

and where we have approximated the activities as concentrations if in mol dm^{-3} and set $a_{\mathrm{H_2O}} = 1$.

and solve Eq. (C.1.9) for θ_1

$$\theta_1 = \frac{\upsilon_3 + \Gamma k_{-3}}{\Gamma k_3 c_{\mathrm{OH^-}} + \Gamma k_{-3}} \tag{C.7.4}$$

where we have also assumed $\theta_2 = 0$ and $\theta_3 = 0$ in the potential region close to zero vs. RHE. Substituting Eq. (C.7.4) into Eq. (C.1.8) gives

$$\upsilon_2 = \Gamma k_2 c_{\mathrm{H_2}} c_{\mathrm{OH^-}} \left\{1 - \left[\frac{\upsilon_2 + \Gamma k_{-3}}{\Gamma k_3 c_{\mathrm{OH^-}} + \Gamma k_{-3}}\right]\right\} - \Gamma k_{-2}\left[\frac{\upsilon_2 + \Gamma k_{-3}}{\Gamma k_3 c_{\mathrm{OH^-}} + \Gamma k_{-3}}\right] \tag{C.7.5}$$

where we have set $\upsilon_3 = \upsilon_2$, which is exact in steady state and approximately true at low scan rates.

$$\upsilon_2\left\{1 + \frac{k_2 c_{\mathrm{H_2}} c_{\mathrm{OH^-}} + k_{-2}}{k_3 c_{\mathrm{OH^-}} + k_{-3}}\right\} = \Gamma k_2 c_{\mathrm{H_2}} c_{\mathrm{OH^-}} \left\{1 - \left[\frac{k_{-3}}{k_3 c_{\mathrm{OH^-}} + k_{-3}}\right]\right\} - \Gamma k_{-2}\left[\frac{k_{-3}}{k_3 c_{\mathrm{OH^-}} + k_{-3}}\right] \tag{C.7.6}$$

$$v_2\left\{1+\frac{k_2 c_{H_2} c_{OH^-}+k_{-2}}{k_3 c_{OH^-}+k_{-3}}\right\}=\Gamma k_2 c_{H_2} c_{OH^-}-\Gamma\left(k_2 c_{H_2} c_{OH^-}+k_{-2}\right)\left(\frac{k_{-3}}{k_3 c_{OH^-}+k_{-3}}\right) \tag{C.7.7}$$

$$v_2\left\{k_3 c_{OH^-}+k_{-3}+k_2 c_{H_2} c_{OH^-}+k_{-2}\right\}=\Gamma k_2 c_{H_2} c_{OH^-}\left(k_3 c_{OH^-}+k_{-3}\right)-\Gamma k_{-3}\left(k_2 c_{H_2} c_{OH^-}+k_{-2}\right) \tag{C.7.8}$$

$$v_2=\frac{\Gamma k_2 c_{H_2} c_{OH^-}\left(k_3 c_{OH^-}+k_{-3}\right)-\Gamma k_{-3}\left(k_2 c_{H_2} c_{OH^-}+k_{-2}\right)}{k_3 c_{OH^-}+k_{-3}+k_2 c_{H_2} c_{OH^-}+k_{-2}} \tag{C.7.9}$$

and the current is

$$i=2Fv_2=2F\Gamma\frac{k_2 c_{H_2} c_{OH^-}\left(k_3 c_{OH^-}+k_{-3}\right)-k_{-3}\left(k_2 c_{H_2} c_{OH^-}+k_{-2}\right)}{k_3 c_{OH^-}+k_{-3}+k_2 c_{H_2} c_{OH^-}+k_{-2}} \tag{C.7.10}$$

where now the rate constants are to be linearized as

$$k_i = k_i^0 \exp\left[(1-\alpha_i)FE/RT\right] \approx k_{-i}^0\left[1+\frac{(1-\alpha_i)FE}{RT}\right];\ i=2,3 \tag{C.7.11}$$

$$k_{-i} = k_{-i}^0 \exp\left(-\alpha_i FE/RT\right) \approx k_{-i}^0\left[1-\frac{\alpha_i FE}{RT}\right];\ i=2,3 \tag{C.7.12}$$

Appendix D

MATLAB code

D.1 Simulation of Voltammogram for Hydrogen Oxidation at Nickel

```
%*************************************************************************
%                                                                        *
%          SIMULATION OF VOLTAMMOGRAM FOR HYDROGEN OXIDATION             *
%                              AT NICKEL                                 *
%                                                                        *
%                                 Svein Sunde                            *
%                NTNU, Sem Saelands veg 12, NO-7491 Trondheim            *
%                             Ver. Jan 25, 2018                          *
%                                                                        *
%       References:                                                      *
%       [1] S. Kabir et al. J. Mater. Chem. A, 5 (2017) 24443            *
%       [2] S. Kabir et al. J. Mater. Chem. A, 5 (2017) 24443, ESI       *
%       [3] S. Schittkowski, "Numerical Data Fitting in Dynamical        *
%           Systems", Springer (2002), pp. 43 - 45                       *
%                                                                        *
```

```
%       Uses: ode23tb.m or ode45.m, dthetadt.m                          *
%                                                                       *
%***********************************************************************
clear all;
global Deli Delta vsweep nusweep aOH tlambda gamma V1 V2 V3 V4 V5 ...
    alpha2 alpha3 alpha4 alpha5 T Gamma iota1 iota2 iota3 iota iotaexp ...
    expi expot plotCoverages p00 isim1 isim2 isim3 timet

%***********************************************************************
%Constants:
%***********************************************************************
Faraday=96485;%Faradays number, C/mol
R = 8.31434;%Gas constant, J/K mol
Temp = 298;%K
NA = 6.022e23;%1/mol
eVtoJ = 0.1602e-18;%J/eV
%***********************************************************************
%Experimental data:
%***********************************************************************
filename = 'Ni-H2-CV-0.5V-20mvs.xlsx';
A = xlsread(filename);
expot = A(:,1); %contains experimental potential in volt
expi = A(:,6)/0.196; %contains experimental current in mA cm^-2
clear A;
%***********************************************************************
%Experimental sweep parameters:
%***********************************************************************
Ei = min(expot);%-0.2;%Initial potential, V (RHE)
Ev = max(expot);%0.5;%Vertex potential, V (RHE)
% vsweep = input('Sweep rate (mV/s) = ');
```

```
vsweep = 5;%Sweep rate, mV/s
vsweep = vsweep * 1e-3;%Sweep rate, V/s
Ttot = 2*(Ev-Ei)/vsweep;
lengthdata = size(expot);
kk=1;
A(kk,1) = expot(1);
A(kk,2) = expi(1);
for ii=2:lengthdata(1)
    if (isnan(expot(ii))==0 && isnan(expi(ii))==0)&& ...
            (abs(expot(ii)-expot(ii-1))>1e-8)
        kk = kk + 1;
        A(kk,1) = expot(ii);
        A(kk,2) = expi(ii);
    end
end
clear expot expi;
expot= A(:,1);
expi= A(:,2);

%************************************************************************
%Default parameters from Ref. [1,2], Table S1, Nipc values default:
%************************************************************************
aH2 =    7e-7;%mol cm^-3 (stated in M in [2], but units do not match)
aOH =    1e-4;%mol cm^-3 (stated in M in [2], but units do not match)
Gamma =  2.2e-9;%mol cm^-2
alpha2 = 0.4;
alpha3 = 0.5;
alpha4 = 0.5;%Missing from the reference [2]
alpha5 = 0.5;%Missing from the reference [2]
k10 =    3.94e7;%cm^3 / s mol
```

```
km10 =   0.01;%/1/s
k20 =    8.0e9;%cm^6 / s mol
km20 =   0.01;%/1/s
k30 =    30;%cm^3 / s mol
km30 =   0.1;%/1/s
k40 =    99.1628;%cm^3 / s mol
km40 =   1.3551%/1/s
E40 =    0.06;%V, not used
k50 =    0.4899;%cm^3 / s mol
km50 =   0.2689;%/1/s
E50 =    0.18;%V, not used
gamma =  0.1;%Frumkin parameter
%************************************************************************
%Revised parameters:
%************************************************************************
Gamma =  0.2e-8;%mol cm^-2
k20 =    1.4e6;%cm^6 / s mol %12
km20 =   0.0007%/1/s         %0.05
k30 =    9.5;%cm^3 / s mol %50
km30 =   0.007;%/1/s        %0.5
k40 =    25;%cm^3 / s mol
km40 =   0.36;%/1/s
k50 =    0.13;%cm^3 / s mol  %1.6
km50 =   0.07;%/1/s          %0.8
%************************************************************************
%Dimensionless parameters
%************************************************************************
p0    = zeros(9,1);
p0(1) = Gamma*k10*aH2/k50/aOH;
p0(2) = Gamma*km10/k50/aOH;
```

```
p0(2) = k20*aH2/k50;
p0(4) = km20/k50/aOH;
p0(3) = k30/k50;
p0(4) = km30/k50/aOH;
p0(5) = k40/k50;
p0(6) = km40/k50/aOH;
p0(7) = k50;
p0(8)= km50/k50/aOH;
p0(9) = gamma;
%************************************************************************
%Find the time for each potential
%************************************************************************
for ii=1:length(expot)
    if ii==1
        t(ii) = 0;
    elseif expot(ii)>expot(ii-1)
        t(ii) = (expot(ii)-expot(1))/vsweep;
        Emax = expot(ii);
        tmax = t(ii);
    else
        t(ii) = tmax - (expot(ii)-Emax)/vsweep;
    end
    if ii>1 && t(ii)-t(ii-1)<1e-6
        str=['Not strictly increasing time: ', num2str(expot(ii)),', ' ...
            ,num2str(expot(ii-1))];
        disp(str);
    end
    T(ii) = t(ii)*p0(7)*aOH;
end
```

```
timet = t;

plotCoverages = false;
%Initial plot
isim0 = cvHORkin(p0,t);
%**************************************************************************
%Fit dimensionless current and plot results
%**************************************************************************
% fitornot=menu('Fit?','Yes','No');
fitornot=1;
if fitornot==1

    options = saoptimset('PlotFcns',{@saplotbestx,...
        @saplotbestf,@saplotx,@saplotf},...
        'InitialTemperature',500,'MaxIter',500);
    ObjectiveFunction = @cvHORkinLsqObjFun;

    lb = 1e-3*p0;
    ub = 1e3*p0;
    [p1,fval,exitflag,output] = simulannealbnd(ObjectiveFunction,p0,...
        lb,ub,options);
    %Final plot
    plotCoverages = true;
    isim1 = cvHORkin(p1,t);

    %Plot after fitting
    figure(1);
    title('Current');
    grid on;
    box on;
```

```
    plot(expot,isim0,'-g',expot,isim1,'-b',expot,expi,'-r');
    legend('i_{sim}^0 \mu A/cm^2','i_{sim} \mu A/cm^2','i_{exp} \mu A/cm^2' ...
        ,'Location','SouthEast');
    xlabel('E / V');
    ylabel('i_{sim} A/cm^2');
    axis([min(expot) max(expot) min(expi) max(max(expi),max(isim1))]);
    str = ['[',num2str(p1(1)),';',num2str(p1(2)),';',num2str(p1(3)),';',...
        num2str(p1(4)),';',num2str(p1(5)),';',num2str(p1(6)),';',...
        num2str(p1(7)),';',num2str(p1(8)),';',num2str(p1(9)),']'];
    fid=fopen('fitresult.dat','a+');
    if fid>0
        fprintf(fid,'%6e\n',p1);
        fclose(fid);
    end
    string=sprintf('%6e\n',p1);
    disp(string);
    string = ['[',num2str(p1(1)),';',num2str(p1(2)),';',num2str(p1(3)),';'...
        ,num2str(p1(4)),';',num2str(p1(5)),';',num2str(p1(6)),';'...
        ,num2str(p1(7)),';',num2str(p1(8)),';',num2str(p1(9)),']']
    disp(string);
else
    figure(1);
    title('Current');
    grid on;
    box on;
    if plotCoverages
        plot(expot,isim0,'-r',expot,isim1,'--k',expot,isim2,'-.m',...
            expot,isim3,':c',expot,expi,'-b');
        legend('i_{sim}^0 \mu A/cm^2','i_{H_2} \mu A/cm^2','i_{OH} \mu A/cm^2',...
            'i_{OH_2} \mu A/cm^2','i_{exp} \mu A/cm^2','Location','SouthEast');
```

```
    else
        plot(expot,isim0,'-r',expot,expi,'-b');
        legend('i_{sim}^0 \mu A/cm^2','i_{exp} \mu A/cm^2','Location','SouthEast');
    end
    xlabel('E / V');
    ylabel('i_{sim} A/cm^2');
end

%***************************END*****************************************
```

D.2 Plotting Coverage

```
function isim = cvHORkin(p0,t)

global Deli Delta vsweep nusweep aOH tlambda gamma V1 V2 V3 V4 V5 ...
    alpha2 alpha3 alpha4 alpha5 T Gamma iota1 iota2 iota3 iota iotaexp ...
    expi expot plotCoverages p00 isim1 isim2 isim3 timet

    %**************************************************************************
    %Constants:
    %**************************************************************************
    Faraday=96485;%Faradays number, C/mol
    R = 8.31434;%Gas constant, J/K mol
    Temp = 298;%K
    NA = 6.022e23;%1/mol
    eVtoJ = 0.1602e-18;%J/eV
    %**************************************************************************
    %Dimensionless parameters:
    %**************************************************************************

    %Dimensionless sweep rate
    nusweep = Faraday*vsweep/R/Temp/p0(7)/aOH;

    %Dimensionless time
    for ii=1:length(t)
        Delta(ii) = expot(ii)*Faraday/R/Temp;
        T(ii) = t(ii)*p0(7)*aOH;
    end
    Deli = Delta(1);%Initial potential
```

```
%Dimensionless experimental current
for ii=1:length(expot)
    iotaexp(ii) = expi(ii)/Faraday/Gamma/p0(7)/aOH;
end

%**************************************************************************
%Solve differential equations for theta
%**************************************************************************
y0 = zeros(3,1);
if Deli<0
    y0(1) = .7;%A high coverage is expected below 0V.
    y0(2) = .3;%A high coverage is expected below 0V.
end
p00    = zeros(11,1);
p00(1) = p0(1);
p00(2) = p0(1)*(p0(3)/p0(4))^2;
p00(3) = p0(2);
p00(4) = p0(2)*p0(3)/p0(4);
p00(5) = p0(3);
p00(6) = p0(4);
p00(7) = p0(5);
p00(8) = p0(6);
p00(9) = p0(7);
p00(10)= p0(8);
p00(11)= p0(9);
options = odeset('RelTol',1e-4,'AbsTol',1e-4,'Jacobian','JacobianThetadt');
o = odeget(options,'Jacobian');
[T,theta] = ode15s(@dthetadtHOR,T,y0,options);

DeltaOH20 = 0.16*Faraday/R/Temp;
```

```
theta3eq = zeros(length(expot),1);
theta2eq = theta3eq;
for ii=1:length(expot)
    theta3eq(ii) = ((p0(6)/p0(5))*exp(-Delta(ii))+1)...
        *(p0(8)/p0(7))*exp(-Delta(ii)) + 1;
    theta3eq(ii) = 1/theta3eq(ii);
    theta2eq(ii) = (p0(8)/p0(7))*exp(-Delta(ii))*theta3eq(ii);
end

if plotCoverages
    figure(5);
    title('Coverages');
    grid on;
    box on;
    plot(expot,theta(:,1),'-k',expot,theta(:,2),':b',expot,theta(:,3),'-r',...
        expot,(1 - theta(:,1)-theta(:,2)-theta(:,3)),'-g',expot,theta3eq,...
        '--b',expot,theta2eq,'--r');
    legend('\theta_{H}','\theta_{OH}','\theta_{OH_2}','1 - \sum\theta_{i}',...
        '\theta_{OH_2}^0','\theta_{OH}^0','Location','NorthWest');
    xlabel('E vs. RHE / V');
    ylabel('\theta');
end

%************************************************************************
%Convert to microampsvalues
%************************************************************************

for ii=1:length(T)
    dy = dthetadtHOR(T(ii),theta(ii,:));
    iota(ii) = V2 + V3 + V4 + V5;
```

```
        iota1(ii) = V2 + V3;
        iota2(ii) = V4;
        iota3(ii) = V5;
        V22(ii) = V2;
        V33(ii) = V3;
        V44(ii) = V4;
        V55(ii) = V5;
        isim(ii) = iota(ii)*Faraday*Gamma*p0(7)*aOH;
        isim1(ii) = iota1(ii)*Faraday*Gamma*p0(7)*aOH;
        isim2(ii) = iota2(ii)*Faraday*Gamma*p0(7)*aOH;
        isim3(ii) = iota3(ii)*Faraday*Gamma*p0(7)*aOH;
    end

    isim = 1e6*isim';%Simulated current in micro amps
    isim1 = 1e6*isim1';%Simulated current in micro amps
    isim2 = 1e6*isim2';%Simulated current in micro amps
    isim3 = 1e6*isim3';%Simulated current in micro amps

    if plotCoverages
        figure(6);
        title('Reaction rates');
        grid on;
        box on;
        plot(expot,V22,'-k',expot,V33,':b',expot,V44,'-r',expot,V55,'g');
        legend('V_{2}','V_{3}','V_{4}','V_{5}','Location','NorthWest');
        xlabel('E vs. RHE / V');
        ylabel('V_i');
    end

end
```

D.3 Conversion to Dimensionless Parameters

```
function dy = dthetadtHOR(t,y)

global Deli Delta vsweep nusweep aOH tlambda gamma V1 V2 V3 V4 V5 ...
    alpha2 alpha3 alpha4 alpha5 T Gamma iota1 iota2 iota3 iota iotaexp ...
    expi expot plotCoverages p00 isim1 isim2 isim3 timet

    %Find the index of t in T
    Tlambda = T(length(T)/2);%This is where the sweep returns
    %Note: nusweep*t is independent of k50 and aOH, see MS. Therefore
    %the results in this routine are independent of p0(7) = k50.
    if t < Tlambda
        DeltaLoc = Deli + nusweep*t;
    else
        DeltaLoc = Deli + 2*nusweep*Tlambda - nusweep*t;
    end

    theta1 = y(1);
    theta2 = y(2);
    theta3 = y(3);

    K1  = p00(1);
    Km1 = p00(2);
    K2  = p00(3)*exp((1-alpha2)*DeltaLoc);
    Km2 = p00(4)*exp(-alpha2*DeltaLoc);
    K3  = p00(5)*exp((1-alpha3)*DeltaLoc);
    Km3 = p00(6)*exp(-alpha3*DeltaLoc);
    K4  = p00(7)*exp((1-alpha4)*DeltaLoc-(gamma/2)*theta2);
    Km4 = p00(8)*exp(-alpha4*DeltaLoc+(gamma/2)*theta2);
```

```
    K5 = exp((1-alpha5)*DeltaLoc);
    Km5 = p00(10)*exp(-alpha5*DeltaLoc);
    gamma = p00(11);

    V1 = K1*(1-theta1-theta2-theta3)^2 - Km1*theta1^2;
    V2 = K2*(1-theta1-theta2-theta3) - Km2*theta1;
    V3 = K3*theta1 - Km3*(1-theta1-theta2-theta3);
    V4 = K4*(1-theta1-theta2-theta3) - Km4*theta2;
    V5 = K5*theta2 - Km5*theta3;

    %Differential equations for theta:
    dy(1) = 2*V1 + V2 - V3;%H
    dy(2) = V4 - V5;%OH
    dy(3) = V5;%OH2

    dy = dy';

end
```

D.4 Finding Forward Sweep

```
function Fobj = cvHORkinLsqObjFun(p0)

global Deli Delta vsweep nusweep aOH tlambda gamma V1 V2 V3 V4 V5 ...
    alpha2 alpha3 alpha4 alpha5 T Gamma iota1 iota2 iota3 iota iotaexp ...
    expi expot plotCoverages p00 isim1 isim2 isim3 timet

    Fobj = 0.;
    %Find forward sweep maximum:
    isim0 = cvHORkin(p0,timet);
    Ihalf = round(length(isim0)/2);
    [maxi0f,Imaxi0f] = max(isim0(1:Ihalf));
    [maxexpif,Imaxexpif] = max(expi(1:Ihalf));
%     Fobj = (maxexpif-maxi0f)^2 + (expot(Imaxi0f) - expot(Imaxexpif))^2;
    %Find reverse sweep maximum:
    I34 = round(3*length(isim0)/4);
    [maxi0b,Imaxi0b] = max(isim0(I34+1:length(isim0)));
    Imaxi0b = Imaxi0b + I34 + 1;
    [maxexpib,Imaxexpib] = max(expi(I34+1:length(isim0)));
    Imaxexpib = Imaxexpib + I34 + 1;
%     Fobj = (maxexpib-maxi0b)^2 + (expot(Imaxi0b) - expot(Imaxexpib))^2;
    for ii=1:length(isim0)
        Fobj = Fobj + (isim0(ii) - expi(ii))^2;
    end
%     expot(Imaxi0b)
%     isim0(Imaxi0b)
end
```

Appendix E

Pourbaix

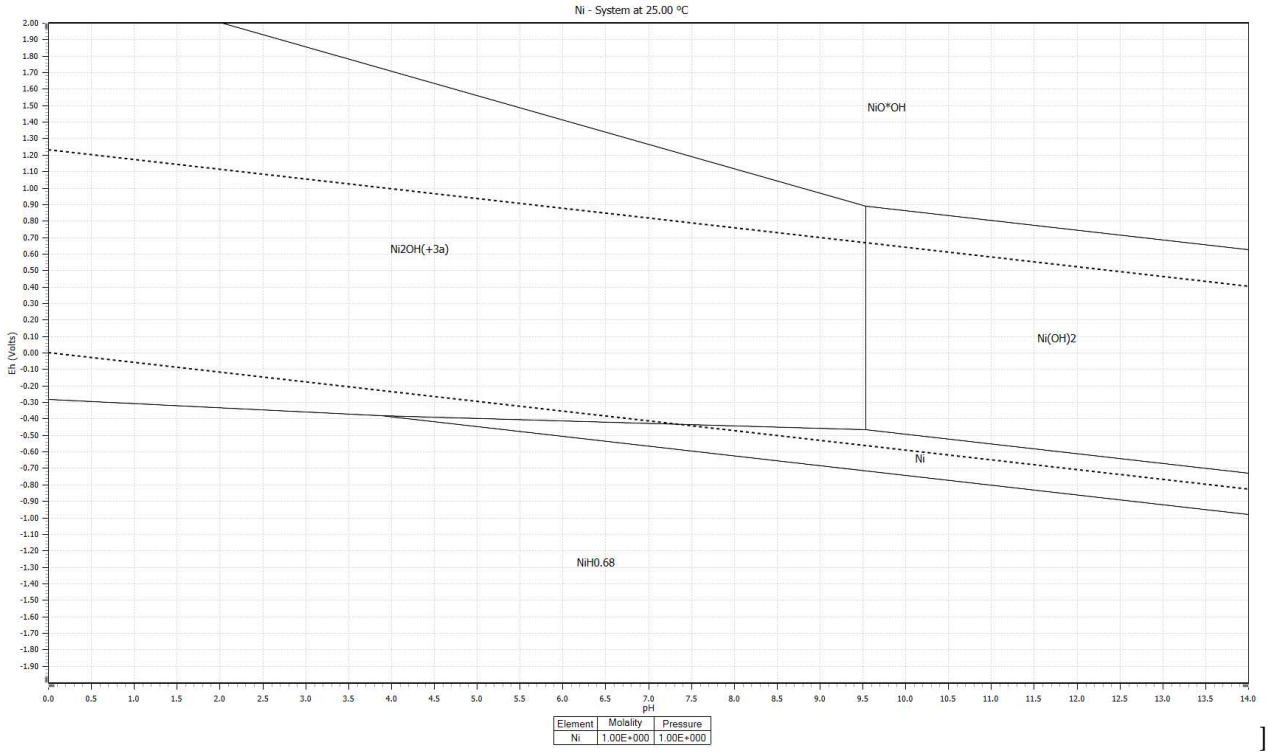

]

Figure E.0.1: Pourbaix diagram of the nickel-water system at 25°C, generated in HSC Chemistry Software

Sigrid Strand

An Investigation of HOR Activity in Alkaline Solution on Nickel Electrode

NTNU
Norwegian University of
Science and Technology